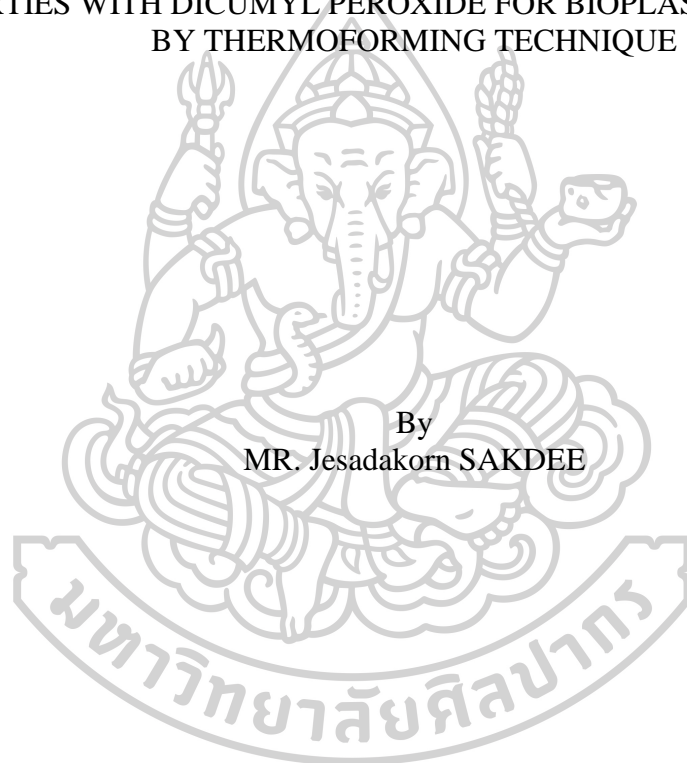




DEVELOPMENT OF POLY(LACTIC ACID)/POLY(BUTYLENE
SUCCINATE)/EPOXIDIZED NATURAL RUBBER TERNARY BLENDS
PROPERTIES WITH DICUMYL PEROXIDE FOR BIOPLASTIC PACKAGING
BY THERMOFORMING TECHNIQUE



By
MR. Jesadakorn SAKDEE

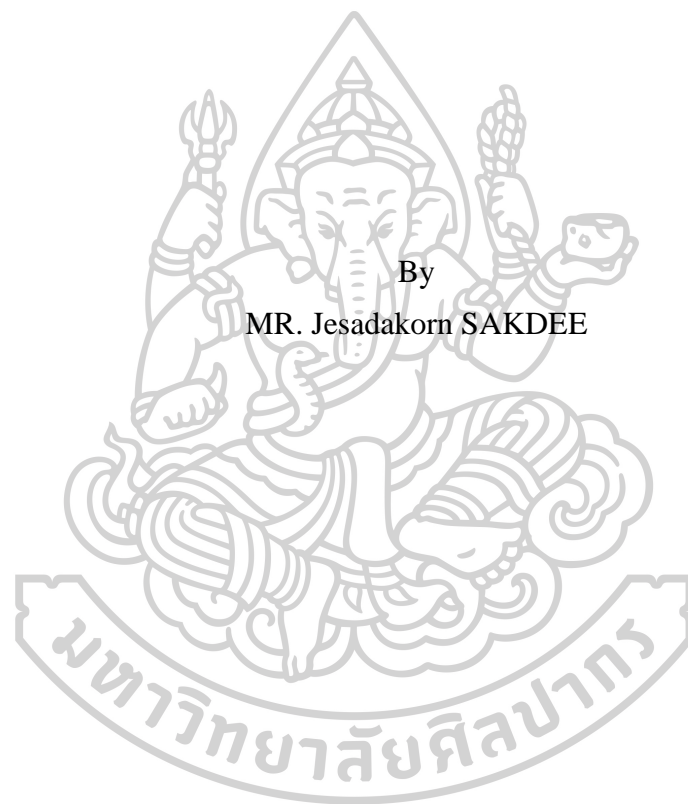
A Thesis Submitted in Partial Fulfillment of the Requirements
for Master of Engineering (CHEMICAL ENGINEERING)
Department of CHEMICAL ENGINEERING
Graduate School, Silpakorn University
Academic Year 2021
Copyright of Silpakorn University

การพัฒนาสมบัติพอลิเมอร์ผสมสามองค์ประกอบของพอลิแลคติกแอซิด พอลิบิวทิลีน
ซักซิเนตและยางธรรมชาติอีพอกไซค์ด้วยไดควิมิลเปอร์ออกไซค์สำหรับบรรจุภัณฑ์
พลาสติกชีวภาพด้วยเทคนิคเทอร์โมฟอร์มมิ่ง



วิทยานิพนธ์นี้เป็นส่วนหนึ่งของการศึกษาตามหลักสูตรวิศวกรรมศาสตรมหาบัณฑิต
สาขาวิชาวิศวกรรมเคมี แผน ก แบบ ก 2 ระดับปริญญาโทมหาบัณฑิต
ภาควิชาวิศวกรรมเคมี
บัณฑิตวิทยาลัย มหาวิทยาลัยศิลปากร
ปีการศึกษา 2564
ลิขสิทธิ์ของมหาวิทยาลัยศิลปากร

DEVELOPMENT OF POLY(LACTIC ACID)/POLY(BUTYLENE
SUCCINATE)/EPOXIDIZED NATURAL RUBBER TERNARY
BLENDS PROPERTIES WITH DICUMYL PEROXIDE FOR
BIOPLASTIC PACKAGING BY THERMOFORMING TECHNIQUE



By
MR. Jesadakorn SAKDEE

A Thesis Submitted in Partial Fulfillment of the Requirements
for Master of Engineering (CHEMICAL ENGINEERING)
Department of CHEMICAL ENGINEERING
Graduate School, Silpakorn University
Academic Year 2021
Copyright of Silpakorn University

Title Development of poly(lactic acid)/poly(butylene succinate)/epoxidized natural rubber ternary blends properties with dicumyl peroxide for bioplastic packaging by thermoforming technique
By MR. Jesadakorn SAKDEE
Field of Study (CHEMICAL ENGINEERING)
Advisor Associate Professor Sirirat Wacharawichanant, D.Eng.

Graduate School Silpakorn University in Partial Fulfillment of the Requirements for the Master of Engineering

.....Dean of graduate school
(Associate Professor Jurairat Nunthanid, Ph.D.)

Approved by

.....Chair person
(Associate Professor Prakorn Ramakul, D.Eng.)

.....Advisor
(Associate Professor Sirirat Wacharawichanant, D.Eng.)

.....Committee
(Sunthon Piticharoenphun, Ph.D.)

.....External Examiner
(Assistant Professor Sunan Tiptipakorn, D.Eng.)

620920030 : Major (CHEMICAL ENGINEERING)

Keyword : poly(lactic acid), poly(butylene succinate), epoxidized natural rubber, dicumyl peroxide, polymer blends

MR. JESADAKORN SAKDEE : DEVELOPMENT OF POLY(LACTIC ACID)/POLY(BUTYLENE SUCCINATE)/EPOXIDIZED NATURAL RUBBER TERNARY BLENDS PROPERTIES WITH DICUMYL PEROXIDE FOR BIOPLASTIC PACKAGING BY THERMOFORMING TECHNIQUE THESIS ADVISOR : ASSOCIATE PROFESSOR SIRIRAT WACHARAWICHANANT, D.Eng.

This main work aims to study the effect of dicumyl peroxide (DCP) contents on the morphological, mechanical, and thermal properties of poly(lactic acid) (PLA)/poly(butylene succinate) (PBS)/epoxidized natural rubber (ENR) ternary blends. The contents of DCP were 0.2, 0.3, 0.5, 1 and 2 parts per hundred of resin (phr). The DCP loading of 0.3 and 0.5 phr increased the percent strain at break of PLA/PBS/ENR 80/15/5 and 80/10/10. The highest percent strain at break was observed in PLA/PBS/ENR 80/10/10 with DCP 0.3 phr at about 42%, which is possibly due to the improved dispersion of DCP. The tensile strength and Young's modulus of PLA/PBS/ENR with DCP increased when compared to those of the blends without DCP. The morphology properties, SEM micrograph showed the effective miscibility changed to the mechanical properties with addition of DCP and good dispersion state of all materials results in interfacial compatibility and enhanced the percent strain at break, compared with PLA. For FTIR showed the same peaks of polymer blends compared to pure PLA after adding all components. In addition, thermal properties, the melting temperature of all of the PLA blends was approximately 150°C. For the decomposition temperature at 10% weight loss of PLA was about 330°C which the PLA/PBS/ENR blends with various DCP were shifted lower the decomposition temperatures than PLA. Nevertheless, in comparison with the decomposition temperature of PLA/PBS/ENR blends with the various DCP, especially at PLA/PBS/ENR (80/15/5) blends with DCP 0.3 and 0.5 phr had more thermal stability than PLA and other blends. The XRD patterns of PLA/PBS/ENR with various DCP were investigated to obtain further insight into the material's crystallinity. A wide diffraction peak at $2\theta=16^\circ$ was observed for PLA. The PLA/PBS/ENR blends were observed at $2\theta=19.5^\circ$ and 22.5° , indicating that the PBS crystalline structure remained in the blends. However, the diffraction peak of PBS in blends did not appear as over ENR loading. For UV-vis spectrophotometer, A huge absorption band of wavelength below 225 nm belonging to PLA absorption was observed and its intensity of blends increased when PBS and ENR were added. The absorption spectra showed a strong absorption

band in the visible region (400-800 nm) due to discoloration of the blends as a result of ENR loading.



ACKNOWLEDGEMENTS

The author wished to express her gratitude and appreciation to their advisor, Associate Professor Sirirat Wacharawichanant, D.Eng. for their support, stimulating, useful discussions throughout this research and devotion to revise this thesis otherwise it cannot be completed in a short time. In addition, the author would like to gratefully acknowledge Associate Professor Prakorn Ramakul, D.Eng. as the chairman of the committee, Sunthon Piticharoenphun, Ph.D. and Assistant Professor Sunan Tiptipakorn, D.Eng. as the members of the thesis committee for their kind evaluation of work and valuable suggestions that could be beneficially used to improve working behavior.

In particular, special thanks for the kind suggestions and useful help to members of Polymer Innovation Laboratory and members of the research zone for their assistance. The author would like to thank the Department of Chemical Engineering, Faculty of Engineering, Chulalongkorn University for Differential Scanning Calorimeter (DSC), Thermogravimetric Analysis (TGA), Ultraviolet-Visible Spectroscopy (UV-vis), Fourier Transform Infrared Spectroscopy (FTIR), and X-Ray Diffractometers (XRD).

Most importantly, the author would like to express the highest gratitude to my family and my friends, who always supported pay attention to though these years for their encouragement, love, care, and other their wills.

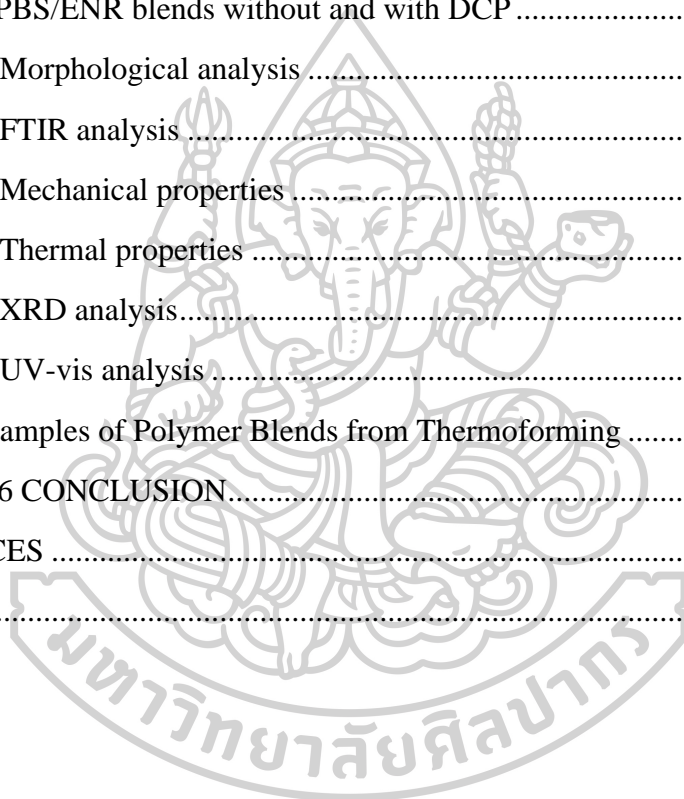
MR. Jesadakorn SAKDEE

TABLE OF CONTENTS

	Page
ABSTRACT.....	D
ACKNOWLEDGEMENTS.....	F
TABLE OF CONTENTS.....	G
LIST OF TABLES.....	J
LIST OF FIGURES.....	K
CHAPTER 1 INTRODUCTION.....	1
CHAPTER 2 THEORY.....	5
2.1 Poly(lactic acid) (PLA).....	5
2.2 Polybutylene Succinate (PBS).....	6
2.3 Epoxidized Natural Rubber (ENR).....	7
2.4 Dicumyl Peroxide (DCP).....	8
2.5 Polymer blends.....	9
2.6 Internal Mixer.....	9
2.7 Compression Molding.....	10
2.8 Thermoforming.....	11
2.9 Mechanical Analysis.....	11
2.9.1 Tensile Test.....	11
2.10 Thermal Analysis.....	13
2.10.1 Differential Scanning Calorimetry (DSC).....	13
2.10.2 Thermogravimetric Analysis (TGA).....	14
2.11 Morphology Analysis.....	15
2.11.1 Scanning electron microscopy (SEM).....	15
2.12 Chemical Structure and Interaction.....	17
2.12.1 Fourier-Transform Infrared Spectroscopy (FTIR).....	17
2.13 Crystal Structure.....	18

2.13.1 X-Ray Diffraction (XRD)	18
2.14 Ultraviolet-Visible Spectroscopy (UV-vis)	19
CHAPTER 3 LITERATURE REVIEWS	20
3.1 Polymer Blends.....	20
3.2 Elastomer	21
3.3 Radical initiator	22
3.4 Thermoforming.....	24
CHAPTER 4 EXPERIMENTAL PROCEDURE.....	25
4.1 Materials	25
4.1.1 Poly(lactic acid) (PLA)	25
4.1.2 Polybutylene Succinate (PBS).....	25
4.1.3 Epoxidized Natural Rubber (ENR)	25
4.1.4 Dicumyl Peroxide (DCP)	25
4.2 Samples Preparation	25
4.2.1 Preparation of Polymer Blends without DCP.....	25
4.2.2 Preparation of polymer blends with DCP.....	26
4.3 Samples Preparation for Testing.....	27
4.3.1 Dog bone-shaped or dumbbells-shaped samples.....	27
4.3.2 Film shaped	27
4.4 Samples Preparation for Thermoforming	27
4.5 Samples Characterizations	27
4.5.1 Scanning Electron Microscopy (SEM).....	27
4.5.2 Universal Tensile Testing (UTM)	27
4.5.3 Differential Scanning Calorimetry (DSC).....	28
4.5.4 Thermogravimetric Analysis (TGA)	28
4.5.5 Fourier-Transform Infrared Spectroscopy (FTIR)	28
4.5.6 X-Ray diffraction (XRD)	28
4.5.7 Ultraviolet-visible spectroscopy (UV-vis)	28
CHAPTER 5 RESULTS AND DISCUSSION.....	29

5.1 Binary Blends of PLA/PBS and PLA/ENR without and with DCP	29
5.1.1 Morphology analysis	29
5.1.2 FTIR analysis	34
5.1.3 Mechanical properties	36
5.1.4 Thermal Properties	41
5.1.5 XRD analysis.....	49
5.1.6 UV-vis analysis	52
5.2 PLA/PBS/ENR blends without and with DCP	53
5.2.1 Morphological analysis	53
5.2.2 FTIR analysis	59
5.2.3 Mechanical properties	61
5.2.4 Thermal properties	66
5.2.5 XRD analysis.....	76
5.2.6 UV-vis analysis	79
5.3 The Samples of Polymer Blends from Thermoforming	82
CHAPTER 6 CONCLUSION.....	85
REFERENCES	86
VITA.....	92



LIST OF TABLES

	Page
Table 1 Physical properties of PBS and PBSA compared with PLA and some commodity plastics [22].....	7
Table 2 Young's modulus and tensile strength of PLA/PBS and PLA/ENR blends with various DCP contents.....	40
Table 3 Stress at break and strain at break of PLA/PBS and PLA/ENR blends with various DCP contents.....	40
Table 4 Melting point temperature of PLA/PBS and PLA/ENR blends with various DCP contents.	44
Table 5 Crystallinity of PLA/PBS and PLA/ENR blends with various DCP contents.	44
Table 6 Decomposition temperature of PLA/PBS and PLA/ENR blends with various DCP contents.	46
Table 7 Normalized crystallinity of PLA/PBS and PLA/ENR blends with various DCP contents.	51
Table 8 Young's modulus and tensile strength of PLA/PBS/ENR blends with various DCP.....	65
Table 9 Stress at break and strain at break of PLA/PBS/ENR blends with various DCP contents.	66
Table 10 Melting point temperature of PLA/PBS/ENR blends with various DCP contents.	71
Table 11 Crystallinity of PLA/PBS/ENR blends with various DCP contents.....	72
Table 12 Decomposition temperature of PLA/PBS/ENR blends with various DCP contents.	76
Table 13 Normalized crystallinity of PLA/PBS/ENR blends with various DCP contents.	79

LIST OF FIGURES

	Page
Figure 1 Synthesis of PLA: (a) Three stereochemical forms of PLA and (b) Direct and ring-opening polymerization method of PLA [2].	5
Figure 2 Scheme of PBS synthesis from SA and BDO (a) esterification,	6
Figure 3 Compatibilization techniques commonly used in polymer blends [24].	8
Figure 4 Chemical structure of DCP [26].	9
Figure 5 Compression molding sequence: (a) molding material is placed into open cavities, (b) the press closes the mold, compressing material in the hot mold for cure and (c) the press opens and molded parts are ejected from the cavities [30].	10
Figure 6 Drape Forming [31].	11
Figure 7 Tensile stress-strain curves for several categories of plastic material [34]. .	12
Figure 8 Stress-strain relationship under uniaxial tensile loading [35].	13
Figure 9 Illustrates typical polymer DSC thermograms [38].	14
Figure 10 TGA and DTG curves of calcium oxalate monohydrate decomposition [39].	15
Figure 11 The electron column shows all of the elements that pertain to the signals from their emission until their capture. In the cabinet, the signals are processed for easy display [41].	16
Figure 12 The optical diagram of an FTIR spectrometer [43].	17
Figure 13 Schematic diagram of X-ray diffraction pattern [44].	18
Figure 14 X-ray diffraction pattern of (a) amorphous sample and (b) Semicrystalline polymer sample [44].	19
Figure 15 SEM micrographs of PLA/NR and PLA/ENR blended at various rubber contents stated in the micrograph [50].	22
Figure 16 Scheme of possible in situ compatibilization and the transition layer at the interface between PLA and ENR phases [17].	23
Figure 17 SEM micrograph of binary blends without DCP; (a) PLA, (b) PLA/PBS (80/20) blends and (c) PLA/ENR (80/20) blends.	31

Figure 18 SEM micrograph of (a) PLA/PBS (80/20) blends and PLA/PBS (80/20) blends with various DCP contents; (b) 0.2 phr, (c) 0.3 phr, (d) 0.5 phr, (e) 1 phr and (f) 2 phr.	32
Figure 19 SEM micrograph of (a) PLA/ENR (80/20) blends and PLA/ENR (80/20) blends with various DCP contents; (b) 0.2 phr, (c) 0.3 phr, (d) 0.5 phr, (e) 1 phr and (f) 2 phr.	33
Figure 20 FTIR spectra of PLA, PBS, ENR and DCP.	35
Figure 21 FTIR spectra of PLA/PBS (80/20) blends with various DCP contents.....	35
Figure 22 FTIR spectra of PLA/ENR (80/20) blends with various DCP contents.	36
Figure 23 Young's modulus of PLA, PLA/PBS (80/20) blends and PLA/ENR (80/20) blends with various DCP contents.	38
Figure 24 Tensile strength of PLA, PLA/PBS (80/20) blends and PLA/ENR (80/20) blends with various DCP contents.	38
Figure 25 Stress at break of PLA, PLA/PBS (80/20) blends and PLA/ENR (80/20) blends with various DCP contents.	39
Figure 26 Strain at break of PLA, PLA/PBS (80/20) blends and PLA/ENR (80/20) blends with various DCP contents.	39
Figure 27 DSC of PLA and PLA/PBS blends with various DCP contents.	42
Figure 28 DSC of PLA and PLA/ENR blends with various DCP contents.....	43
Figure 29 TGA of PLA and PLA/PBS blends with various DCP contents.	47
Figure 30 TGA of PLA and PLA/ENR blends with various DCP contents.	48
Figure 31 XRD of PLA, PBS and ENR.....	50
Figure 32 XRD of PLA and PLA/PBS (80/20) blends with various DCP contents... ..	50
Figure 33 XRD of PLA and PLA/ENR blends with various DCP contents.	51
Figure 34 UV-vis of PLA and PLA/PBS blends with various DCP contents.	52
Figure 35 UV-vis of PLA and PLA/ENR blends with various DCP contents.....	53
Figure 36 SEM micrograph of PLA/PBS/ENR blends without DCP; (a) PLA, (b) PLA/PBS/ENR (80/15/5), (c) PLA/PBS/ENR (80/10/10) and (d) PLA/PBS/ENR (80/5/15).....	55
Figure 37 SEM micrograph of PLA/PBS/ENR (80/15/5) blends with various DCP contents; (a) no DCP, (b) 0.2 phr, (c) 0.3 phr, (d) 0.5 phr, (e) 1 phr and (f) 2 phr.	56

Figure 38 SEM micrograph of PLA/PBS/ENR (80/10/10) blends with various DCP contents; (a) no DCP, (b) 0.2 phr, (c) 0.3 phr, (d) 0.5 phr, (e) 1 phr and (f) 2 phr.	57
Figure 39 SEM micrograph of PLA/PBS/ENR (80/5/15) blends with various DCP contents; (a) no DCP, (b) 0.2 phr, (c) 0.3 phr, (d) 0.5 phr, (e) 1 phr and (f) 2 phr.	58
Figure 40 FTIR spectra of PLA/PBS/ENR (80/15/5) blends with various DCP contents.	60
Figure 41 FTIR spectra of PLA/PBS/ENR (80/10/10) blends with various DCP contents.	60
Figure 42 FTIR spectra of PLA/PBS/ENR (80/5/15) blends with various DCP contents.	61
Figure 43 Young's modulus of PLA/PBS/ENR blends with various DCP contents.	63
Figure 44 Tensile strength of PLA/PBS/ENR blends with various DCP contents.	63
Figure 45 Stress at break of PLA/PBS/ENR blends with various DCP contents.	64
Figure 46 Strain at break of PLA/PBS/ENR blends with various DCP contents.	64
Figure 47 DSC of PLA/PBS/ENR (80/15/5) blends with various DCP contents.	68
Figure 48 DSC of PLA/PBS/ENR (80/10/10) blends with various DCP contents.	69
Figure 49 DSC of PLA/PBS/ENR (80/5/15) blends with various DCP contents.	70
Figure 50 TGA of PLA/PBS/ENR (80/15/5) blends with various DCP contents.	73
Figure 51 TGA of PLA/PBS/ENR (80/10/10) blends with various DCP contents.	74
Figure 52 TGA of PLA/PBS/ENR (80/5/15) blends with various DCP contents.	75
Figure 53 XRD of PLA/PBS/ENR (80/15/5) blends with various DCP contents.	77
Figure 54 XRD of PLA/PBS/ENR (80/10/10) blends with various DCP contents.	78
Figure 55 XRD of PLA/PBS/ENR (80/5/15) blends with various DCP contents.	78
Figure 56 UV-vis of PLA/PBS/ENR (80/15/5) blends with various DCP contents.	80
Figure 57 UV-vis of PLA/PBS/ENR (80/10/10) blends with various DCP contents.	81
Figure 58 UV-vis of PLA/PBS/ENR (80/5/15) blends with various DCP contents.	81
Figure 59 Thermoforming equipment in Polymer Innovation Laboratory.	82
Figure 60 Sample 1 of PLA/PBS (80/20) blends with DCP 0.3 phr.	82
Figure 61 Sample 2 of PLA/PBS (80/20) blends with DCP 0.3 phr.	83
Figure 62 Samples 3 and 4 of PLA/PBS/ENR (80/10/10) blends with DCP 0.3 phr.	83
Figure 63 Samples 5 and 6 of PLA/PBS/ENR (80/10/10) blends with DCP 0.3 phr.	84

Figure 64 The sample 7 of PLA/PBS/ENR (80/15/5) blends with DCP 0.3 phr.....84



CHAPTER 1

INTRODUCTION

Petroleum-based polymers have been widely used in the production of numerous polymeric products for diverse commodities, engineering, and advanced applications. However, the use of petroleum-based polymers has been a serious concern of the environmentalists because the majority of these polymers linger in the environment as non-degradable wastes. As a result, efforts have been directed toward the creation of biodegradable polymers from renewable agricultural resources in order to address these concerns [1-3]. There is a rise in interest in bioplastics, which stems from increased concern about the disposal of plastic waste and the need to discover alternatives. Bio-degradable polymers may provide an alternate answer to fossil fuel feedstocks, such as plastic. Furthermore, the emphasis on polymers generated from renewable resources, such as plant-based compounds [4].

To circumvent the growing problem of plastic waste and pollution, research has concentrated on the development of alternative bio-packaging materials produced from renewable sources that are compostable or biodegradable. Biopolymers or bio-materials can be used to replace non-biodegradable plastics. There are many bio-based polymers or biodegradable polymers that were used to solve this problem, such as poly(lactic acid) (PLA), polyhydroxybutyrate (PHB), polycaprolactone (PCL), polybutylene adipate-co-terephthalate (PBAT), polybutylene succinate (PBS) or other polymers. For the development and improvement of polymers, PLA is an aliphatic thermoplastic polyester that is widely used in commercial bio-based, biodegradable, and biocompatible polymers. It is derived from the fermentation of polysaccharide sources like sugarcane, cornstarch, and other renewable bio-mass products and wastes. PLA can be produced via direct condensation polymerization of the lactic acid monomer or ring-opening polymerization of the lactide, which is a cyclic lactide dimer consisting of two lactic acid molecules. In general, the ring-opening strategy is utilized commercially to create solvent-free high molecular weight PLA, because water is produced as an unwanted coproduct during polymerization in the other way [3-5]. PLA, in addition to being a competitive material, has appealing physical and mechanical qualities such as non-toxicity, high strength and modulus, and good clarity. These properties make PLA a

suitable candidate in commodity and engineering applications to replace some important petroleum-based polymers, but some PLA properties have disadvantages, such as inherent brittleness, very low toughness, low elongation at break, low degree of crystallization, and poor thermal stability, which limits its wide application, particularly for packaging products.

To overcome such disadvantages, studies on the suitable formulations of PLA mixes with other biodegradable polymers have been done. Many researchers have now shown that PLA may be combined with a wide range of flexible biodegradable polymers, with PBS being of particular interest due to its mechanical properties and biodegradability. It is a ductile polymer with the potential for great elongation. Xue et al. [6], Ji et al. [7], and Monika et al. [8] investigated the mechanical properties of PLA blended with PBS and the results revealed an increase in toughness, impact strength, and high elongation when PBS was incorporated in PLA. However, most of the blends showed poor mechanical characteristics due to phase separation, low miscibility, and interfacial adhesion. Incorporation between PLA and PBS, PLA as the matrix had revealed to aid in PLA crystallization due to the capability of PBS to well disperse in the PLA matrix. A high-intensity, crystallization peak emerged at a low PBS level of 10-20 wt%, corresponding to PLA crystallization, implying that PBS may promote PLA crystallization [9, 10]. In terms of mechanical qualities, including a rigid material such as PLA into PBS increases tensile strength while decreasing flexibility, resulting in hard-produced miscible blends. In previous research, a minor shift in glass transition temperature to lower temperatures was seen at PBS concentrations greater than 40 wt%, most likely due to a well-dispersed PBS phase with a plasticization influence on the PLA matrix [11].

For this reason, the immiscibility of polymer blends leads many researchers to try to improve by finding other polymers or additives. Epoxidized natural rubber (ENR) is a biopolymer and a co-agent that was modified from natural rubber (NR). But ENR shows a higher T_g than NR which ENR has good toughness, high strength, and adhesion [12]. Effective properties included bio-based material, susceptibility for non-toxic, low cost, and biocompatibility which enabled ENR to be utilized for producing heat resistance, impact resistance, eco-friendly, and naturally degradable blends. The addition of ENR to PBS blends increased versatility. The morphology shifted to co-continuous phase

morphology at 40 wt% of ENR as the ENR dosage increased [13]. The excellent interfacial adhesion between ENR and PLA is exhibited by Zhang et al. [14], who described the mechanical properties increased because ENR reduced the tensile strength and elongation at break of PLA. The crystallization increased with ENR and NR because tiny molecules in the rubber phase and droplet surfaces might act as nucleating agents.

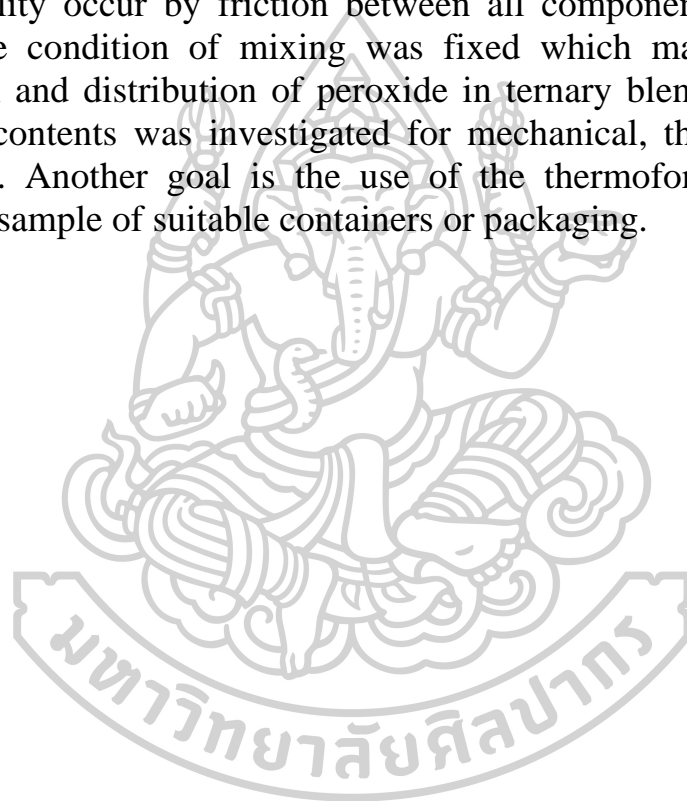
However, the majority of the blends showed poor properties due to low miscibility and interfacial adhesion. In-situ reactive compatibilization is thought to be a viable approach for enhancing the miscibility of PLA blends. Reactive processing is frequently used compatibilizers or additives for the production of miscible polymer. One of the organic additives was used which is dicumyl peroxide (DCP). The role of DCP and the compatibilizing process was well documented for these bio-polymer blends. In the reaction, the DCP induced free-radical interaction between the distinct phases to generate a grafting copolymer and a partly cross-linked network, which considerably increased the compatibility of the polymer blends. Wang et al. have observed the impacts of DCP as a free-radical initiator on the mechanical properties of PLA/PBS blends. They discovered the rising impact strength with increasing DCP. In addition, DCP has been used as a compatibilizer in the process, which could decrease the domain phase of PBS and increase interfacial adhesion [15].

In previous research, Srimalanon et al. [16] employed DCP as a free radical. The inclusion of PBS into PLA was found to increase the toughness, however poor adhesion and miscibility resulted in poor mechanical qualities. At 20 wt% of PBS changed the fracture behavior from brittle to ductile. The highest elongation at break and toughness were obtained at 0.2 pph of DCP, improved the distribution of PBS, and also reduced the particle size. Ji et al. and Monika et al. revealed the impact of DCP on mechanical properties increased. Research by Wang et al. [17] showed the toughening mechanism, no voids resulting from pull-out were observed by scanning electron microscope (SEM), indicating that the crosslinked ENR phase was very compatible in PLA. When adding the DCP and ENR, can be improved and also increased the mechanical properties, especially for the toughness [18, 19].

In the polymer packaging business, thermoforming is an important shaping mechanism for thermoplastic plastic film and sheets. The thermoforming method is one of the few procedures utilized in the

manufacture of plastics. The improvement of process factors is becoming increasingly important in the industry. All of this has allowed for a wide spectrum of plastic production [20]. Thermoforming, also known as vacuum forming, is an industrial process that is used to create many products, such as food packaging, disposable plates, plastic toys, and another packaging.

Consequently, the main proposal of this work is the use of peroxide, DCP as a compatibilizer in the biodegradable process of ternary blends (PLA/PBS/ENR). In the process, the mixing, melting, and compatibility occur by friction between all components, and peroxide within the condition of mixing was fixed which may lead to better dispersion and distribution of peroxide in ternary blends. The effect of different contents was investigated for mechanical, thermal, and other properties. Another goal is the use of the thermoforming process to provide a sample of suitable containers or packaging.



CHAPTER 2

THEORY

2.1 Poly(lactic acid) (PLA)

PLA's monomer is lactic acid, which can be generated through starch and sugar fermentation. Lactic acid has two optically active forms due to L-lactic acid and D-lactic acid. PLA can be produced from lactide which has three different structures; the LL-lactide made from two L-lactates, the DD-lactide made from two D-lactates, and the DL made from a combination of one L- and one D-lactate. PLA can occur in three stereochemical structures which are poly (L-lactide) (PLLA), poly (DL-lactide) (PDLLA), and poly (D-lactide) (PDLA), as shown in Figure 1a. PLA is primarily synthesized through chemical and biological polymerization. Several studies have been published on the polymerization of PLA, although the most commonly used methods are direct polymerization and ring-opening polymerization, as shown in Figure 1b [2].

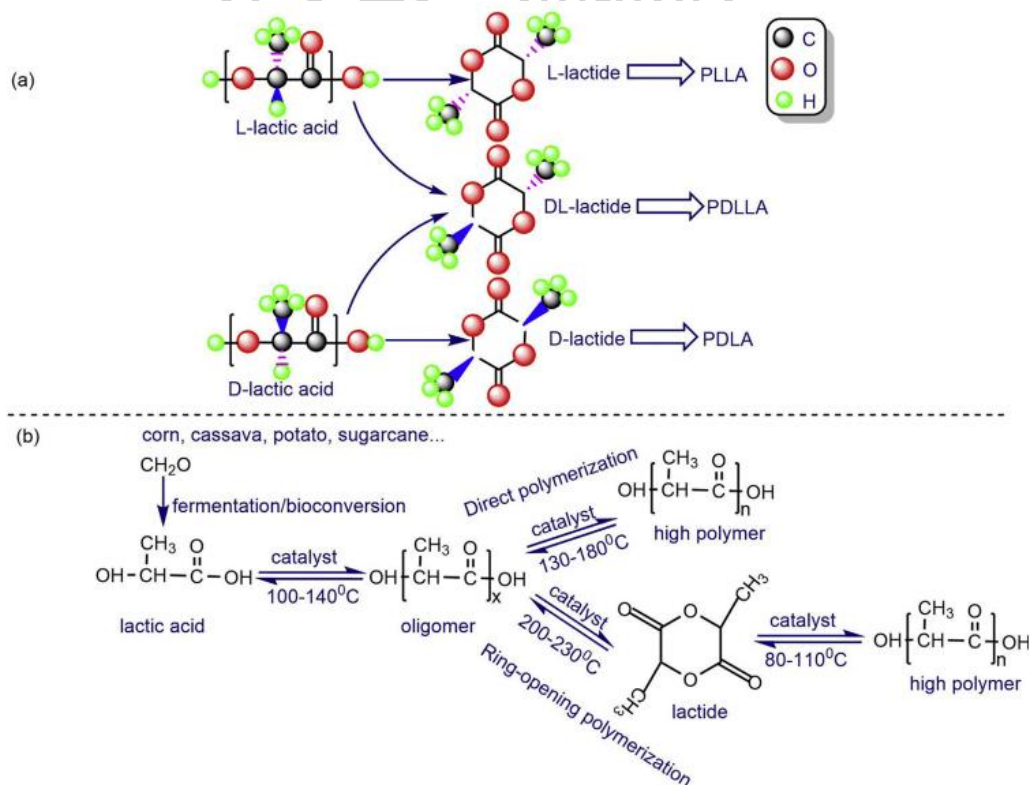


Figure 1 Synthesis of PLA: (a) Three stereochemical forms of PLA and (b) Direct and ring-opening polymerization method of PLA [2].

The former demonstrates that lactic acid generates PLA through a dehydration-condensation reaction at a catalyst and controlled temperature, but the output is lower. The latter demonstrates that lactic acid first produces lactide by raising the catalyst and temperature, and then lactide forms PLA by ring-opening polymerization at a catalyst and controlled temperature. PLA is compostable and derived from renewable sources, making it ideal for consumer goods and packaging applications. It has been suggested as a potential remedy for the issue of properly disposing of solid waste and reducing the use of packaging materials made of petroleum-based plastics.

2.2 Polybutylene Succinate (PBS)

Figure 2 illustrates the two-step melt by polycondensation reaction used to create PBS. This reaction took place in a 7.5-L stainless steel batch reactor that was provided with a heating system, a mechanical stirrer with torque monitoring, a distillation column, a vacuum line, and a nitrogen gas intake. PBS is a biopolymer derived from the polycondensation of succinic acid and 1-4 butanediol (BDO), and it offers plastics manufacturers an intriguing building block for biopolymer compounds.

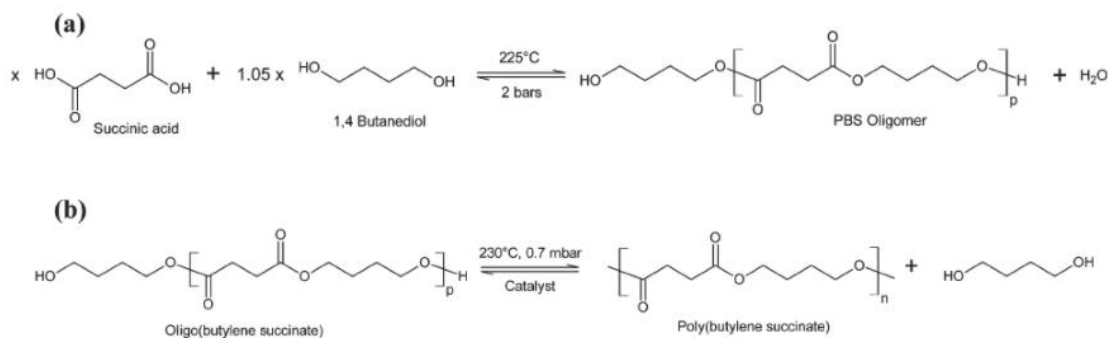


Figure 2 Scheme of PBS synthesis from SA and BDO (a) esterification, (b) transesterification [21].

PBS is a crystalline polyester with a melting temperature of more than 100°C, which is crucial for high-temperature applications. Table 1 provides a summary of the mechanical properties of PBS and PBSA, a typical copolymer of PBS including adipic acid, in comparison to other biopolymers and common Petro-based polymers. PBS has good processability and can be processed in the textile industry into melt-blow,

multifilament, thermoforming, flat, and split yarn, as well as in the plastics industry into injection molded items, making it a promising polymer for a wide range of possible applications [22].

Table 1 Physical properties of PBS and PBSA compared with PLA and some commodity plastics [22].

Items	PLA (LACEA)	PBS (Bionolle) #1000	PBSA #3000	PP MA210	HDPE	LDPE F082
Glass transition temperature (°C)	55	-32	-45	-5	-120	-120
Melting point (°C)	170-180	114	96	163	129	110
Heat distortion temperature (°C)	55	97	69	110	82	49
Tensile strength (Mpa)	66	34	19	33	28	10
Elongation at break (%)	4	560	807	415	700	300
Izod impact strength (J/m)	29	300	>400	20	40	>400
Degree of crystallinity (%)		35-45	20-30	56	69	49

2.3 Epoxidized Natural Rubber (ENR)

Natural rubber is a renewable resource that is also environmentally friendly. Chemical modification has emerged as an important method for improving the properties of NR and expanding its range of applications. It was first developed at the beginning of the nineteenth century, some 50 years earlier than the chemical modification of synthetic polymers. Having a highly cis-1,4-polyisoprenic structure, the chemical reactivity of the carbon-carbon double bond of NR is considered to be similar to that of simple olefins. Chemical reactions under environmentally friendly conditions such as water phase or original latex form of NR are of increasing interest. Based on the fundamentals of organic chemistry, the hydrogenation of NR latex has been successfully investigated, despite the lack of a clear understanding of the reaction at the interface of the rubber particles in latex form. Epoxidation is another chemical modification of NR which has been explored by researchers. The reaction can be carried out with NR latex, which is available in rubber-producing countries and is commercially viable via in-situ epoxidation using formic acid and hydrogen peroxide.

The chemical reaction that converts the carbon-carbon double bond into oxiranes by using a variety of reagents such as organic peracid is known as epoxidation. The epoxidation of NR is an attractive method of modification as it improves properties. Peroxycarboxylic acid was first used to react with NR. Commercial production of epoxidized NR (ENR), ENR-10 (having 10% mole of epoxide content), ENR-25 (having 25%

mole of epoxide content), and ENR-50 (having 50% mole of epoxide content) [23].

2.4 Dicumyl Peroxide (DCP)

As shown in Figure 3, various methods for polymer blend compatibilization can be used. Copolymer addition is one of the most commonly used compatibilizations. In general, the copolymer should be miscible with one component and miscible with another blend component. The presence of the copolymer at the interface reduces the interfacial tension of an immiscible blend. It also shrinks the dispersed phase and prevents coalescence. Compatibility through reactive polymer addition is currently used to replace the addition of prefabricated copolymers. The polymer used in the blend is miscible with one of the components [24].

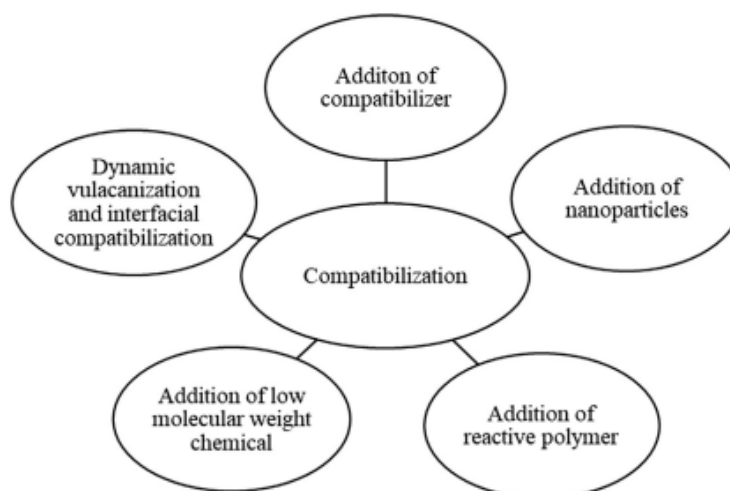


Figure 3 Compatibilization techniques commonly used in polymer blends [24].

Reactive processing is a popular compatibilization strategy for producing new multiphase polymeric materials with excellent physical and chemical properties at a low cost. The successful application of reactive processing principles has resulted in significant technological opportunities for the compatibilization of immiscible polymer blends. During the extrusion process, terminal or graft groups react with the terminal group of the other polymers. Figure 4 illustrates the chemical structure of dicumyl peroxide, a free radical producer [25].

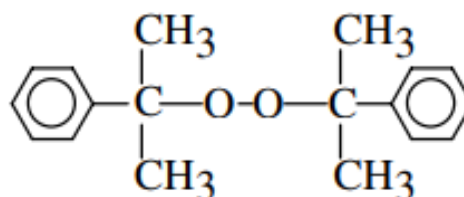


Figure 4 Chemical structure of DCP [26].

2.5 Polymer blends

Polymer blends are the combination of two or more polymers that have been combined to form a new material with distinct physical properties. Polymer blending has gained popularity as a simple and cost-effective method of developing polymeric materials with commercial applications in mind. In other words, by carefully selecting the component polymers, the properties of the blends can be tailored to their intended use [27]. Polymer blends can be three categorized as follows; (1) Immiscible polymer blends, (2) Compatible polymer blends, and (3) Miscible polymer blends [28].

2.6 Internal Mixer

An internal mixer is a machine where the materials are mixed and blended. An internal mixer consists usually of two rotors enclosed in a mixing chamber. The internal mixer is classified into two types which are the Banbury mixer (tangential rotor design) and the Intermix mixer (interlocking rotor design). The Banbury Mixer is one of the most popular designs. The design features a mixing chamber with a counter-rotating rotor in each section. The mixing action of the two mixer designs contrasts due to the shape of the rotors used. Previously, an internal mixer was operated by fixed-speed motors through the use of gears. They are now frequently equipped with controllable motors for increased versatility. Temperature is controlled by fluid flow through channels in the steel chamber walls, rotors, and drop doors, as well as alternately within the ram. An internal mixer can process materials more rapidly than mills, sometimes by an order of magnitude more rapidly [29].

2.7 Compression Molding

A composite manufacturing technique called compression molding is typically used to create large quantities of composite parts, like those for automobiles. Cold compression molding and hot compression molding are the two different types of compression molding. The molding compound is typically used as an intermediate material in this process for thermosetting matrices.

It is a semi-cured composite. The thermosetting-based molding compounds known as sheet molding compounds are very popular. An internal mixer and twin-screw extruder are typically used to make composite pellets. Pressure is applied during cold compression molding and pressure and temperature are applied during hot compression molding before the molding is completed and placed in a mold cavity. While the curing process for the hot press occurs by heating the mold and then transferring that heat to the composites, cold compression molding takes place at room temperature. Figure 5 shows an upward-closing press [30].

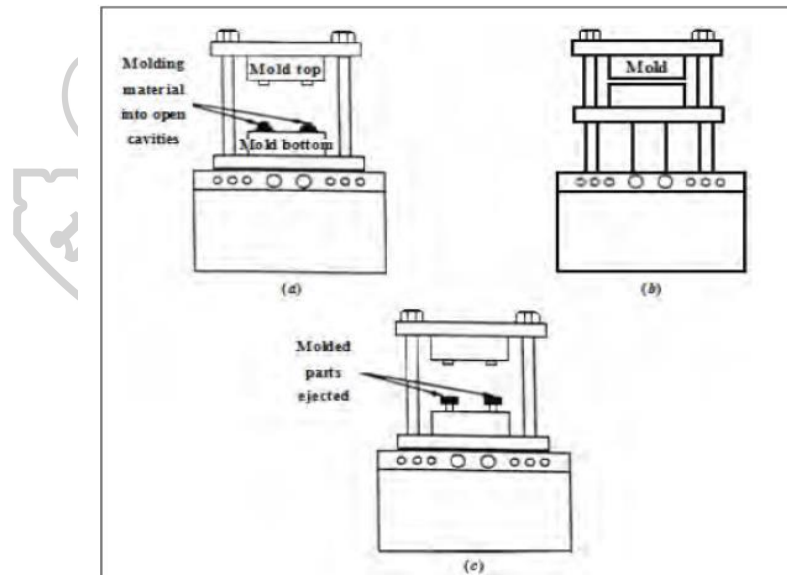


Figure 5 Compression molding sequence: (a) molding material is placed into open cavities, (b) the press closes the mold, compressing material in the hot mold for cure and (c) the press opens and molded parts are ejected from the cavities [30].

2.8 Thermoforming

Thermoforming is the process of shaping a plastic sheet (or film) into useful packaging by shaping it into or around a mold. The thermoforming process has three basic steps: heating the sheet, *forming the sheet*, and trimming the part.

After the plastic sheet has been softened by heat, there are numerous methods for molding it. *Drape forming*, vacuum forming, and pressure forming are the most basic. Other thermoforming techniques are variations or combinations of these fundamental techniques. The influence of gravity on the hot plastic sheet is the main forming force in drape forming, as shown in Figure 6. A positive, or male, a mold of the part with a convex shape is typically used. The forming process is aided by the use of a vacuum to pull the material down around the shape [31].

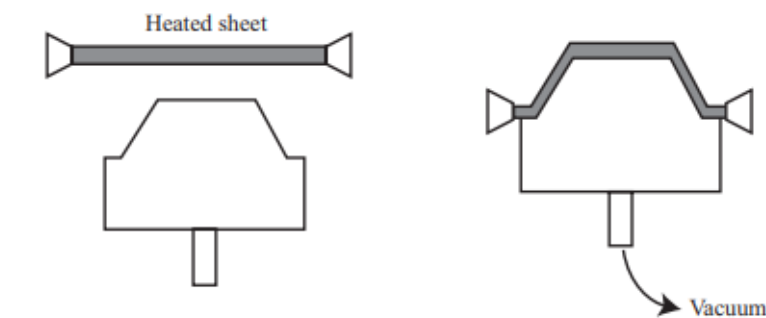


Figure 6 Drape Forming [31].

2.9 Mechanical Analysis

2.9.1 Tensile Test

Mechanical properties are properties that relate to the material's response to external forces. Tensile strength, stiffness, and ductility are examples of mechanical properties. These material properties are critical for engineering applications to use properly and efficiently and safely [32].

Tensile tests are performed for various reasons. Tensile test results are used to select materials for applications. Tensile properties are frequently measured during the development of new materials and processes. Tensile properties are often used to predict a material's behavior under loading conditions other than uniaxial tension. The force

required to separate the specimen is calculated, as well as how far the material can stretch before breaking. A force is applied to the specimen sample in the universal testing machine. As a result, the change in length of the specimen is measured with the original length. A tensile test can provide information about a material's strength, Young's modulus, and ductility. These values from testing are then converted into a stress-strain curve. It is further analyzed for material properties. The modulus is essentially a measure of stiffness. As shown in Figure 7, The overall amount under a stress-strain curve represents overall toughness [33].

The stress-strain curve follows Hook's law during elastic deformation, and the slope of the curve indicates Young's modulus (E), as follows;

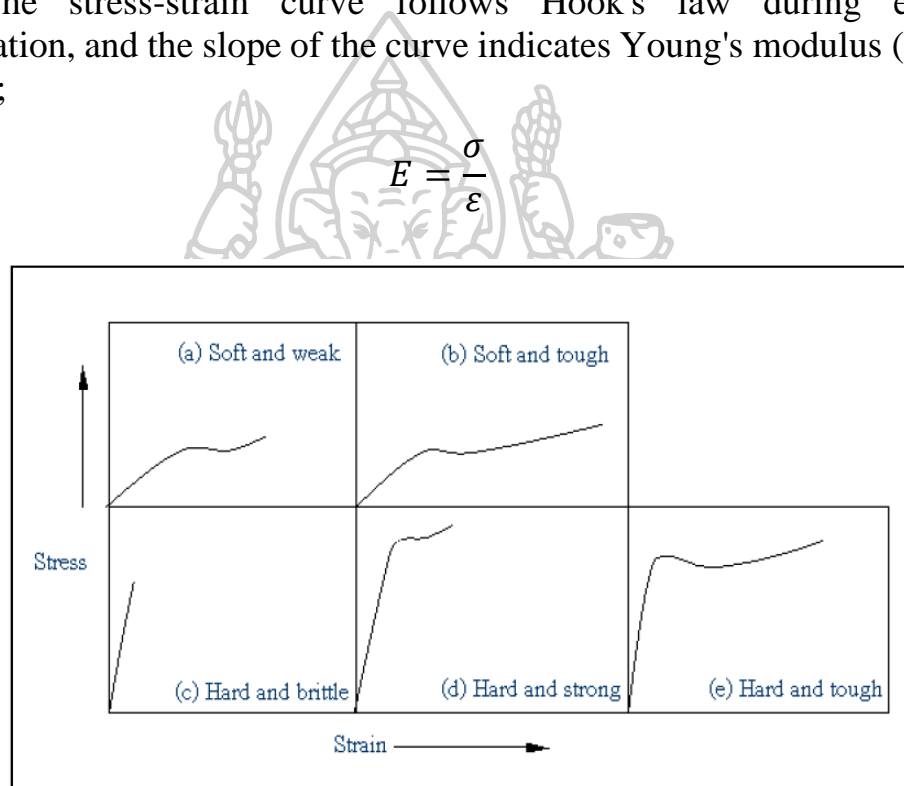


Figure 7 Tensile stress-strain curves for several categories of plastic material [34].

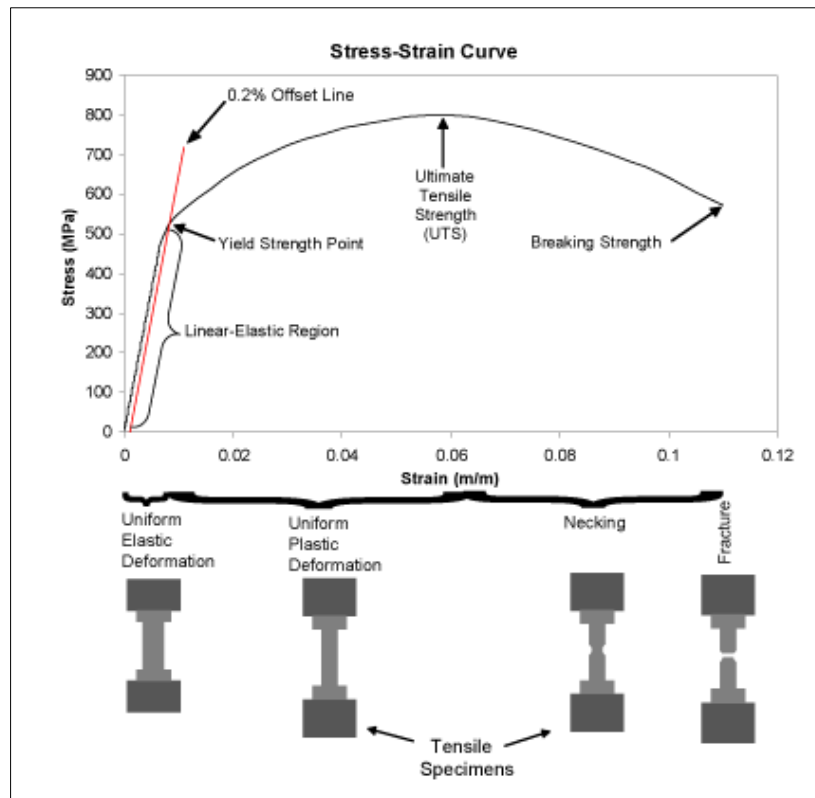


Figure 8 Stress-strain relationship under uniaxial tensile loading [35].

2.10 Thermal Analysis

2.10.1 Differential Scanning Calorimetry (DSC)

DSC is the most commonly used technique for the thermal analysis of polymeric materials. It calculates the difference in energy inputs into a substance and reference material while subjecting them to a temperature control program. Almost all chemical and physical processes involve the change in enthalpy heat. DSC is almost universally applicable to condensed phase systems [36]. It is measured quantitatively, and the change in enthalpy is typically a linear function of the reaction coordinate. Figure 9 illustrates a DSC endothermic or exothermic peak. The area between a DSC curve and its extrapolated baseline indicates the total heat of reaction because DSC measurement gives the rate of change of enthalpy. The reacted fraction is calculated by dividing the fractional area by the total area. The rate of reaction is measured by the amplitude between the baseline and the DSC curve [37].

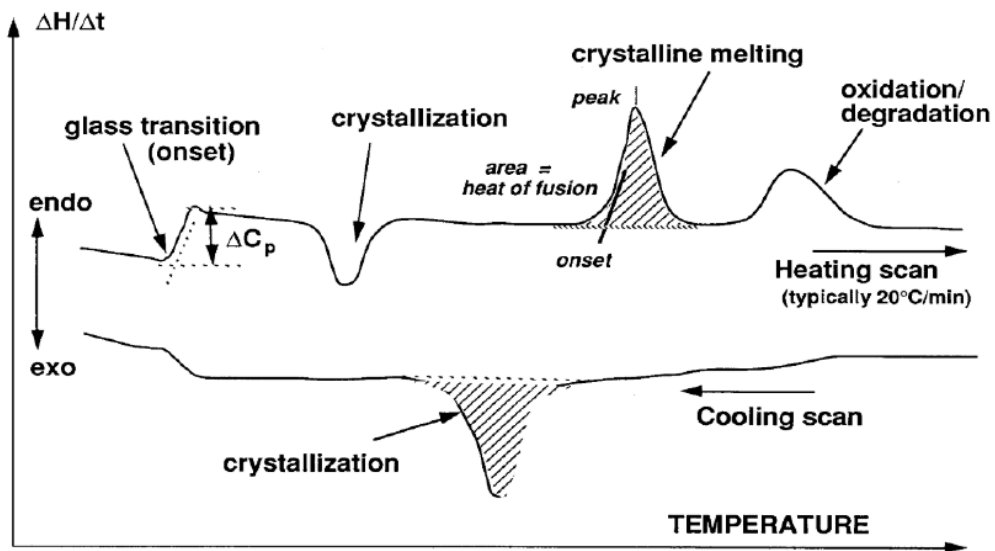


Figure 9 Illustrates typical polymer DSC thermograms [38].

In the formation of crystals, the results of the analysis with the DSC can be calculated as a percentage of crystal (% X_c) as shown in the equation;

$$\%X_c = \left(\frac{\Delta H_m}{\Delta H_m^\circ} \right) \times \frac{100}{W}$$

Where W = the fraction of polymer matrix in the polymer blends
 ΔH_m = enthalpy of annealing polymer matrix
 ΔH_m° = enthalpy of annealing of 100% crystalline polymer

2.10.2 Thermogravimetric Analysis (TGA)

Thermogravimetric Analysis is a technique that detects the mass of a substance as a function of temperature while exposing the sample specimen to a controlled temperature program in a controlled atmosphere. The TGA curve plots percent mass versus temperature. The first derivative of the TGA curve to temperature is an alternative and complementary presentation. This is referred to as the DTG curve, and it represents the rate of mass change. Mass changes occur when a sample loses some materials. Various effects can cause a sample to lose or gain mass, resulting in steps in the TGA curve. The instrument can measure water loss, plasticizer loss, decarboxylation, and decomposition, as well

as weight percent filler and weight percent ash. Figure 10 shows an example of stepwise decomposition of calcium oxalate monohydrate measured at 30 K/min under nitrogen atmosphere by the temperature range of the three mass losses, which is especially visible in the normalized first derivative or DTG curve [39].

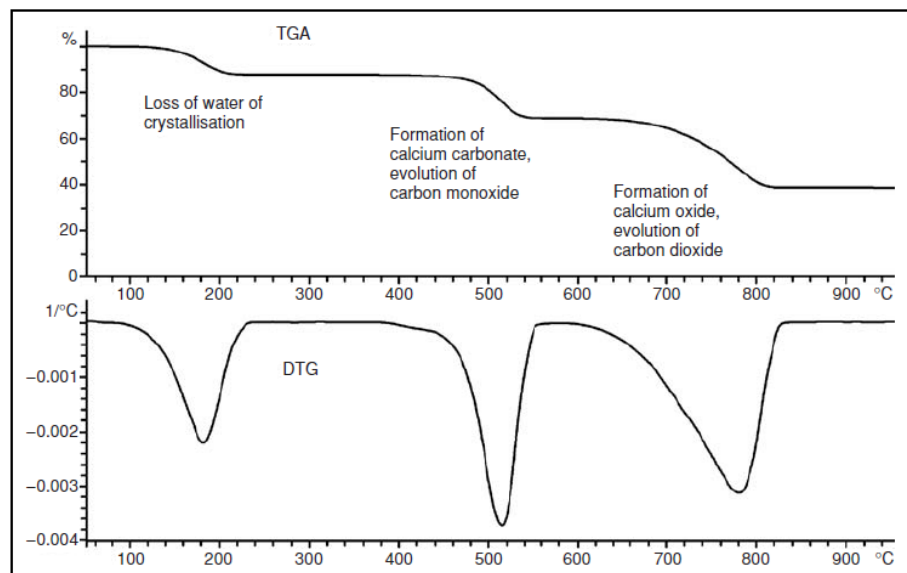


Figure 10 TGA and DTG curves of calcium oxalate monohydrate decomposition [39].

2.11 Morphology Analysis

2.11.1 Scanning electron microscopy (SEM)

A variety of morphologies can be formed by combining dissimilar polymers. Morphology control is critical in polymer blends. There are several techniques for studying the morphology of polymer blends. SEM is commonly used to examine polymer surfaces. The SEM can provide different contrast modes, wherein information such as surface voltage is embedded in its output signals, in addition to providing a rising topographical image of a specimen's surface [40].

The column and the cabinet are the two main components of SEM (Figure 11). The column is the path electrons take from their emission to the sample, where the detectors installed will capture the scattered signals caused by the electrons' interaction with the sample. The detectors are energy transducers that convert one type of signal into an electrical signal that is transmitted to the control cabinet [41]. The control cabinet is

outfitted with electronic systems capable of quantifying the electrical signals sent by the detectors and switching them into data that can be analyzed, such as images.

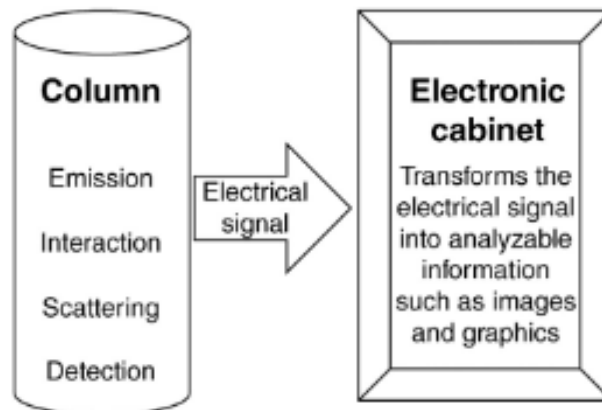


Figure 11 The electron column shows all of the elements that pertain to the signals from their emission until their capture. In the cabinet, the signals are processed for easy display [41].

SEM provides surface information by tracing a sample with an electron beam in a raster pattern. An electron gun fires a beam of energetic electrons down the column and onto a series of electromagnetic lenses, which starts the process. These lenses are solenoids, which are tubes wrapped in a coil. The coils are placed so that the incident electron beam is concentrated on the sample. These adjustments cause voltage fluctuations, increasing or decreasing the rate at which the electrons come into contact with the specimen surface. SEM operators can adjust the beam to control magnification and determine the surface area to be scanned using a computer. It is focused on the stage, which contains a solid sample. The two common preparation processes used before SEM analysis are sputter coating for non-conductive samples and dehydration for most biological specimens. Furthermore, the acceleration rate of incident electrons determines the interaction between incident electrons and the surface of the sample. The scatter patterns produced by the interaction provide information about the sample's size and composition. To attract various types of scattered electrons are used [42].

2.12 Chemical Structure and Interaction

2.12.1 Fourier-Transform Infrared Spectroscopy (FTIR)

The Fourier Transform Infrared Spectrometer (FTIR) is widely used in several sections such as organic synthesis, polymer science, and petrochemical engineering. Furthermore, FTIR spectrometers can be used to investigate the mechanism of chemical reactions in materials.

A typical FTIR spectrometer is made up of a source, an interferometer, a sample compartment, a detector, an amplifier, an A/D converter, and a computer. The source emits radiation, which passes through the interferometer and into the detector. The device and analog-to-digital converter then enhance the signal and convert it to digital. Finally, the signal is transferred to a computer, where the Fourier transform is performed. Figure 12 represents an FTIR spectrometer diagram. Infrared spectroscopy can be used to qualitatively identify substances because different molecules with different atom combinations produce distinct spectra. The intensity of the peaks in the spectrum is proportional to the amount of substance present, allowing for quantitative analysis [43].

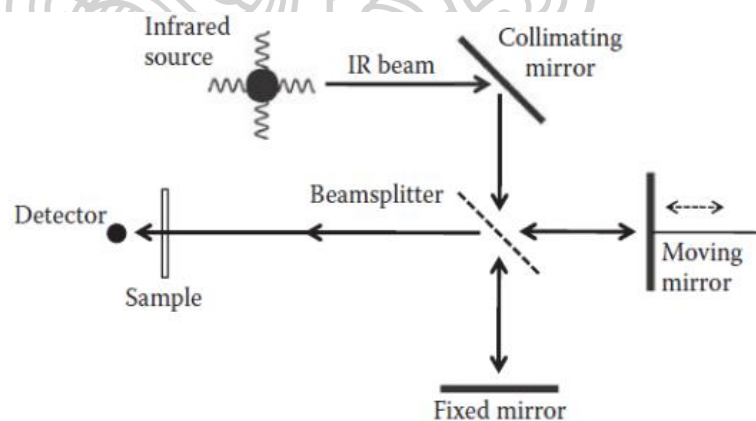


Figure 12 The optical diagram of an FTIR spectrometer [43].

2.13 Crystal Structure

2.13.1 X-Ray Diffraction (XRD)

X-ray diffraction is also used to determine the type of polymer and the degree of crystallinity in a polymer sample. The schematic diagram of an x-ray diffraction pattern is shown in Figure 13. The polymer's crystalline regions seated in a well-defined manner act as a diffraction grating. As a result, the emerging diffracted pattern on the screen alternates between dark and light bands. Polymer X-ray diffraction patterns contain both sharp and defused bands. Sharp bands represent crystalline regions, while defused bands represent amorphous regions [44].

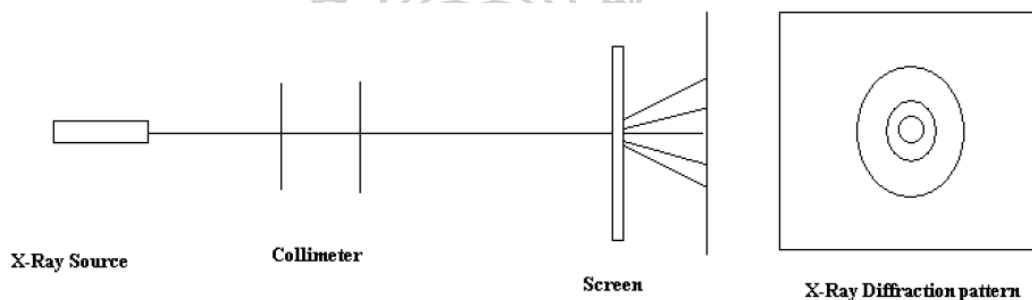


Figure 13 Schematic diagram of X-ray diffraction pattern [44].

The regular arrangement of atoms in a crystalline structure. According to our discussion, polymers contain both crystalline and amorphous phases that are randomly arranged. When an X-ray beam is passed through a polymer sample, some of the regularly arranged atoms constructively reflect the X-ray beam and produce an enhanced intense pattern. Figure 14 depicts a schematic x-ray diffraction pattern. Because the intensity of the emerging rays is greater in amorphous samples, sharp arcs are produced, whereas crystalline components scatter the incident rays. The arc length of a diffraction pattern is affected by its orientation [45].

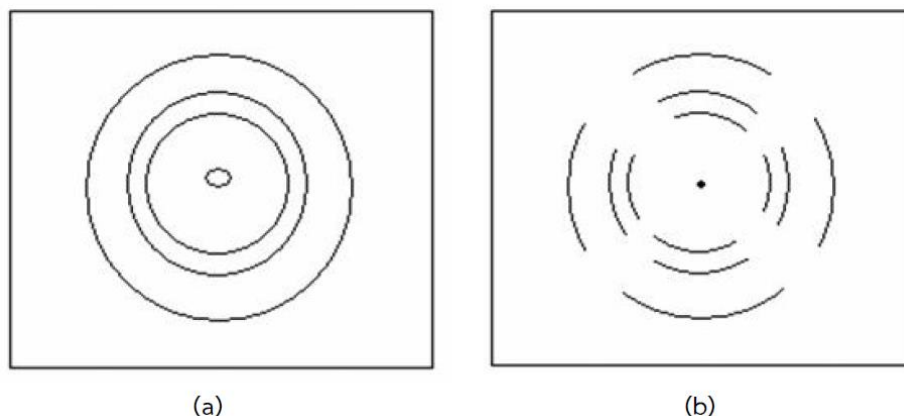


Figure 14 X-ray diffraction pattern of (a) amorphous sample and (b) Semicrystalline polymer sample [44].

The equation can be used to calculate the degree of crystallinity.

$$\% \text{Crystallinity (Xc)} = \frac{A_c}{A_c + A_a} \times 100$$

Where A_c and A_a refer to the area of the crystalline peaks and amorphous peaks, respectively.

2.14 Ultraviolet-Visible Spectroscopy (UV-vis)

The ultraviolet-visible spectroscopy is regarded as an important tool in analytical chemistry. It is one of the most common techniques used in chemical laboratories because it is used for qualitative chemical analysis and identification. Its primary application, however, is the quantitative determination of organic and inorganic compounds in solution. Spectroscopy studies the interaction of light with matter. When light is absorbed by matter, the energy content of the molecules enhances. A chemical compound's absorption of visible or ultraviolet light results in a distinct spectrum. When ultraviolet radiations are absorbed, electrons are excited from their ground state and moved to a higher energy state. According to the theory underlying this concept, the energy absorbed from ultraviolet radiation is equal to the energy difference between the ground state and the higher energy state [46].

CHAPTER 3

LITERATURE REVIEWS

3.1 Polymer Blends

PLA is a thermoplastic material that, when compared to non-biodegradable fossil-based polymers, is biodegradable and compostable. It is a bio-based material derived from renewable resources such as sugarcane or corn starch [47]. PLA is one of the most biodegradable thermoplastic materials available. Several studies examined the factors that influence the mechanism and rate of PLA degradation under different environmental conditions. Furthermore, the present authors have reviewed several properties of PLA, including rheological, thermal, and mechanical properties. As is well known, the application of PLA on wide surface products was thought to be difficult due to several factors such as strength, stickiness, and high brittleness. As a result, several authors have investigated ways to improve the properties of PLA by combining it with other polymers, particularly biopolymers or biodegradable polymers like PBS. PBS is a well-known biodegradable aliphatic co-polyester with notable properties such as melt processability and biodegradability including thermal resistance. PBS has been used to improve the ductility and melt processability of PLA [48]. According to Bhatia et al. [11], the viscosity measurements of the blends containing 10 and 20 wt %. PBS had viscosities similar to PLA, indicating that PBS blends containing less than 20 wt% showed a high degree of compatibility. For blends containing small amounts of PBS, SEM of fractured surfaces revealed a good distribution of the PBS phase in the PLA matrix. Y. Deng et al. [4] investigated the effects of blending PLA and PBS on ductility and phase inversion. With 10% wt PBS added, the result explained an increase in ductility of over 250 percent elongation-to-break.

Hassan et al. [49] reported similar behavior for PLA/PBS blends, stating that the modulus and tensile strength of the blends decreased as the PBS content increased. The addition of PBS may reduce tensile strength and modulus, but impact strength has increased approximately twofold when compared to pure PLA. This demonstrated that the PLA/PBS blends affected thermal stability due to PBS's thermal stability. As a result, the mechanical properties of PLA/PBS blends have been enhanced using a variety of modification techniques. The immiscibility of PLA and PBS in which PBS was converted into spherical inserts in the

PLA matrix The presence of large voids around spherical PBS indicated a lack of interfacial adhesion and confirmed their poor compatibility [6].

3.2 Elastomer

The incorporation of biodegradable polyesters as an additive into rubber offers a promising environmentally friendly opportunity to create rubber blends. Natural rubber (NR) is a bio-based material extracted from a natural resource in the form of latex. ENR epoxy groups would improve the polarity of rubber, promoting compatibility with PLA. There is also the possibility of chemical interactions between epoxy functional groups and reactive terminal PLA groups. Pongtanayut et al. [50] demonstrated phase-separated morphology in PLA/NR blends, with PLA/ENR having better blend compatibility, as shown in Figure 15. It was attributed to chemical bonds formed between ENR's oxirane ring and PLA's hydroxyl groups. Even though small molecules in the rubber phase and the surface of droplets could act as nucleating agents, the crystallization of blends increased with NR or ENR. W. Tissanan et al. [51] reported that they investigated properties by melt-blending with a specific modified natural rubber. Rubber that has been modified with hydrogenated and epoxide moieties has improved compatibility with PLA. The results showed the increment in elongation and impact performance. M. Zheng et al. [18] revealed the grafting of PLA chains onto the ENR network during dynamic vulcanization of a PLA/ENR blends. SEM revealed that the PLA/ENR blends was a bi-continuous structure both before and after dynamic vulcanization.

Moreover, D. Yuan et al. [19] demonstrated that the mechanical properties, specifically the tensile strength, were significantly improved. However, with a lower ENR phase, elongation decreased while hardness increased only slightly. As a result, ENR with more epoxy groups could improve interfacial compatibility with PLA, resulting in improved mechanical properties. exhibited good interfacial adhesion between PLA and ENR, which increased mechanical properties. ENR could reduce PLA's tensile strength while increasing its elongation and impact strength. The addition of ENR to PBS blends increased the material's flexibility. The morphology changed to co-continuous phase morphology at 40% ENR loading as the ENR loading increased. The degree of crystallinity of PBS in ENR/PBS blends increased as ENR content increased, while ENR content greater than 60 wt% caused crystallinity to decrease. Furthermore, biodegradability was assessed using a soil burial

test, which revealed a significant difference in weight loss, indicating the degree of degradation with different proportions [13].

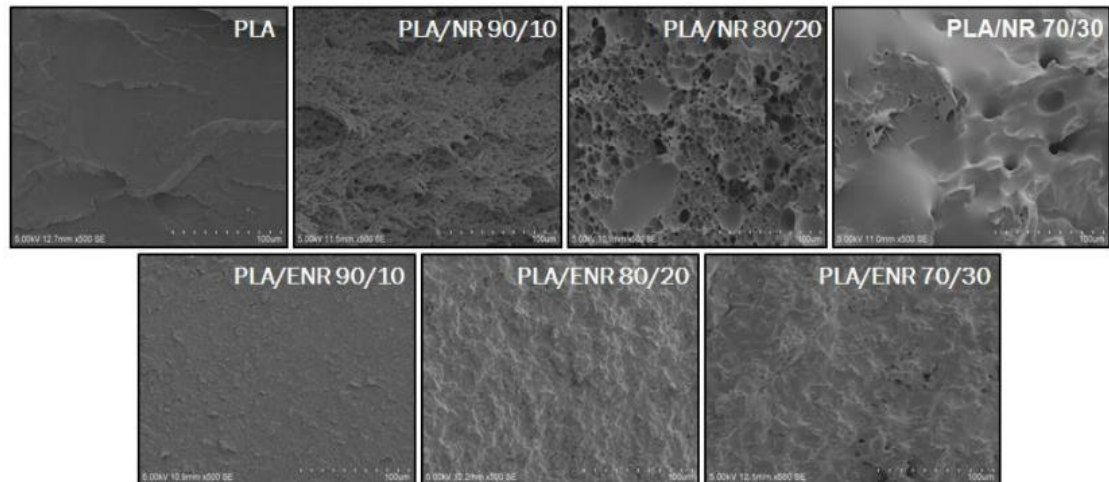


Figure 15 SEM micrographs of PLA/NR and PLA/ENR blended at various rubber contents stated in the micrograph [50].

3.3 Radical initiator

To produce polymer radicals on polymer blends, crosslinking reactions of polyesters in the presence of radical initiators have been developed. The radical combinations produce crosslinked materials with improved mechanical properties. DCP is the most commonly used radical initiator and is the most efficient due to its relatively high hydrogen abstraction efficiency and the addition of low-molecular-weight reactive chemicals to the blend during the mixing process. The mechanism by which additives improve blend compatibility is primarily related to the type of blended polymers as well as the additives themselves. Wang et al. [17] demonstrated by SEM the morphological properties that the synergistic effect of improved interfacial adhesion due to no voids caused by pull-out, indicating that the cross-linked ENR phase was well compatible with the PLA matrix. According to the results of the dynamic mechanical analysis, a small amount of DCP was consumed in the PLA phase, causing a slight branching and cross-linking of PLA molecules. Figure 16 represents a significant improvement in toughness and a scheme of possible in situ compatibilization. DCP is used to create a dynamically vulcanized PLA/NR blend with a cross-linked NR phase. At 35 wt% of NR, a continuous crosslinked network-like structure was observed, resulting in increased impact strength [52].

Ma et al. [53] demonstrated that DCP initiates branching and network structures. A reduction in domain size and an increase in interfacial adhesion improve the compatibility of the two components. The optimal amount of DCP to improve blend toughness was 0.5 wt%, after which the blend toughness decreased. The mechanical properties of polymer blends that showed improvement, particularly elongation at break and impact toughness, were increased. Srimalanon et al. [16] demonstrated that increasing the PBS content increased the toughness of PLA. PBS was added to PLA, causing it to transform from brittle to ductile. Furthermore, DCP increased elongation and toughness [26].

Mishra et al. developed 70/30 or 50/50 Polycaprolactone (PCL)/ENR blends by melt blending with DCP (0.5 and 1 phr). Biodegradable thermoplastic elastomers with higher tensile strength and elongation at break and good elastic recovery were created. Peroxide crosslinking improved the degree of crystallinity of PCL in terms of thermal properties. DCP and ENR significantly improved the compatibility of the system's phases, enhancing and playing dual roles as an effective coupling agent and impact modifier in polymer blends. DCP, as an effective free radical initiator, has recently been widely used as a reactive compatibilizer [54].

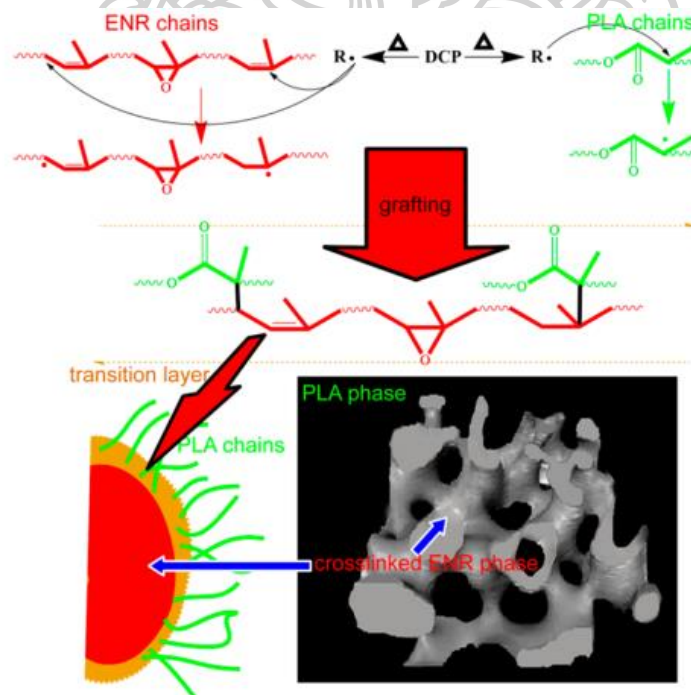
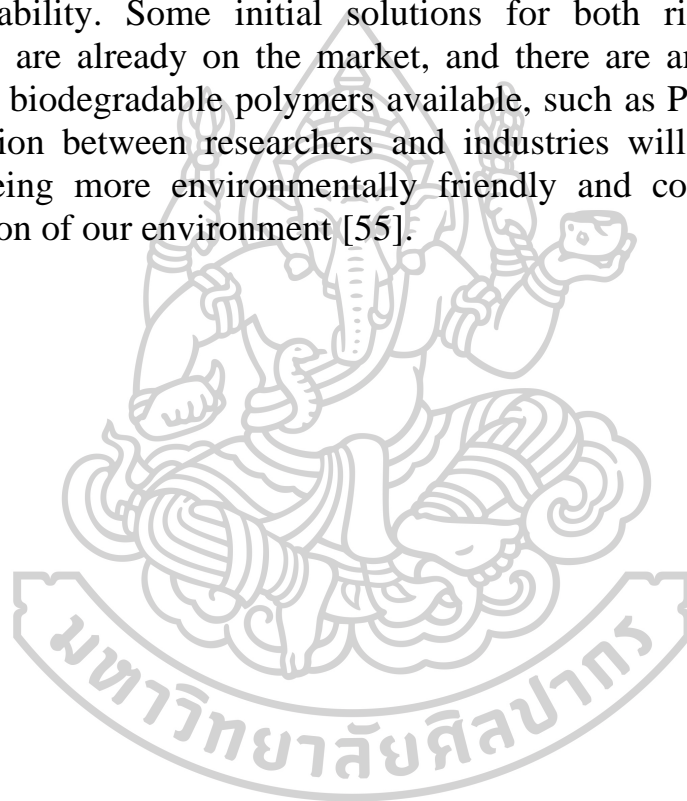


Figure 16 Scheme of possible in situ compatibilization and the transition layer at the interface between PLA and ENR phases [17].

3.4 Thermoforming

Thermoforming is an effective shaping mechanism for thermoplastic plastic film and sheets in the polymer packaging industries. One of the least used techniques for producing plastic objects is thermoforming. Nowadays, the process is expanding in the industry due to the improvement of process variables. All of this has allowed for a wide variety of plastic production [20]. P. Cinelli et al. had previously focused on modifying bio-based and biodegradable polymers to meet the demanding requirements for cosmetic preservation while retaining biodegradability. Some initial solutions for both rigid and flexible packaging are already on the market, and there are an amount of bio-based and biodegradable polymers available, such as PLA. A successful collaboration between researchers and industries will drive the sector toward being more environmentally friendly and contributing to the preservation of our environment [55].



CHAPTER 4

EXPERIMENTAL PROCEDURE

4.1 Materials

4.1.1 Poly(lactic acid) (PLA)

NatureWorks LLC, USA, produced PLA with a melt flow index of 6.0 g/10 min and a specific gravity of 1.24 g/cm³ under the trade name “Ingeo biopolymer 2003D”. The melting temperature of PLA was around 210°C.

4.1.2 Polybutylene Succinate (PBS)

In this study, PBS with a melt flow index of 5.0 g/10 min and a density of 1.26 g/cm³ was used. PBS was produced by Nature works LLC, USA.

4.1.3 Epoxidized Natural Rubber (ENR)

ENR was used to mix, type ENR-25 that was produced by Muang Mai Guthrie Public Company Limited. The percentage of epoxidation was 24.65.

4.1.4 Dicumyl Peroxide (DCP)

DCP with a specific gravity of 1.56 g/cm³, Molecular weight 270.37 g/mol, and the melting temperature was around 39-41°C. DCP was produced by Sigma-Aldrich Chemistry.

4.2 Samples Preparation

4.2.1 Preparation of Polymer Blends without DCP

4.2.1.1 PLA/PBS Blends

All polymers were dried before blending, PLA and PBS were dried in an oven at 80°C for 4 hours. PLA/PBS blend was prepared by an internal mixer at temperature and rotor speed was 180°C and 70 rpm for 15 min. PBS contents were added at 20 wt%.

4.2.1.2 PLA/ENR Blends

All polymers were dried before blending, PLA and PBS were dried in an oven at 80°C for 4 hours. PLA/ENR blend was prepared by an internal mixer at temperature and rotor speed was 180°C and 70 rpm for 15 min. ENR contents were added at 20 wt%.

4.2.1.3 PLA/PBS/ENR blends

All polymers were dried before blending, PLA and PBS were dried in an oven at 80°C for 4 hours. PLA/PBS/ENR blend was prepared by an internal mixer at temperature and rotor speed was 180°C and 70 rpm for 15 min which PBS and ENR were mixed in various contents that equal to 20 wt%.

4.2.2 Preparation of polymer blends with DCP

4.2.2.1 PLA/PBS/DCP blends

All polymers were dried before blending, PLA and PBS were dried in an oven at 80°C for 4 hours. PLA/PBS blends were prepared by an internal mixer at temperature and rotor speed was 180°C and 70 rpm for 15 min. PBS contents were added at 20 wt% and DCP contents were added at 0, 0.2, 0.3, 0.5, 1 and 2 phr.

4.2.2.2 PLA/ENR/DCP Blends

All polymers were dried before blending, PLA and PBS were dried in an oven at 80°C for 4 hours. PLA/ENR blends were prepared by an internal mixer at temperature and rotor speed is 180°C and 70 rpm for 15 min. ENR contents were added at 20 wt% and DCP contents were added at 0, 0.2, 0.3, 0.5, 1 and 2 phr.

4.2.2.3 PLA/PBS/ENR/DCP blends

All polymers were dried before blending, PLA and PBS were dried in an oven at 80°C for 4 hours. PLA/PBS/ENR blends were prepared by an internal mixer at temperature and rotor speed was 180°C and 70 rpm for 15 min which PBS and ENR were mixed in various contents that equal to 20 wt% and DCP contents were added at 0, 0.2, 0.3, 0.5, 1 and 2 phr.

4.3 Samples Preparation for Testing

All samples were prepared from an internal mixer which were dried before compressing in an oven at 100°C for 1 hour in order to get rid of the moisture for characterization.

4.3.1 Dog bone-shaped or dumbbells-shaped samples

The dumbbell-shaped samples of Universal tensile testing (UTM) were prepared by compression molding at 180°C. The specimen was prepared following ASTM standards.

4.3.2 Film shaped

The film-shaped samples of Thermogravimetric analysis (TGA), Differential scanning calorimetry (DSC), X-Ray diffraction (XRD), Fourier-transform infrared spectroscopy (FTIR), and Ultraviolet-visible spectroscopy (UV-vis) was prepared by compression molding at 180°C.

4.4 Samples Preparation for Thermoforming

The samples were prepared by thermoforming equipment in Polymer Innovation Laboratory at the Department of Chemical engineering, Silpakorn University. The sample size was 20×20 cm at a temperature of 250°C. The thickness of samples for thermoforming was about 0.3 mm.

4.5 Samples Characterizations

4.5.1 Scanning Electron Microscopy (SEM)

SEM (MIRA3, TESCAN, Czech) is used to observe the morphology and distribution of polymers. All specimens were sputter-coated with gold and were detected by scattered electrons (SE) with an accelerating voltage of 5 kV.

4.5.2 Universal Tensile Testing (UTM)

Universal tensile testing (EZ-LX model, Shimadzu, Japan) observed the mechanical properties of the polymer blends following ASTM standards. The gage length was 65 mm. Tensile testing was carried out with a crosshead speed of 50 mm/min and a preload of 0.01 N. The obtained results represented the average triplicate specimens.

4.5.3 Differential Scanning Calorimetry (DSC)

DSC (SDT Q600, TA Instruments, UK) was used to characterize the thermal properties of the polymer blends. The polymer blends were cut into small pieces weighing 10-20 mg and placed in aluminum pans. The experiment was conducted in a nitrogen atmosphere at a temperature range of 40-600°C at a heating rate of 10°C/min.

4.5.4 Thermogravimetric Analysis (TGA)

TGA (SDT Q600, TA Instruments, UK) was used to characterize the thermal degradation process of the polymer blends. The polymer blends were cut into small pieces of a mass range between 10-20 mg. The measurement was carried out in a nitrogen atmosphere at a temperature range of 40-600°C at a heating rate of 10°C/min.

4.5.5 Fourier-Transform Infrared Spectroscopy (FTIR)

FTIR (Nicolet 6700, Thermo Scientific, USA), was used to measure the surface functional groups of samples in the wavenumber range from 400 to 4000 cm⁻¹.

4.5.6 X-Ray diffraction (XRD)

XRD (D8 advance, Bruker, USA) operated at 40 kV and 30 mA with a wavelength about 0.154 nm was used to examine the diffraction pattern of samples. The samples were scanned in the 2θ range from 20 to 80° with a step size of 0.02°.

4.5.7 Ultraviolet-visible spectroscopy (UV-vis)

UV-vis spectrophotometer (Cary 5000, Varian, USA) was used to evaluate the UV absorption of the polymer blends in the wavelength range of 200-800 nm.

CHAPTER 5

RESULTS AND DISCUSSION

This research studied the effect of peroxide (DCP) on the properties of the binary blends (PLA/PBS and PLA/ENR) and ternary blends (PLA/PBS/ENR) with various proportions. This chapter showed the characterization of polymer blends that are divided into three sections. The first section is the characterization of PLA/PBS and PLA/ENR blends with DCP. The second section is the characterization of PLA/PBS/ENR blends with DCP which is the main section of this research. For final section is the samples of polymer blends from thermoforming.

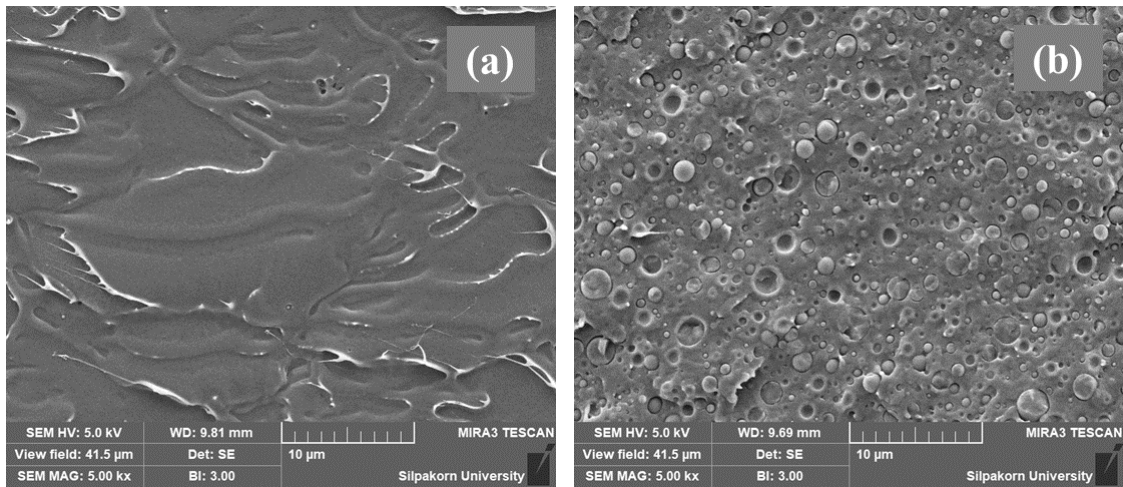
5.1 Binary Blends of PLA/PBS and PLA/ENR without and with DCP

5.1.1 Morphology analysis

SEM micrographs of the tensile fracture surface of polymer blends were examined by SEM to study the phase morphology of PLA, PLA/PBS, and PLA/ENR blends without DCP are presented in Figure 17. The fracture surface of PLA was quite smooth which indicated the brittle properties of PLA as shown in Figure 17(a). Figure 17(b-c) showed phase separation of PLA/PBS and PLA/ENR blends due to weak interaction between PBS and ENR phases. From Figure 17(b), the PBS phase was dispersed as a spherical domain in the PLA matrix, and the observation of voids surrounding the spherical PBS phase confirmed the weak interfacial adhesion between the PBS and PLA phases. As can be seen in Figure 17(c), all of the PLA/ENR blends showed similar phase separation, with the rubber dispersed as small droplets in the PLA matrix. The phase morphology revealed weak interfacial adhesion, as evidenced by the presence of empty spherical grooves on the surface of the PLA and ENR phases [56]. However, after PBS and ENR adding, the results illustrated that the compatibility of blends did not improve and also affected the mechanical properties. Therefore, adding DCP into the previous blending to improve the interfacial adhesion and compatibility that the results showed SEM micrograph of PLA/PBS and PLA/ENR with various DCP as shown in Figures 18 and 19. Figure 18 (b-f) shows PLA/PBS blends with various DCP, at 0.2-2 phr, that were partially compatible with each

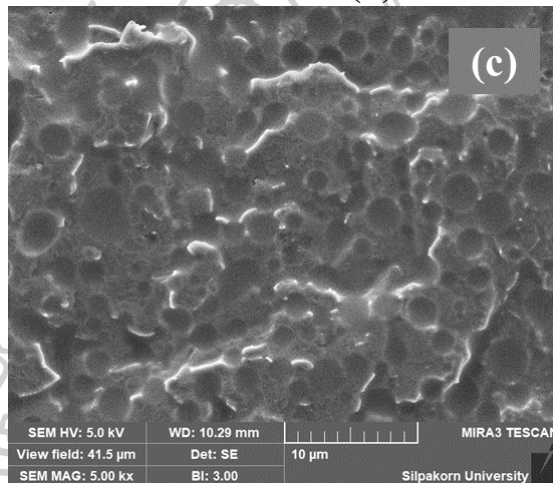
other due to effective DCP loading could increase the compatibility of the above phases. The observation of voids surrounding spherical PBS phase decreased that was smaller than PLA/PBS blends and could improve the interaction between PLA and PBS when DCP was added from 0.3-2 phr, some small granules dispersed throughout the matrix, referring to some crosslinked structures formed after the addition of DCP [7]. These reasons could improve the mechanical properties, especially the strain at break. Figure 19(b-f) shows PLA/ENR blends with various DCP, the morphology of these blends showed the better compatibility between PLA and ENR phases with DCP loading. After DCP loading, the spherical ENR phase was smaller than in previous blends and the ENR phase decreased after DCP was added from 0.3-2 phr. However, the observation still showed the empty spherical grooves of the ENR phase [50]. The partial compatibility between PLA and ENR phase was responsible for coarse surface as shown in Figure 19(e-f). It has previously been stated that chemical interaction between the oxirane ring on ENR and the hydroxyl group in PLA and DCP occurred, which can be attributed to their compatibility. Despite improved compatibility in both systems, the results of interaction improvement and mechanical properties of PLA/PBS blends with DCP are better than PLA/ENR blends.





(a) PLA

(b) PLA/PBS (80/20) blends



(c) PLA/ENR (80/20) blends

Figure 17 SEM micrograph of binary blends without DCP; (a) PLA, (b) PLA/PBS (80/20) blends and (c) PLA/ENR (80/20) blends.

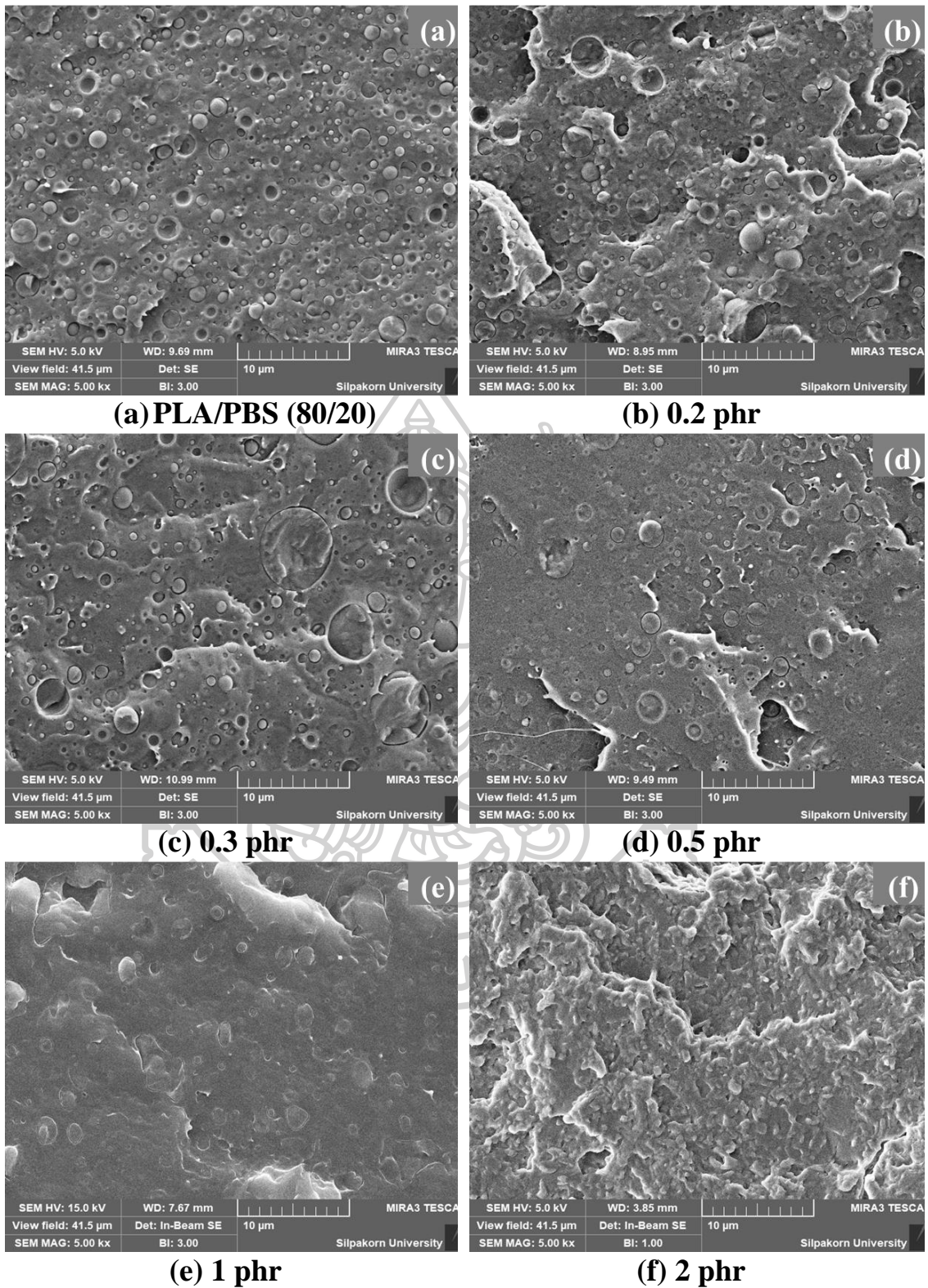


Figure 18 SEM micrograph of (a) PLA/PBS (80/20) blends and PLA/PBS (80/20) blends with various DCP contents; (b) 0.2 phr, (c) 0.3 phr, (d) 0.5 phr, (e) 1 phr and (f) 2 phr.

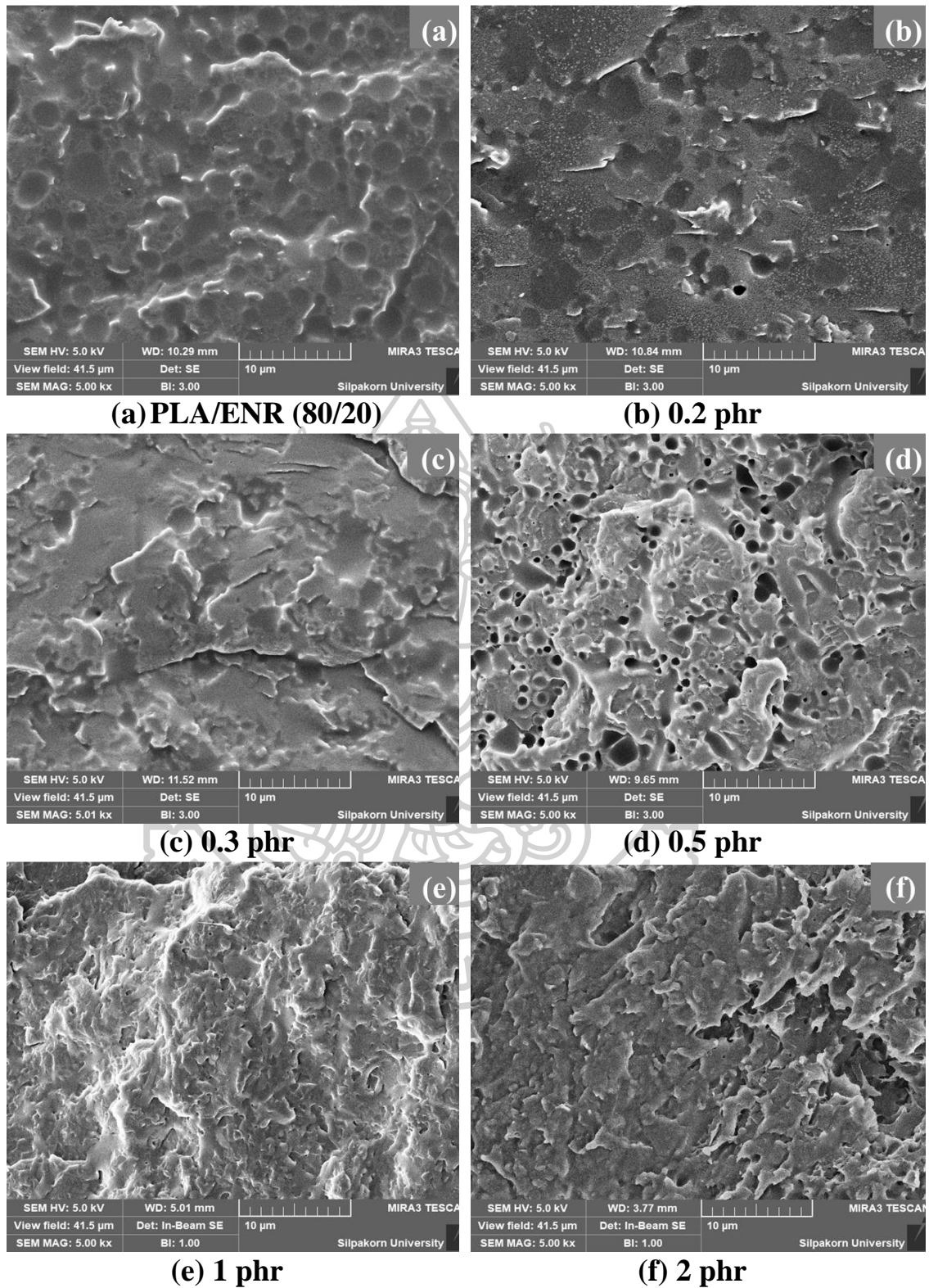


Figure 19 SEM micrograph of (a) PLA/ENR (80/20) blends and PLA/ENR (80/20) blends with various DCP contents; (b) 0.2 phr, (c) 0.3 phr, (d) 0.5 phr, (e) 1 phr and (f) 2 phr.

5.1.2 FTIR analysis

The FTIR was used to obtain information on the surface chemistry of PLA/PBS and PLA/ENR blends with DCP according to the changes in the vibration modes and the band position between 400-4000 cm^{-1} . The FTIR spectra of pure polymers are shown in Figure 20.

Figures 21-22, at around 3000-3600 cm^{-1} could be attributed to the -OH groups of aromatic and aliphatic, which showed the different intensity of this peak depending on the different ratios of materials. Moreover, the decrement of intensities occurred due to the effective formation of DCP in the system [56]. However, PLA and polymer blends around 2900 cm^{-1} are attributed to C-H stretching from the CH_2 group. Furthermore, the C=O stretching vibration peak at around 1750 cm^{-1} , which is attributed to carbonyl groups in the PLA, but the peak of PBS was lower than PLA. As shown in Figure 21, chain modification in PBS chains is confirmed by the presence of a doublet attributed to the C=O group at around 1710 cm^{-1} and a band at 917 cm^{-1} attributed to C-OH bending in the carboxylic group. The spectra revealed that the peak of the PLA/PBS blends, C=O and CH_2 in the presence of DCP shifted to a lower wavenumber in the blends as the DCP contents increased. These may suggest the interaction between PLA and PBS in the presence of DCP existed upon blending [57, 58]. However, a low degree of possible crosslinking interaction was difficult to be detected by FTIR due to peaks overlapping.

FTIR spectra of ENR, the three peaks at around 2900 cm^{-1} are attributed to CH_2 stretching. The peaks at around 1400 cm^{-1} are assigned to CH_3 stretching and around 870 cm^{-1} are assigned to vibration peaks of the epoxy ring [59]. There were no changes in the carbonyl group (C=O) of PLA, implying that no interactions between PLA and ENR occurred in the presence of DCP. The FTIR spectra of blends with DCP showed no difference. Because there were no changes, it confirmed that the blends of PLA and ENR are not miscible.

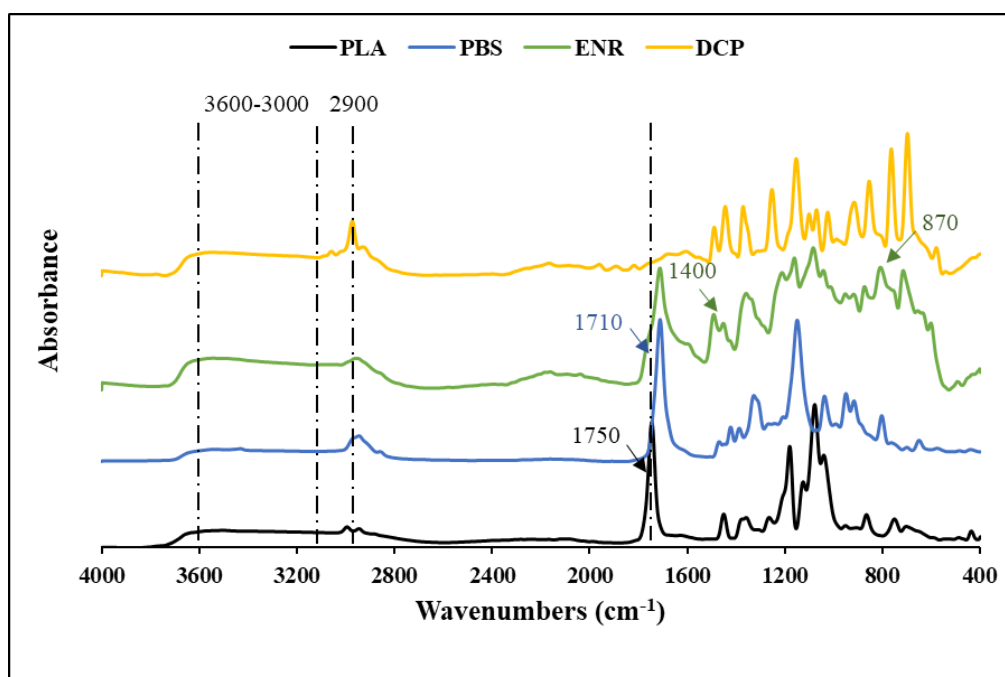


Figure 20 FTIR spectra of PLA, PBS, ENR and DCP.

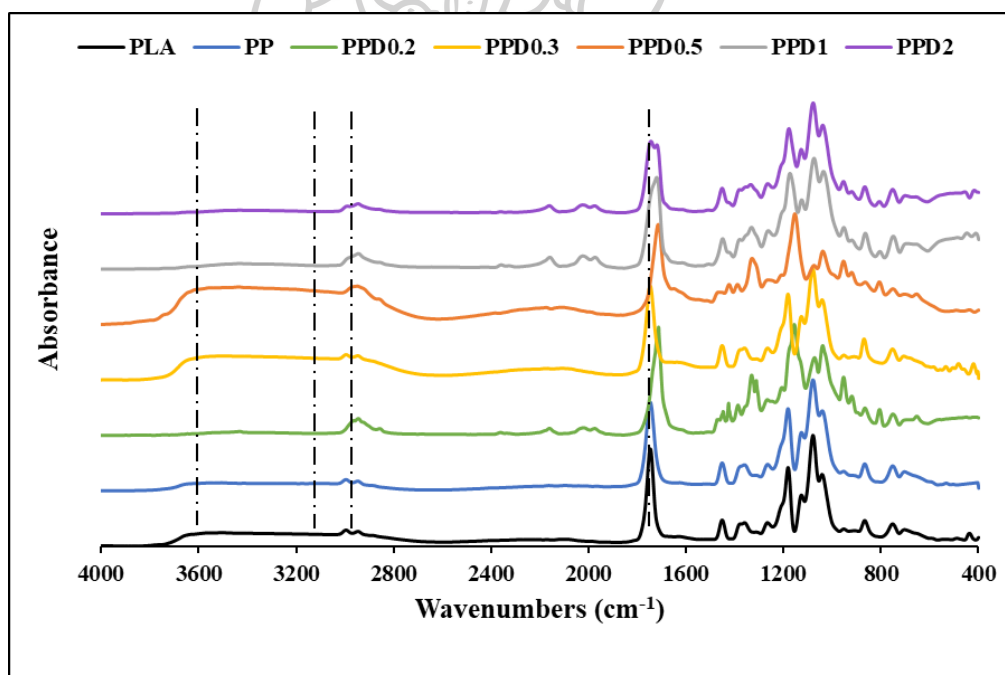


Figure 21 FTIR spectra of PLA/PBS (80/20) blends with various DCP contents.

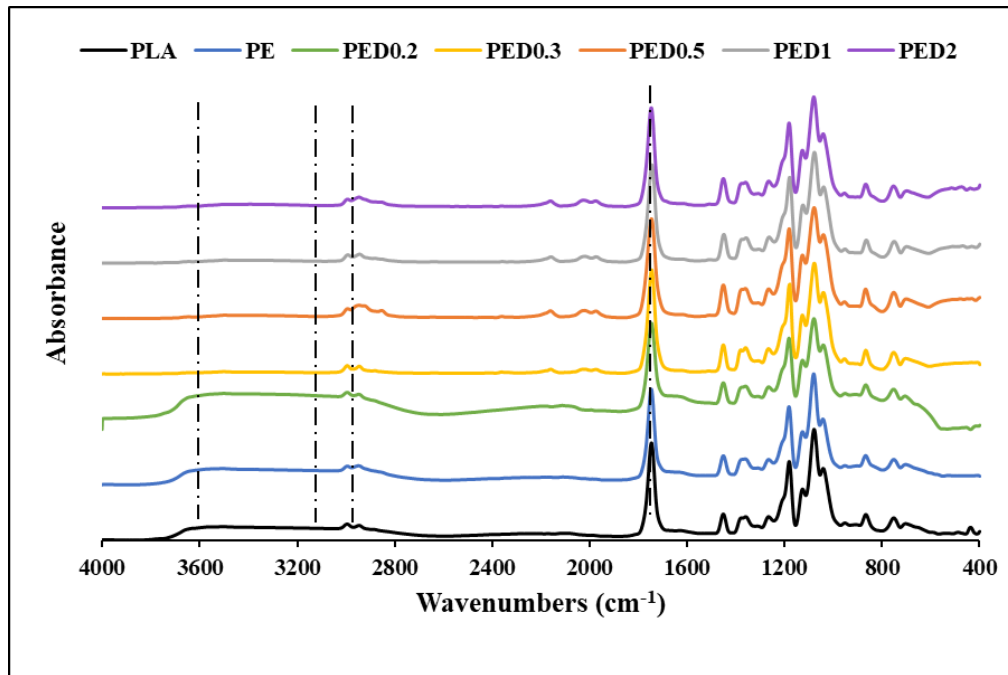


Figure 22 FTIR spectra of PLA/ENR (80/20) blends with various DCP contents.

5.1.3 Mechanical properties

(1) Young's modulus

The Young's modulus of PLA, PLA/PBS, and PLA/ENR blends with various DCP is shown in Figure 23 and Table 2. The results showed that Young's modulus of PLA/PBS and PLA/ENR blends with various DCP decreased when compared to PLA. While the amount of DCP is introduced in these blends, indicating that its fracture changed from brittle to ductile. DCP could improve the miscibility that affected Young's modulus of blends decreased. As PLA/ENR blends with DCP from 0.5-2 phr showed that Young's modulus slightly increased, indicating that amount of DCP could improve Young's modulus in PLA/ENR blends.

(2) Tensile strength

The tensile strength of PLA, PLA/PBS, and PLA/ENR blends with various DCP is shown in Figure 24 and Table 2, showing that the tensile strength of PLA/PBS and PLA/ENR blends with various DCP slightly decreased. While the amount of DCP is introduced in these systems, indicating that DCP loading could change the tensile strength decreased.

Moreover, the slightly increased tensile strength of PLA/ENR blends with DCP, indicating DCP could improve the tensile strength when compared to the PLA/ENR blends without DCP.

(3) Stress at break

The stress at break of PLA, PLA/PBS, and PLA/ENR blends with various DCP is shown in Figure 25 and Table 3. The results showed that the stress at break of PLA/PBS blends with various DCP did not change when compared with PLA/PBS blends without DCP. While the stress at break of PLA/ENR blends with DCP increased when DCP is added more than 0.5 phr, indicating that these blends needed lots of force to break because of their rigid and strength. However, these blends slightly increased due to the empty spherical grooves in polymer, corresponding with the results of morphology analysis is shown in Figure 19.

(4) Strain at break

The strain at break of PLA, PLA/PBS, and PLA/ENR blends with various DCP is shown in Figure 26 and Table 3, showed that the strain at break of PLA/PBS blends with DCP from 0.3-2 phr increased when compared with PLA and PLA/ENR blends. It clearly increased when added DCP 0.3 phr, which is the highest the percent strain at break. From these results, it can be pointed out that the incorporation of PBS and DCP could improve percent strain at break and toughen PLA and PLA to be more flexible. As, the strain at break of PLA/ENR blends with various DCP still decreased when added lower DCP contents but the percent strain at break increased when DCP is added more than 0.3 phr. The results indicated that the amount of DCP could contribute to improving the flexibility of PLA blends if it is added in the proper amount. [6, 7, 15, 50].

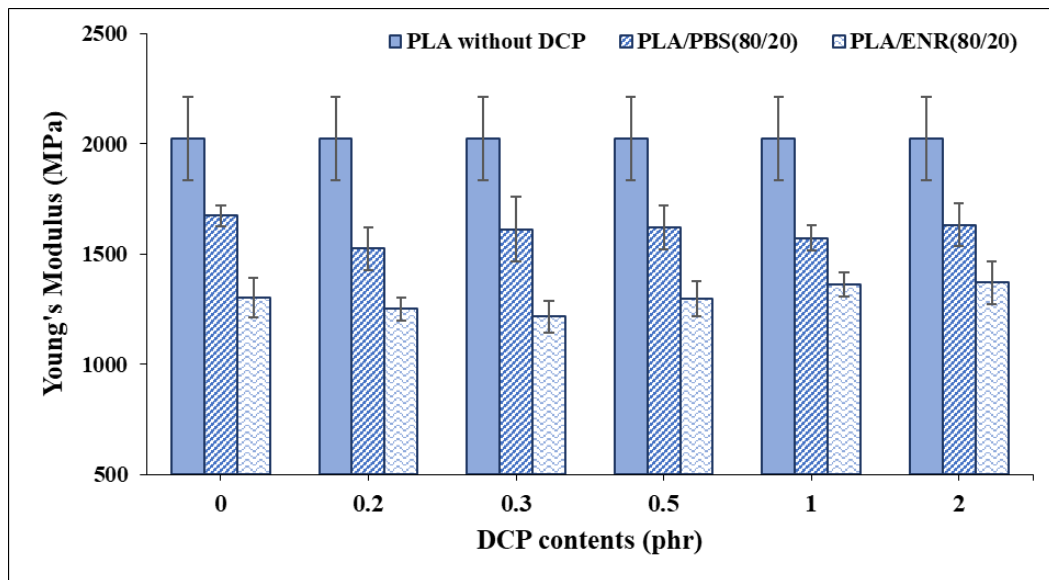


Figure 23 Young's modulus of PLA, PLA/PBS (80/20) blends and PLA/ENR (80/20) blends with various DCP contents.

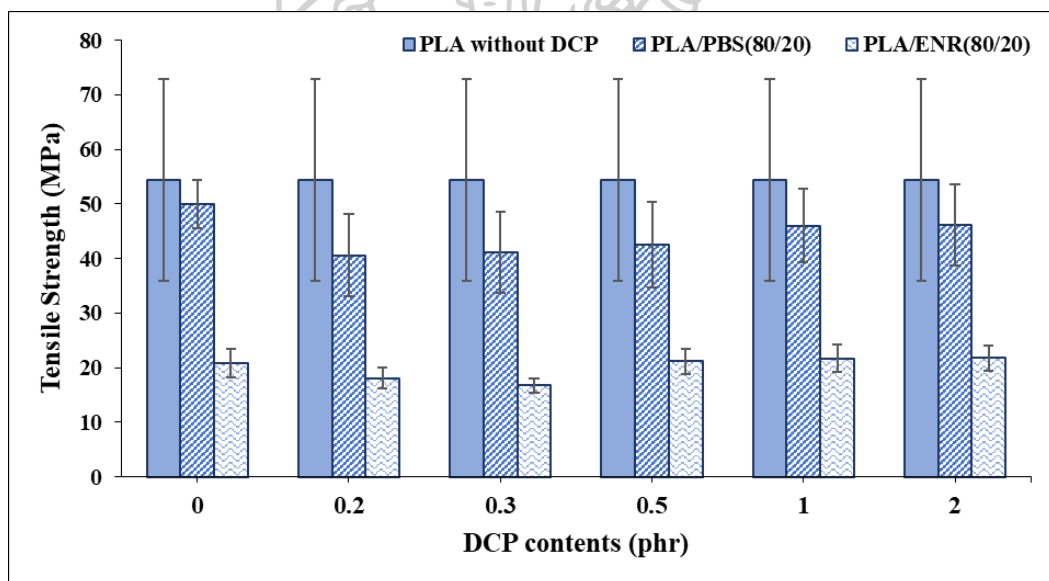


Figure 24 Tensile strength of PLA, PLA/PBS (80/20) blends and PLA/ENR (80/20) blends with various DCP contents.

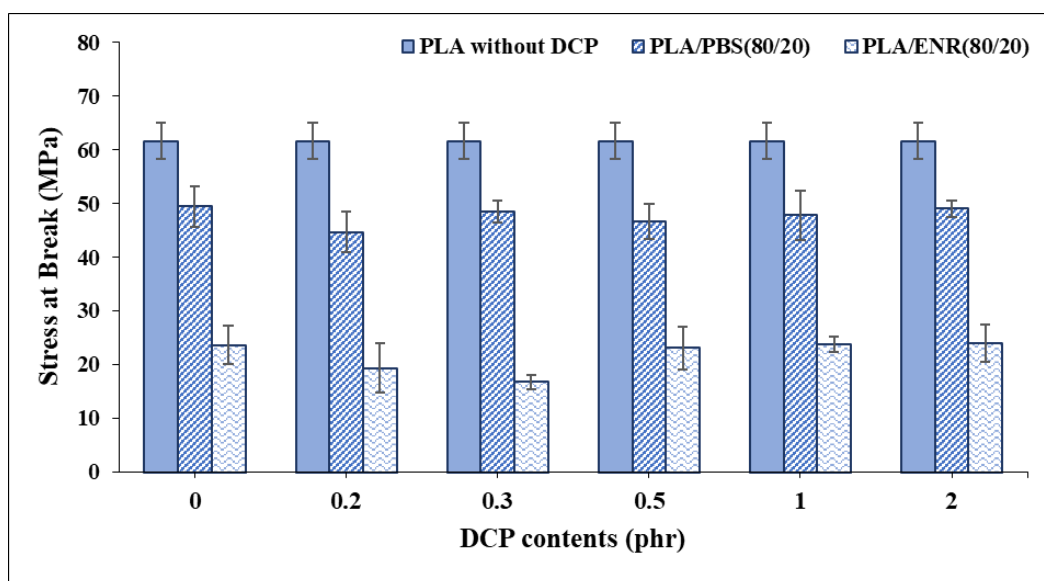


Figure 25 Stress at break of PLA, PLA/PBS (80/20) blends and PLA/ENR (80/20) blends with various DCP contents.

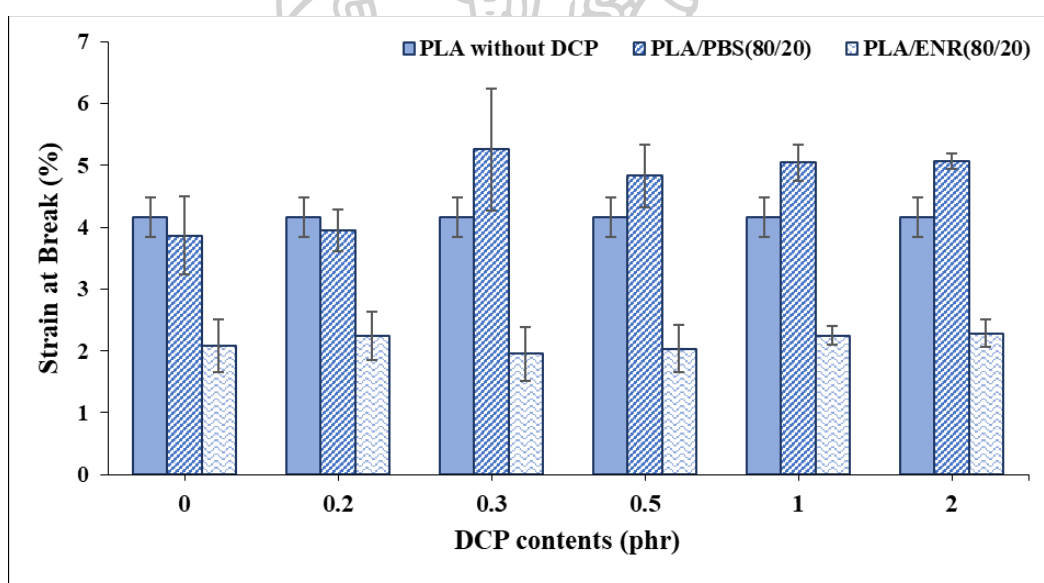


Figure 26 Strain at break of PLA, PLA/PBS (80/20) blends and PLA/ENR (80/20) blends with various DCP contents.

Table 2 Young's modulus and tensile strength of PLA/PBS and PLA/ENR blends with various DCP contents.

Samples	Codes	Young's Modulus (MPa)	Tensile Strength (MPa)
PLA	PLA	2024.37±189.92	54.41±18.50
PLA/PBS 80/20	PP	1673.42±46.02	49.94±4.38
PLA/ENR 80/20	PE	1301.94±90.07	20.88±2.60
PLA/PBS 80/20-0.2DCP	PPD0.2	1524.52±97.53	40.63±7.48
PLA/ENR 80/20-0.2DCP	PED0.2	1251.71±52.30	18.11±1.93
PLA/PBS 80/20-0.3DCP	PPD0.3	1612.11±147.66	41.19±15.46
PLA/ENR 80/20-0.3DCP	PED0.3	1215.15±71.94	16.76±1.29
PLA/PBS 80/20-0.5DCP	PPD0.5	1620.98±98.17	42.56±7.39
PLA/ENR 80/20-0.5DCP	PED0.5	1298.50±79.65	21.20±2.32
PLA/PBS 80/20-1DCP	PPD1	1572.76±55.88	46.05±7.76
PLA/ENR 80/20-1DCP	PED1	1363.73±54.62	21.70±2.46
PLA/PBS 80/20-2DCP	PPD2	1632.62±95.83	46.18±6.71
PLA/ENR 80/20-2DCP	PED2	1369.85±96.05	21.81±2.33

Table 3 Stress at break and strain at break of PLA/PBS and PLA/ENR blends with various DCP contents.

Samples	Codes	Stress at Break (MPa)	Strain at Break (%)
PLA	PLA	61.62±3.36	4.16±0.32
PLA/PBS 80/20	PP	49.45±3.78	3.86±0.63
PLA/ENR 80/20	PE	23.62±3.60	2.08±0.42
PLA/PBS 80/20-0.2DCP	PPD0.2	44.71±3.82	3.95±0.34
PLA/ENR 80/20-0.2DCP	PED0.2	19.35±4.46	2.24±0.39
PLA/PBS 80/20-0.3DCP	PPD0.3	48.45±2.02	5.26±0.99
PLA/ENR 80/20-0.3DCP	PED0.3	16.76±1.29	1.95±0.43
PLA/PBS 80/20-0.5DCP	PPD0.5	46.65±3.19	4.83±0.51
PLA/ENR 80/20-0.5DCP	PED0.5	23.10±4.01	2.04±0.38
PLA/PBS 80/20-1DCP	PPD1	47.79±4.65	5.04±0.29
PLA/ENR 80/20-1DCP	PED1	23.77±1.36	2.24±0.15
PLA/PBS 80/20-2DCP	PPD2	49.05±1.49	5.07±0.13
PLA/ENR 80/20-2DCP	PED2	23.93±3.50	2.28±0.22

5.1.4 Thermal Properties

5.1.4.1 DSC analysis

The melting point temperature (T_m) of PLA, PLA/PBS, and PLA/ENR blends with various DCP is shown in Figures 27-28 and Table 4. The incorporation of DCP significantly changed the thermal behavior of the blends. The results from Figure 27, showed the melting point temperature in PLA/PBS blends with DCP did not change but in these blends with more than 0.5 phr of DCP, it slightly decreased. The PLA/PBS blends with various DCP are slightly shifted to a lower temperature after adding DCP, at DCP 1-2 phr, compared to PLA/PBS blends. This phenomenon indicated that DCP accelerated the melting point temperature of PLA/PBS blends. The cold crystallization peak of PLA blends around 120° C was gradually weakened when DCP was incorporated, illustrating that the crystallinity of PLA in blends is slower and harder to form. As shown in Table 5, the incorporation of DCP increased the crystallization ability of the PLA phase when the DCP content was greater than 0.3 phr.

In case of the PLA/ENR blends with various DCP showed that the melting point temperature is similar to PLA/ENR blends which are shown in Figure 28. The cold crystallization peak of PLA blends around 120°C was slightly weakened when DCP was incorporated in blends without DCP and 0.2 phr of DCP. This indicated that the addition of ENR affected the crystallinity of PLA in blends due to the short chains of PLA and disturbance in crystallization from molecules of ENR. And then, DCP was incorporated above 0.2 phr, affecting the cold crystallization peak increased. This indicated that the crystallinity of PLA in PLA/ENR blends with incorporated DCP was easier to form than in PLA/PBS blends.

The crystallinity (X_c) of PLA/PBS and PLA/ENR blends with various DCP is shown in Table 5, which was calculated from the melting enthalpy. As the melting enthalpy value for 100 % crystalline (93.6 J/g for PLA) [60]. From these results, the PLA/PBS blends with DCP had lower crystallinity than that of PLA. It could be considered that PBS is more efficient in assisting the crystallization of the PLA phase [8]. From these results, with the addition of DCP in the PLA/PBS blends, X_c is slightly decreased. It is found that the X_c was further reduced on the incorporation of DCP when DCP was incorporated above 0.3 phr. In the PLA/ENR

blends, X_c was further increased on the incorporation of DCP, especially at higher loading from 0.3-2 phr.

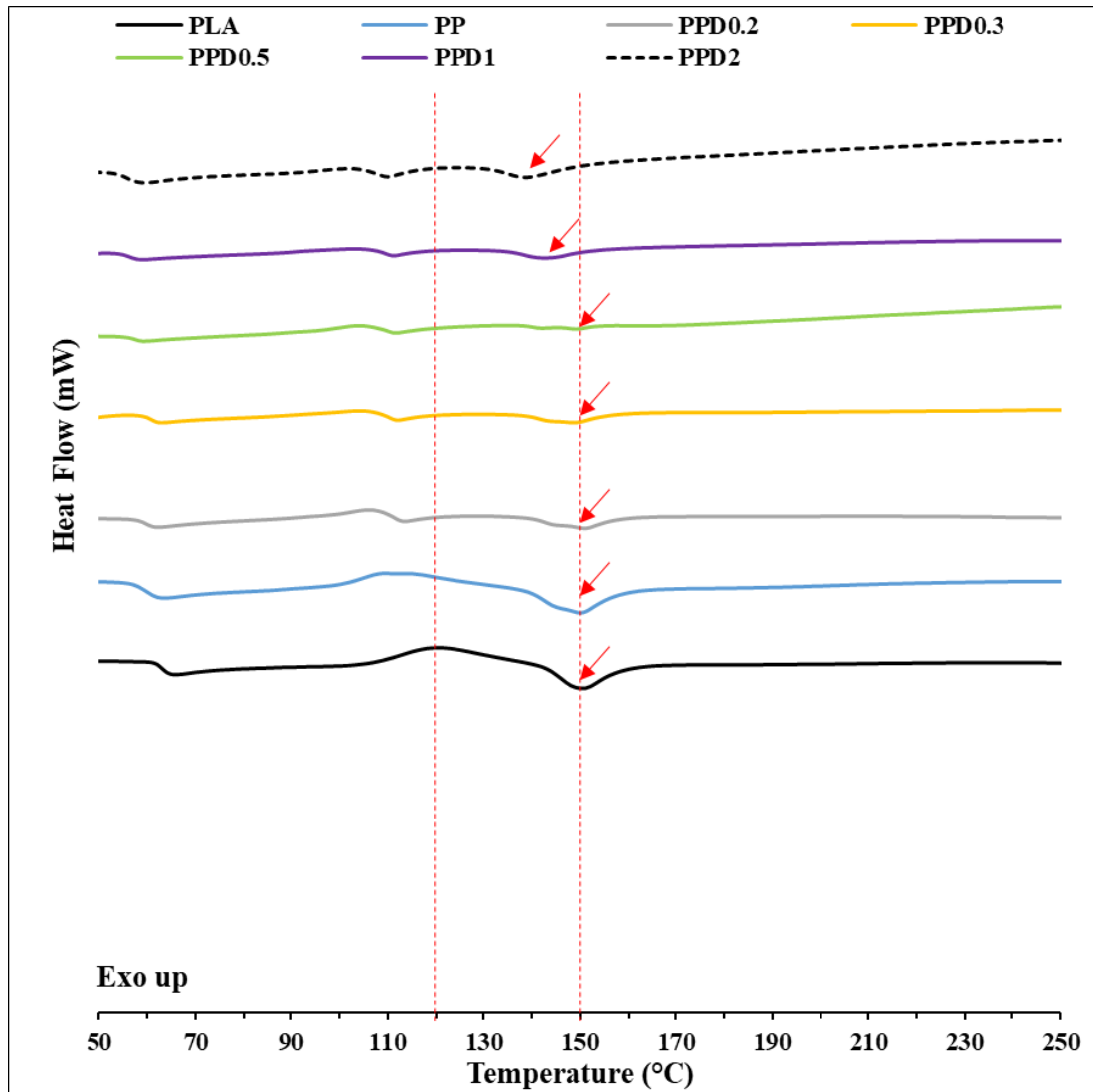


Figure 27 DSC of PLA and PLA/PBS blends with various DCP contents.

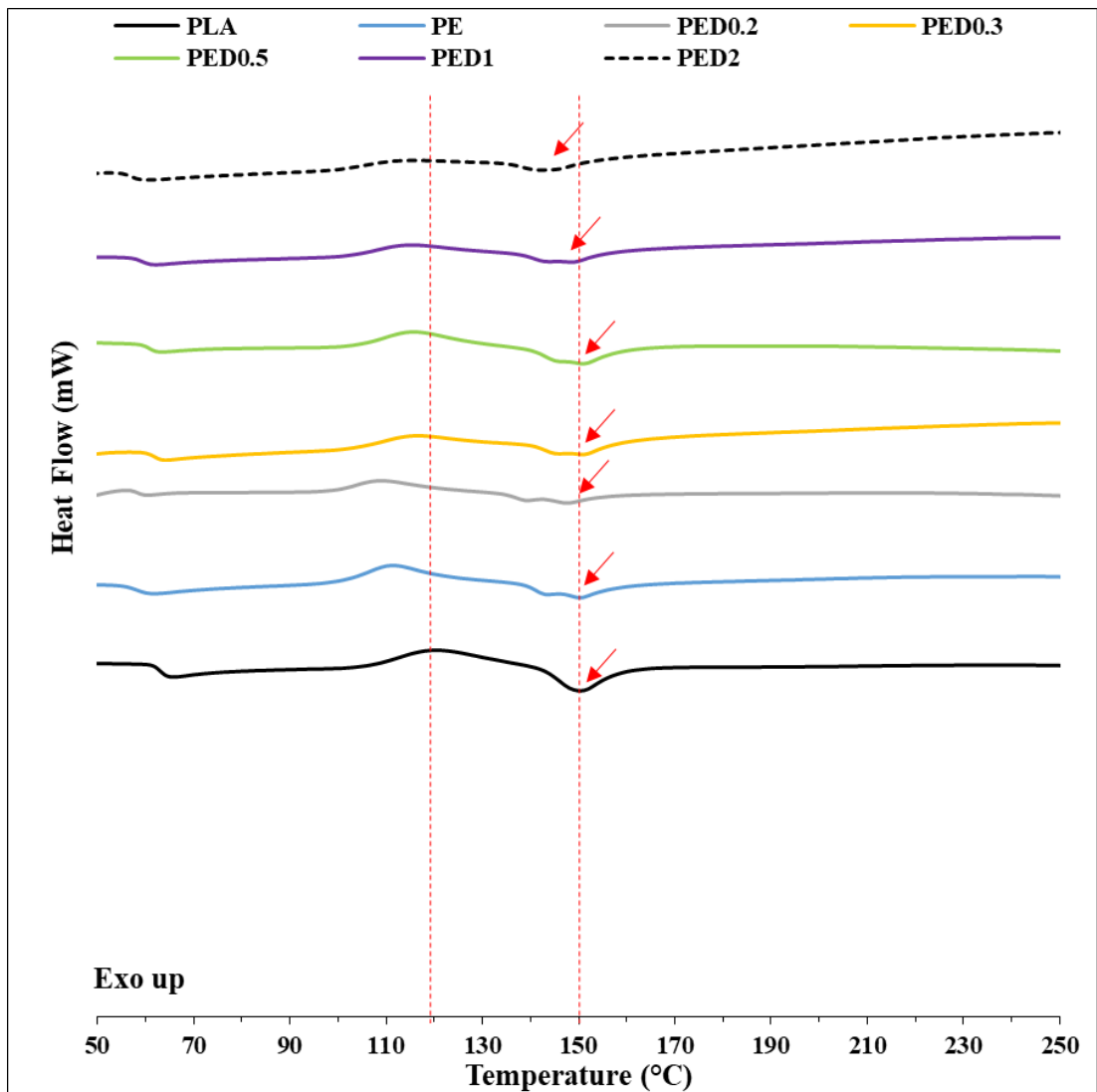


Figure 28 DSC of PLA and PLA/ENR blends with various DCP contents.

Table 4 Melting point temperature of PLA/PBS and PLA/ENR blends with various DCP contents.

Samples	Codes	Melting point temperature (°C)
PLA	PLA	149
PLA/PBS 80/20	PP	150
PLA/PBS 80/20-0.2DCP	PPD0.2	151
PLA/PBS 80/20-0.3DCP	PPD0.3	149
PLA/PBS 80/20-0.5DCP	PPD0.5	149
PLA/PBS 80/20-1DCP	PPD1	144
PLA/PBS 80/20-2DCP	PPD2	140
PLA/ENR 80/20	PE	150
PLA/ENR 80/20-0.2DCP	PED0.2	149
PLA/ENR 80/20-0.3DCP	PED0.3	151
PLA/ENR 80/20-0.5DCP	PED0.5	146
PLA/ENR 80/20-1DCP	PED1	148
PLA/ENR 80/20-2DCP	PED2	145

Table 5 Crystallinity of PLA/PBS and PLA/ENR blends with various DCP contents.

Samples	Codes	Crystallinity (%)
PLA	PLA	41.5
PLA/PBS 80/20	PP	37.4
PLA/PBS 80/20-0.2DCP	PPD0.2	18.1
PLA/PBS 80/20-0.3DCP	PPD0.3	18.3
PLA/PBS 80/20-0.5DCP	PPD0.5	22.1
PLA/PBS 80/20-1DCP	PPD1	21.5
PLA/PBS 80/20-2DCP	PPD2	26.4
PLA/ENR 80/20	PE	45.3
PLA/ENR 80/20-0.2DCP	PED0.2	7.9
PLA/ENR 80/20-0.3DCP	PED0.3	61.5
PLA/ENR 80/20-0.5DCP	PED0.5	54.0
PLA/ENR 80/20-1DCP	PED1	18.7
PLA/ENR 80/20-2DCP	PED2	37.7

5.1.4.2 TGA analysis

Figures 29 and 30 show the thermal degradation of PLA/PBS blends and PLA/ENR blends with various DCP contents, respectively. The decomposition temperature of 5, 10, and 50% weight loss (T_{d5} , T_{d10} , and T_{d50}) of each system is shown in Table 6. These results showed the decomposition temperature at 10% weight loss was 330°C and the PLA/PBS blend with DCP has shifted lower the decomposition temperatures than that of PLA. It could notice the increasing decomposition temperature of 50% weight loss of the PLA/PBS blends with DCP loading. Especially, at T_{d50} of PLA/PBS blends with more than 0.2 phr of DCP was about 5°C higher than PLA. The PLA/PBS blends with 0.3 phr of DCP was the highest thermal stability. In the case of the PLA/ENR blends with various DCP, it was clearly shifted lower the decomposition temperatures than PLA. This indicated that the incorporation of DCP affected the degradation of PLA blends and these blends had thermal stability lower than that of PLA [18, 50].

Furthermore, the degradation of PLA has proceeded in one step, as well as the degradation of PLA/PBS and PLA/ENR blends were two steps. The first step started between 270-380°C, presumably due to the main thermal degradation of PLA. In the second step, the degradation of PBS appeared at around temperature 370-400°C which is shown in Figure 29 and the degradation of ENR appeared at around temperature 350-450°C which is shown in Figure 30. From the result, the amount of DCP loading was incorporated in PLA/ENR blends, indicating that the thermal stability had better than in PLA/PBS blends.

Table 6 Decomposition temperature of PLA/PBS and PLA/ENR blends with various DCP contents.

Samples	Codes	Td5	Td10	Td50
PLA	PLA	319	330	356
PLA/PBS 80/20	PP	319	331	359
PLA/PBS 80/20-0.2DCP	PPD0.2	298	313	352
PLA/PBS 80/20-0.3DCP	PPD0.3	321	334	361
PLA/PBS 80/20-0.5DCP	PPD0.5	308	325	359
PLA/PBS 80/20-1DCP	PPD1	305	320	356
PLA/PBS 80/20-2DCP	PPD2	312	326	359
PLA/ENR 80/20	PE	272	290	329
PLA/ENR 80/20-0.2DCP	PED0.2	258	278	325
PLA/ENR 80/20-0.3DCP	PED0.3	273	291	329
PLA/ENR 80/20-0.5DCP	PED0.5	275	293	329
PLA/ENR 80/20-1DCP	PED1	269	290	330
PLA/ENR 80/20-2DCP	PED2	271	293	331



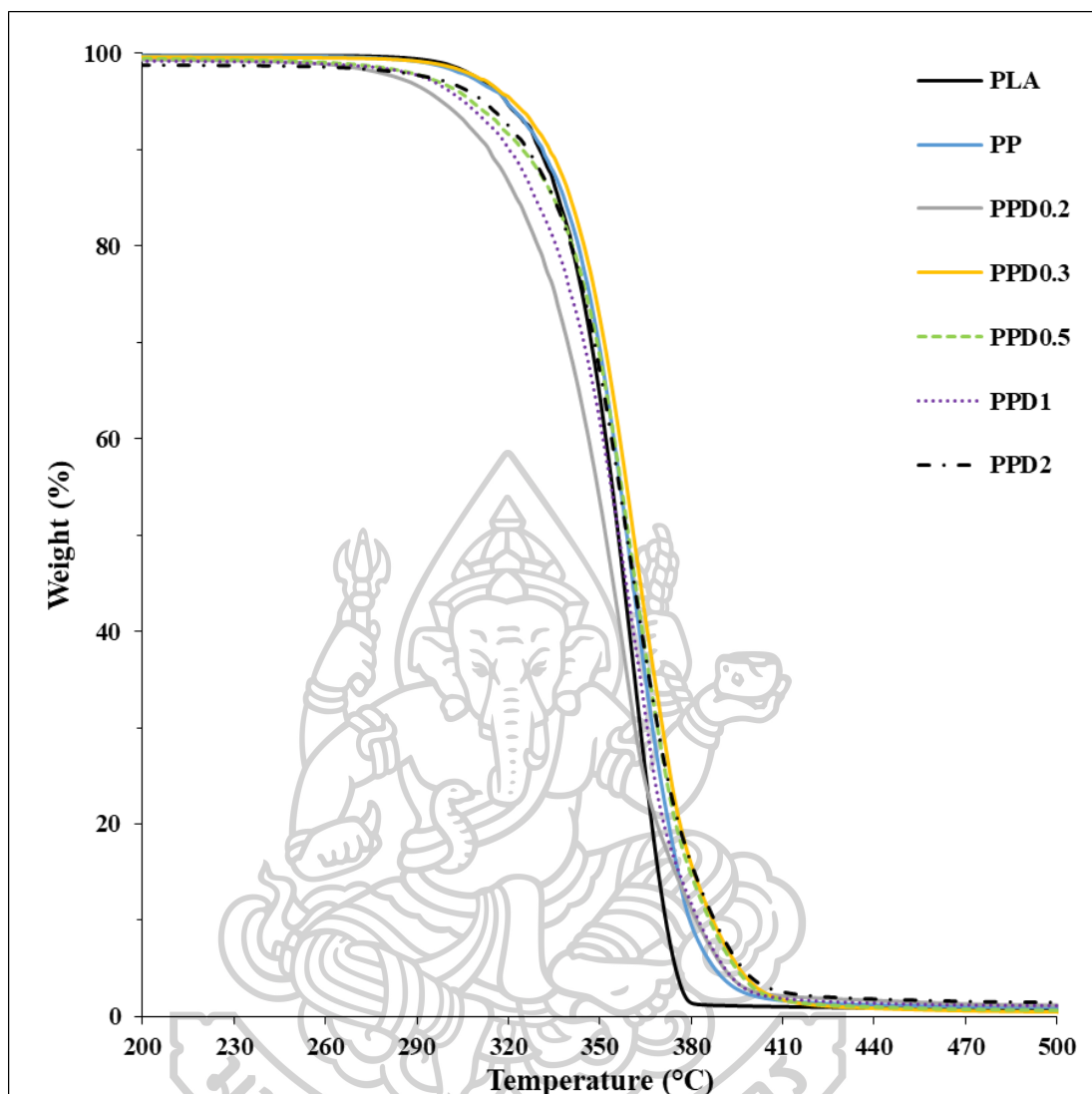


Figure 29 TGA of PLA and PLA/PBS blends with various DCP contents.

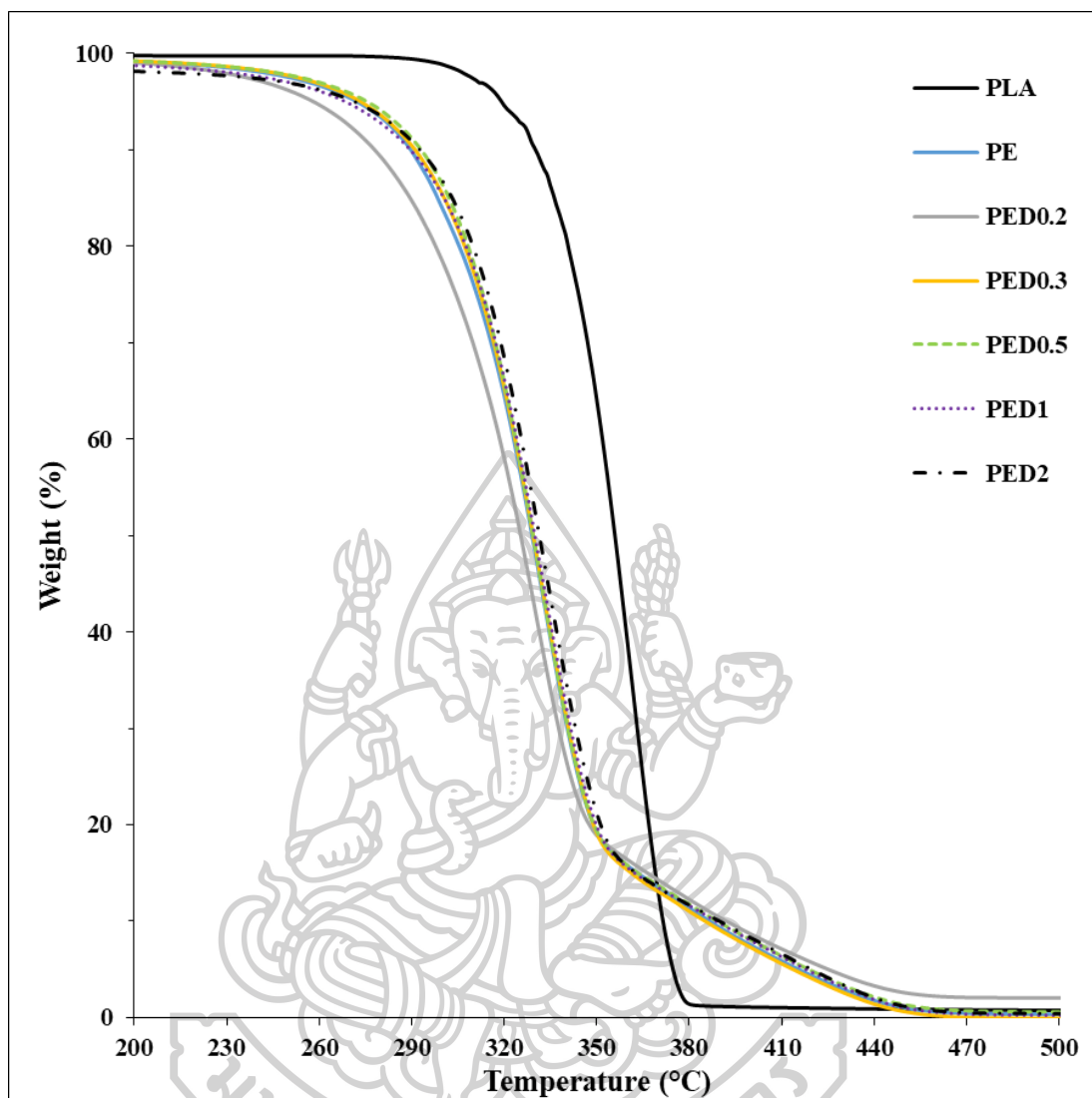


Figure 30 TGA of PLA and PLA/ENR blends with various DCP contents.

5.1.5 XRD analysis

The XRD analysis was used to gain a better understanding of the crystallinity of the material. Figure 31 represents the XRD patterns of PLA, PBS, and ENR. Similar XRD patterns were observed in the studies of Zhou et al. [61]. A wide diffraction peak at $2\theta = 16^\circ$ was observed for PLA, indicating that the processing condition was totally amorphous or the number of crystalline was too low to be traced, but the patterns of PBS shows the peak at $2\theta = 19.5^\circ, 22^\circ, 22.5^\circ$ and 28.5° due to its crystalline of PBS [15, 62]. XRD patterns of amorphous ENR were observed at $2\theta = 18^\circ - 30^\circ$.

Additionally, XRD could be determined the degree of crystallinity of the blends which can be calculated according to the equation.

$$\% \text{Crystallinity (Xc)} = \frac{A_c}{A_c + A_a} \times 100$$

Where A_c and A_a refer to the area of the crystalline peaks and amorphous peaks, respectively.

The normalized area of peaks is shown in Table 7. The results showed that DCP acted as a crosslinker for PLA/PBS blends. The crystallinity slightly increased due to the crystalline of PBS that appeared as peaks of crystalline in the XRD patterns. This indicated that the amount of DCP could affect both crystalline and amorphous blends, observing from are in Table 7. This agreed with the DCS results, which showed the melting temperature of PLA blends slightly decreased. A high amount of DCP and PBS was incorporated, and the sharp and narrow peaks increased as shown in Figure 32. XRD patterns of the PLA/ENR blends with DCP are shown in Figure 33. These showed peaks amorphous which did not appear as the peaks crystalline in the blends. These indicated that it added only PLA and ENR for blending [58, 63].

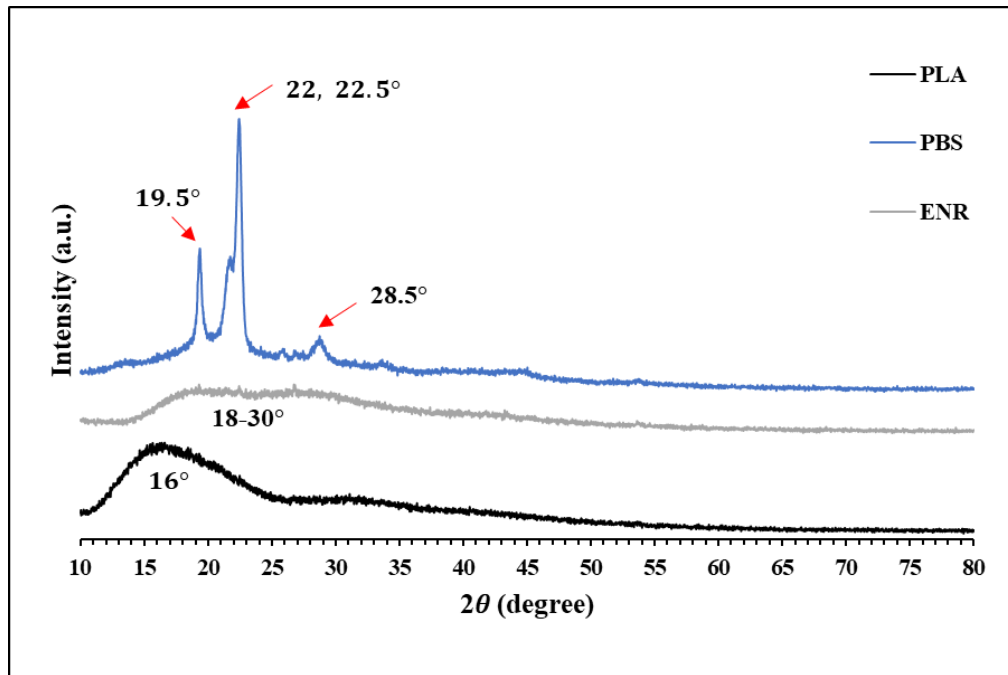


Figure 31 XRD of PLA, PBS and ENR.

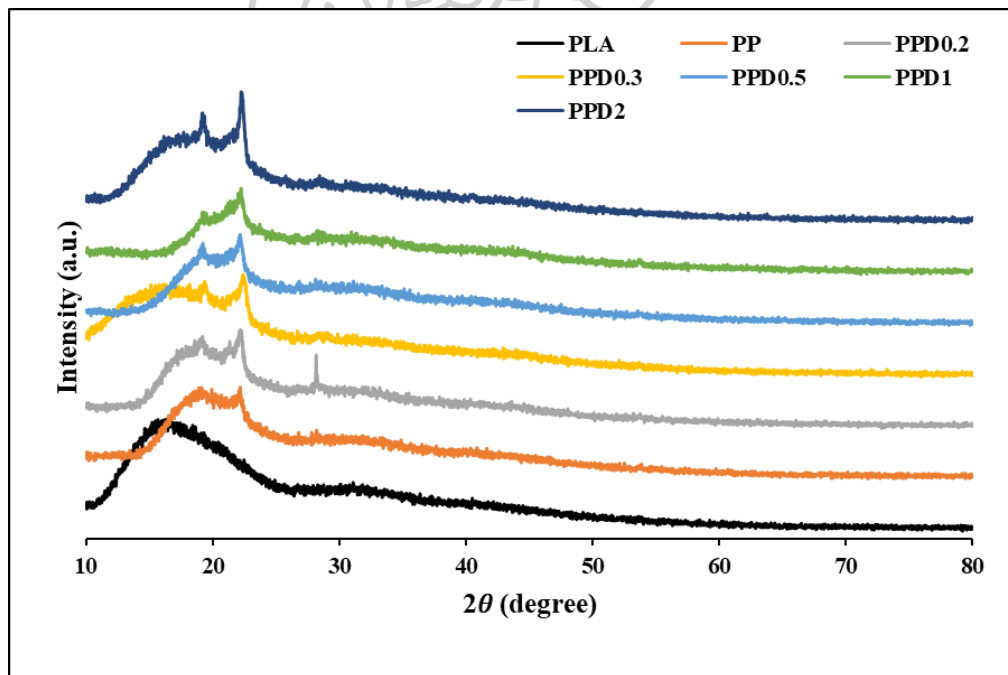


Figure 32 XRD of PLA and PLA/PBS (80/20) blends with various DCP contents.

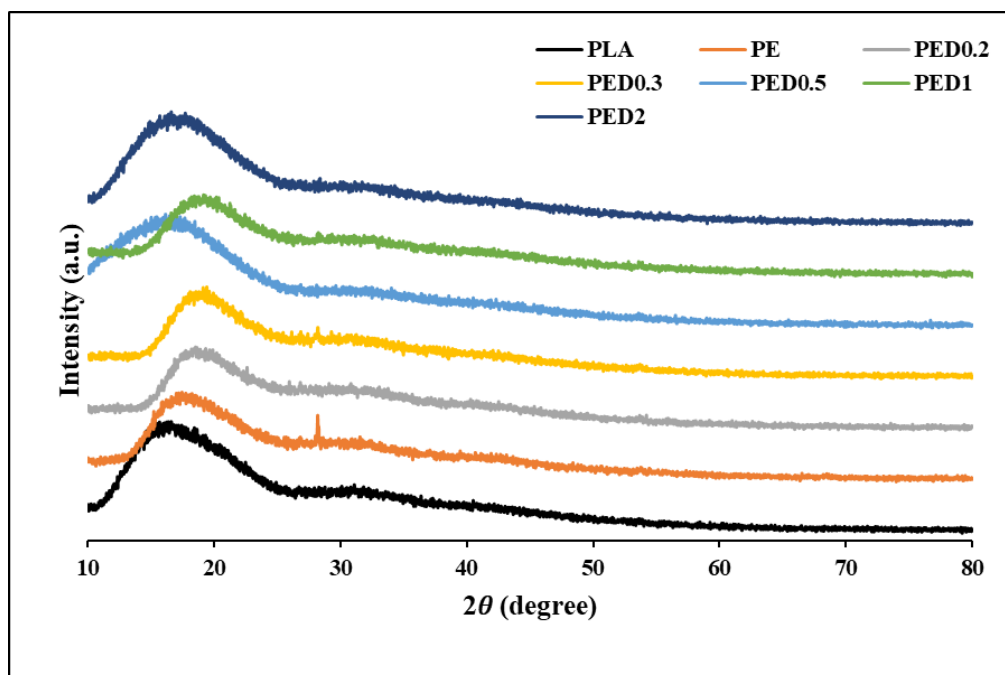


Figure 33 XRD of PLA and PLA/ENR blends with various DCP contents.

Table 7 Normalized crystallinity of PLA/PBS and PLA/ENR blends with various DCP contents.

Samples	Codes	Area		Xc (%)
		Crystalline	Amorphous	
PLA	PLA	-	12696.21	-
PLA/PBS 80/20	PP	616.38	9213.34	6.27
PLA/PBS 80/20-0.2DCP	PPD0.2	781.97	9617.86	7.52
PLA/PBS 80/20-0.3DCP	PPD0.3	625.32	8318.36	6.99
PLA/PBS 80/20-0.5DCP	PPD0.5	490.25	10323.18	4.53
PLA/PBS 80/20-1DCP	PPD1	571.64	7310.39	7.25
PLA/PBS 80/20-2DCP	PPD2	876.35	10889.97	7.45
PLA/ENR 80/20	PE	-	10923.35	-
PLA/ENR 80/20-0.2DCP	PED0.2	-	10184.70	-
PLA/ENR 80/20-0.3DCP	PED0.3	-	9818.85	-
PLA/ENR 80/20-0.5DCP	PED0.5	-	7405.29	-
PLA/ENR 80/20-1DCP	PED1	-	9061.33	-
PLA/ENR 80/20-2DCP	PED2	-	12618.61	-

5.1.6 UV-vis analysis

For this, the UV absorption of PLA, PLA/PBS, and PLA/ENR blends with various DCP contents was evaluated by using a UV-vis spectrophotometer in the wavelength range of 200-800 nm. The UV absorption is divided into two ranges which are the UV region and the visible region. Figures 34 and 35 show the UV absorption of the blends. PLA absorption produced a huge absorption band with a wavelength of less than 225 nm, and its intensity of blends increased when PBS and ENR were added. It was seen that the beige color of PLA/ENR blends with various DCP contents increased as shown in Figure 35. The absorption spectra showed a strong absorption band in the visible region at 400-800 nm due to discoloration of the blends as a result of ENR loading. The higher DCP was incorporated, the more the absorption increased due to DCP loading. During blending, DCP decomposed into free radicals by heating that could facilitate the extraction of Hydrogen from the PLA, PBS, or ENR chains to generate radicals. [7, 8, 56].

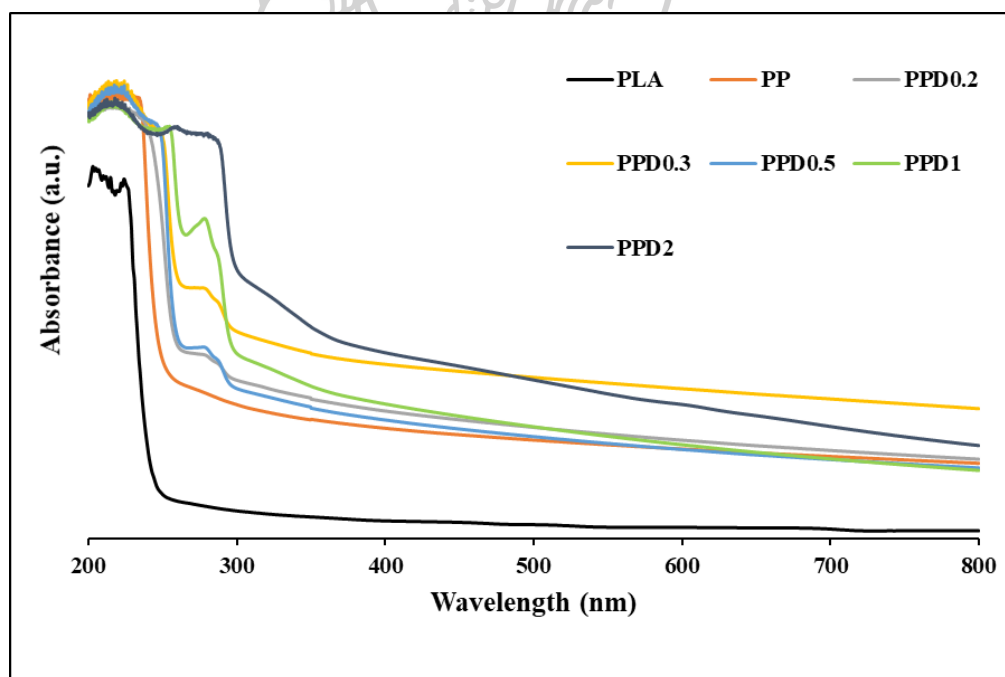


Figure 34 UV-vis of PLA and PLA/PBS blends with various DCP contents.

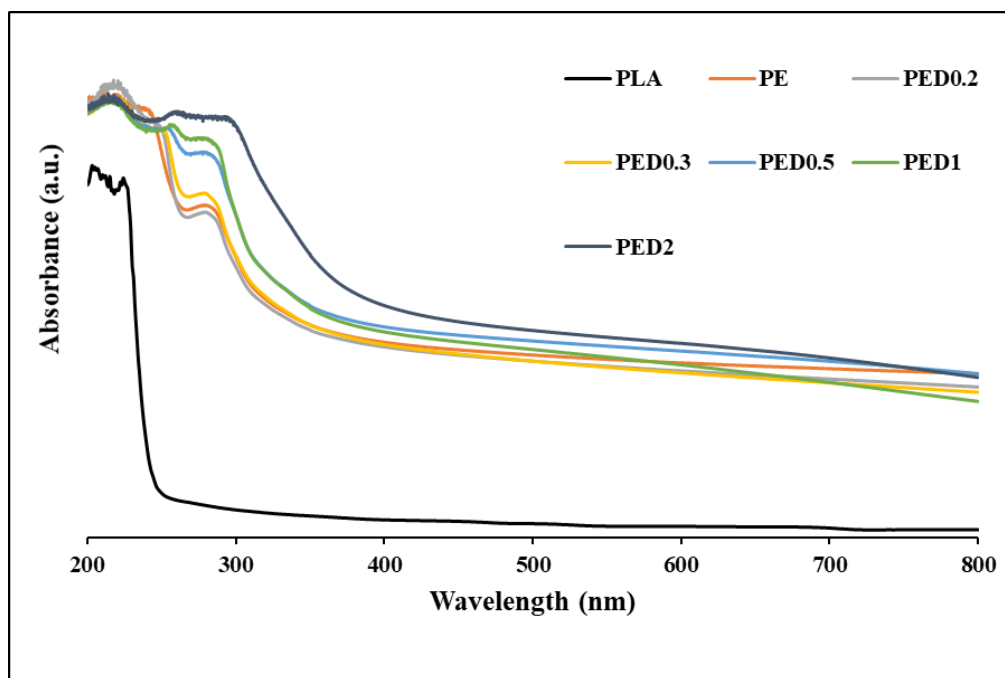


Figure 35 UV-vis of PLA and PLA/ENR blends with various DCP contents.

5.2 PLA/PBS/ENR blends without and with DCP

5.2.1 Morphological analysis

SEM micrographs of the tensile fracture surface of these blends were examined by SEM to study the phase morphology of PLA/PBS/ENR blends without DCP at 80/15/5, 80/10/10, and 80/5/15 as shown in Figure 36. Figure 36 (b-d) shows the phase separation of PLA/PBS/ENR blends. All of the PLA/PBS/ENR blends exhibit phase separation, with the rubber dispersed as small droplets in the PLA matrix. The phase morphology revealed some interfacial adhesion. As the amount of PBS increased, the PBS phase dispersed in the PLA matrix, and the observation of voids surrounding the weak interaction increased, as shown in Figure 36(b). Figure 36 (c-d) showed similarly weak interfacial adhesion by the empty spherical grooves on the surface in Figure 36(c-d) [56], especially 15 wt% of ENR at 80/5/15. The SEM micrograph is similar to binary blends (PLA/ENR). This indicated that it could affect the mechanical properties. Therefore, DCP was incorporated as a compatibilizer to improve the miscibility and interfacial adhesion as shown in Figures 37-39.

SEM micrograph of PLA/PBS/ENR (80/15/5) blends with various DCP, as shown in Figure 37, showed that the morphology had better compatibility with DCP loading and fewer PBS and ENR droplets. From Figure 37(b-e), the effective DCP loading could improve the interfacial adhesion and compatibility of the above phases and occur some granules in these blends. The partially compatible PLA/PBS/ENR (80/15/5) blends with 2 phr of DCP were responsible for coarse surface as shown in Figure 37(f), and very fine particles of dispersion. It indicated that a chemical interaction occurred between the oxirane ring on ENR and the hydroxyl group in PLA, PBS, and DCP, with the high DCP attributed to their compatibility.

The PLA/PBS/ENR (80/10/10) blends with DCP are shown in Figure 38. SEM micrograph showed better compatibility than blends without DCP. The incorporation of DCP as a compatibilizer could improve the interfacial adhesion in these blends. When DCP was incorporated from 0.2-2 phr as shown in Figure 38(b-f), some small granules dispersed in the PLA matrix, which referred to some crosslinked structures after DCP loading. The proper proportion of polymers and DCP loading could improve the interfacial adhesion and compatibility of blends, corresponding with the result of mechanical properties.

SEM micrograph of PLA/PBS/ENR (80/5/15) blends with various DCP, as shown in Figure 39. It still showed that the morphology had better compatibility but occurred some empty spherical grooves on the surface after DCP loading as shown in Figure 39(b-f). Although, DCP could improve the interfacial adhesion and compatibility of the above phases the higher %wt of ENR was added in the blends, indicating that it could improve the miscibility due to weak interfacial adhesion than lower wt% of ENR, when compared with Figure 37 or 38 [7, 50, 56].

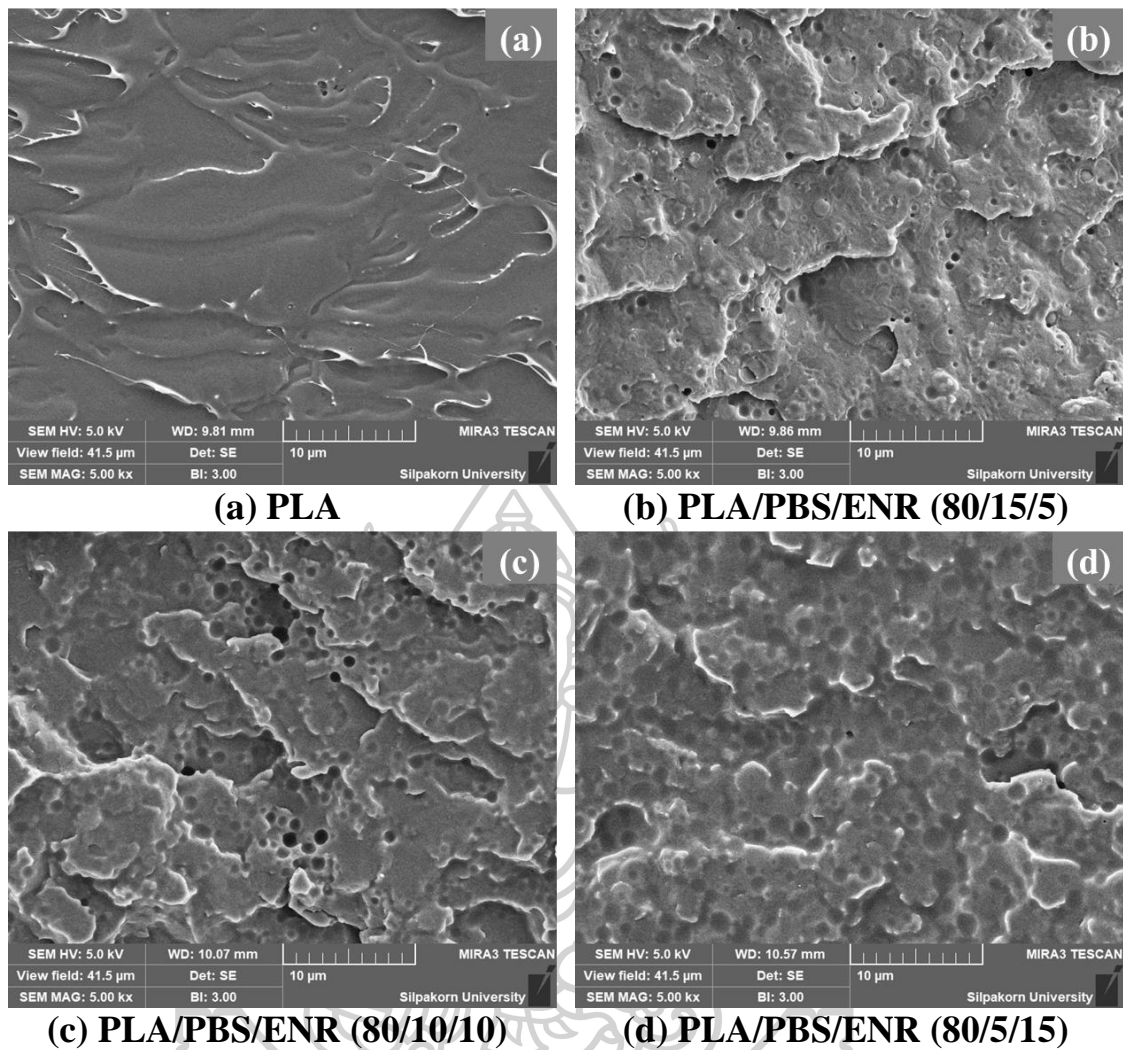


Figure 36 SEM micrograph of PLA/PBS/ENR blends without DCP; (a) PLA, (b) PLA/PBS/ENR (80/15/5), (c) PLA/PBS/ENR (80/10/10) and (d) PLA/PBS/ENR (80/5/15).

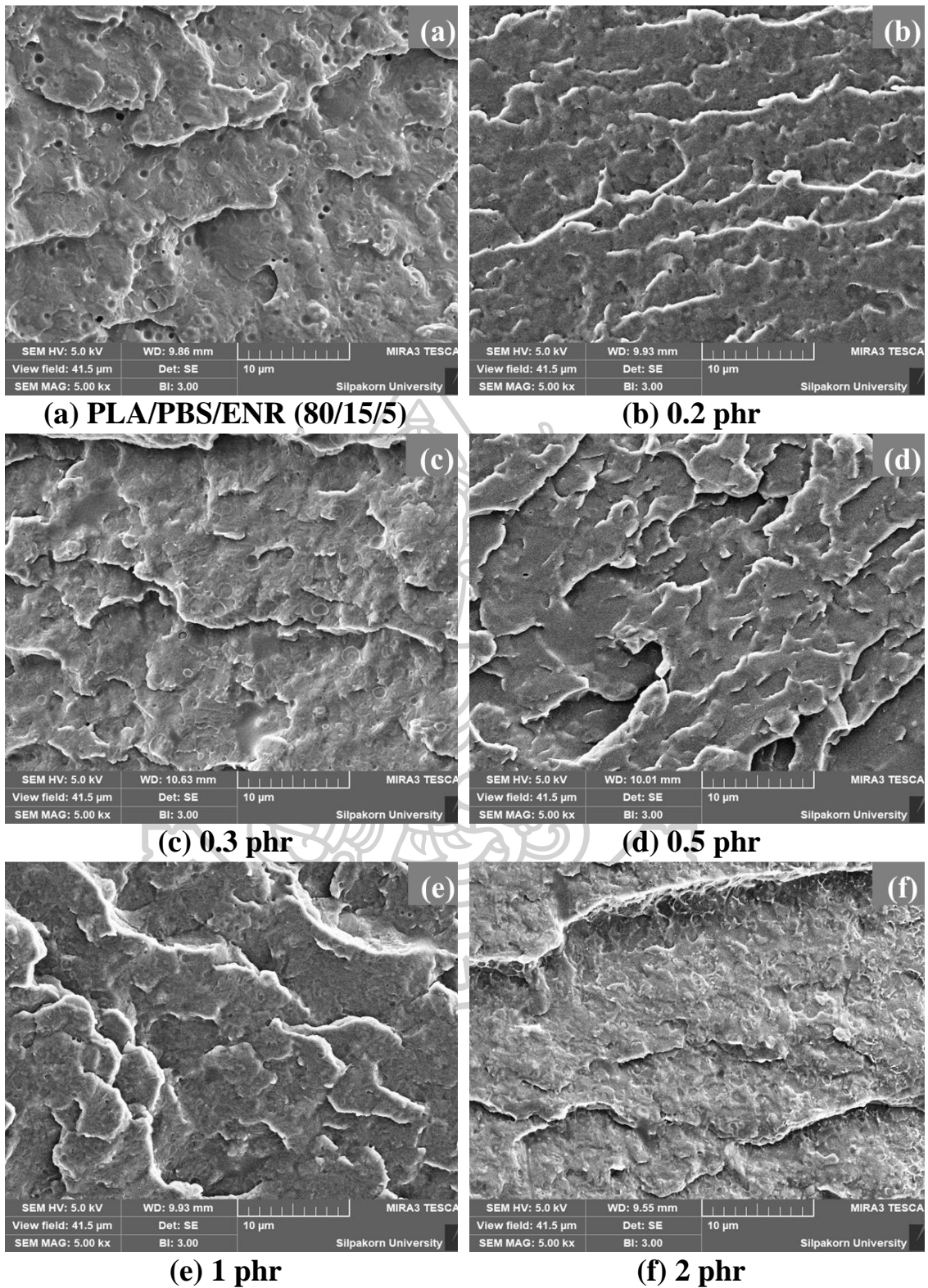


Figure 37 SEM micrograph of PLA/PBS/ENR (80/15/5) blends with various DCP contents; (a) no DCP, (b) 0.2 phr, (c) 0.3 phr, (d) 0.5 phr, (e) 1 phr and (f) 2 phr.

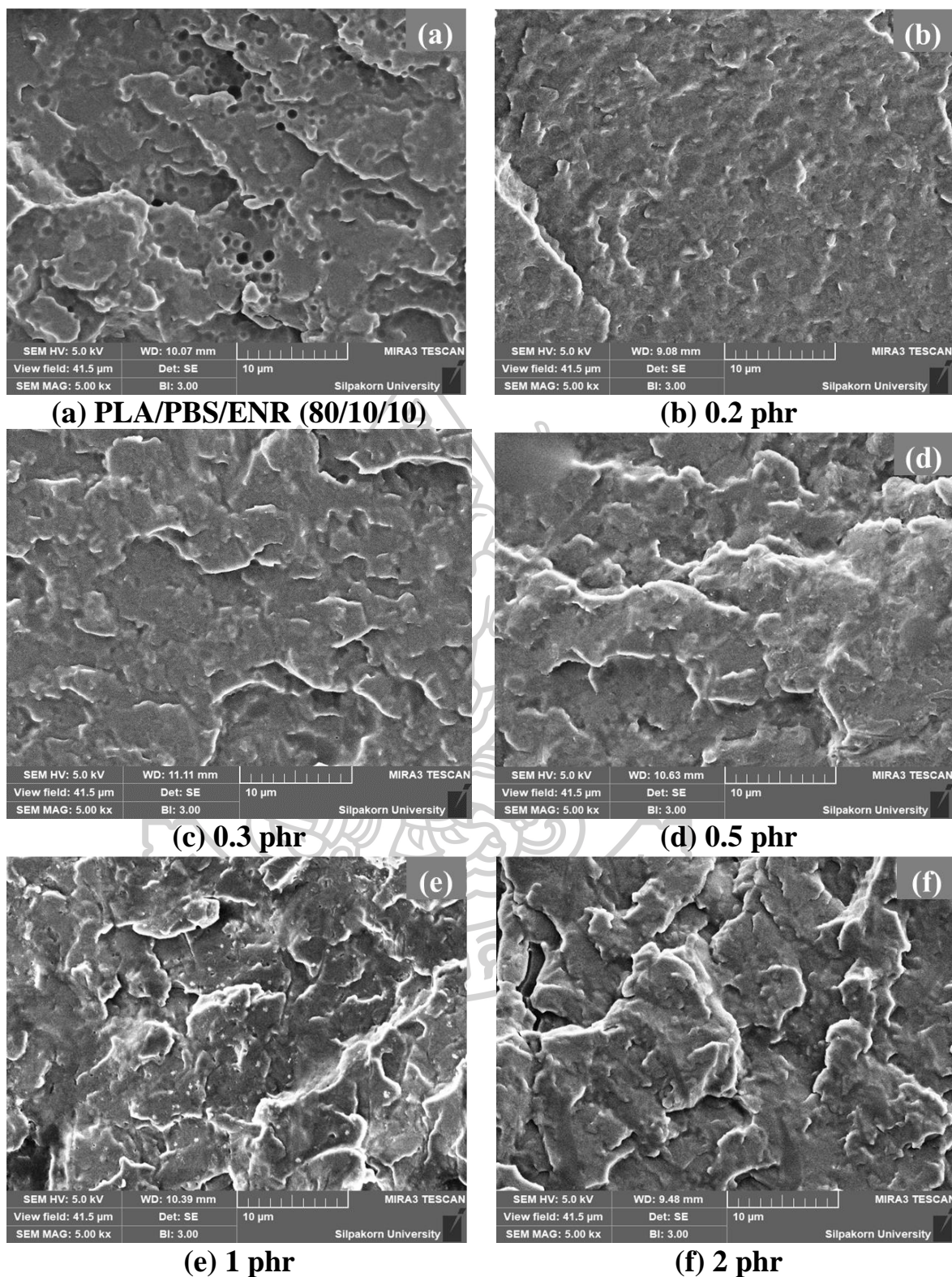


Figure 38 SEM micrograph of PLA/PBS/ENR (80/10/10) blends with various DCP contents; (a) no DCP, (b) 0.2 phr, (c) 0.3 phr, (d) 0.5 phr, (e) 1 phr and (f) 2 phr.

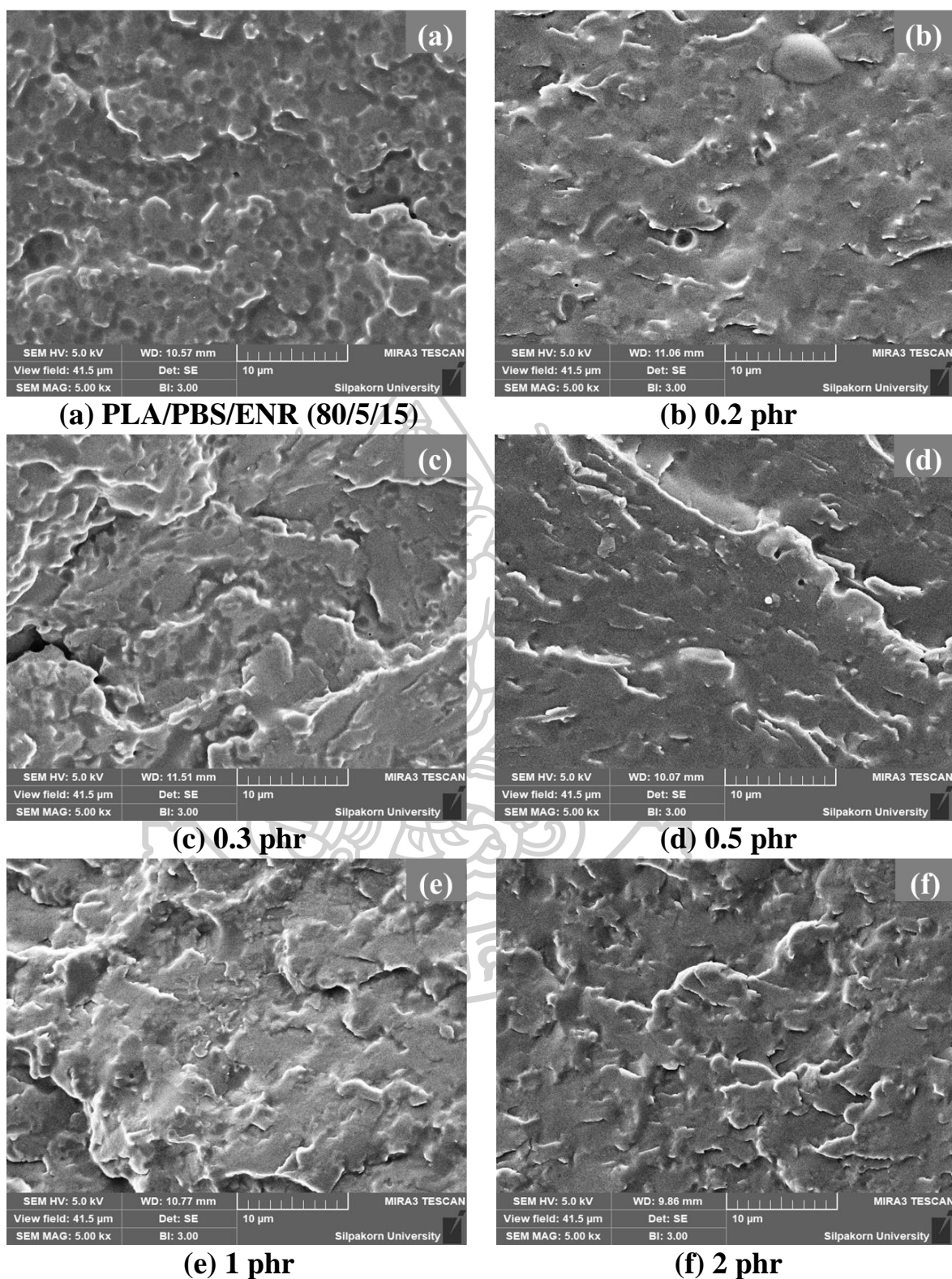


Figure 39 SEM micrograph of PLA/PBS/ENR (80/5/15) blends with various DCP contents; (a) no DCP, (b) 0.2 phr, (c) 0.3 phr, (d) 0.5 phr, (e) 1 phr and (f) 2 phr.

5.2.2 FTIR analysis

According to changes in vibration modes and band position between 400-4000 cm^{-1} , the FTIR was used to obtain information on the surface chemistry of PLA/PBS/ENR blends in the presence of DCP. DCP was used as the compatibilizer for the ternary blends, which possibly improved interfacial compatibilization. Figures 40-42 show that the peaks at 3000-3600 cm^{-1} are attributed to aromatic and aliphatic -OH groups, with the intensity of this peak varying depending on the material ratios.

As the Figures, 40-42 for PLA/PBS/ENR (80/15/5) and (80/10/10) blends, the decrement of intensity occurred due to the effective formation of DCP in the system. However, PLA and polymer blends around 2900 cm^{-1} are attributed to CH_2 stretching. Furthermore, the C=O stretching vibration peak at around 1750 cm^{-1} , is attributed to the stretching vibration of carbonyl groups of PLA including the blends. As the amount of PBS is incorporated at high contents, it indicated that the vibration peaks of carbonyl groups around 1750 cm^{-1} shifted to lower wavenumber. The FTIR spectra showed that the peak of the PLA/PBS/ENR blends, the C=O and CH_2 stretching in the presence of DCP slightly shifted to lower wavenumber in the blends. It could suggest that some interaction between PLA, PBS and ENR in the presence of DCP existed upon blending [57, 58, 64]. Especially, the interaction between PLA and PBS with DCP existed, corresponding the FTIR results in section 1.

Furthermore, no changes in the carbonyl group (C=O) of the blends were observed, thus suggesting that there may not occur any interactions between PLA and ENR in the presence of DCP. The FTIR spectra of blends with DCP showed no difference. Another reason is that it implies a possible interaction between the carboxylic group of PLA chains and the oxirane group of ENR. It further confirmed that the blends between PLA and ENR are partially miscible [7, 63, 64]. However, a low degree of possible crosslinking interaction was difficult to be detected by FTIR due to peaks overlapping.

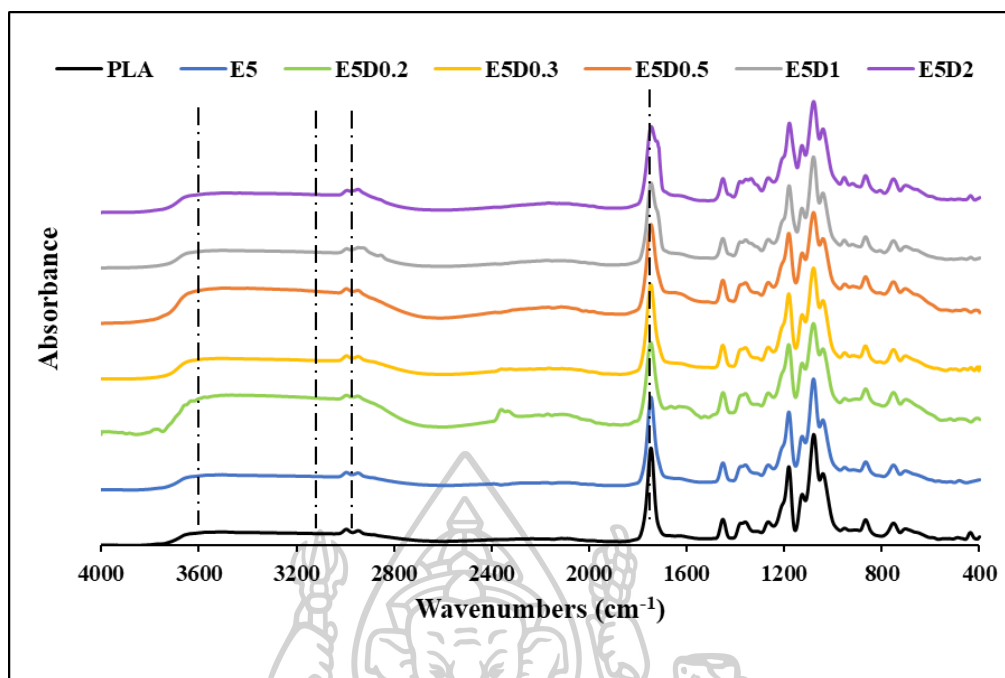


Figure 40 FTIR spectra of PLA/PBS/ENR (80/15/5) blends with various DCP contents.

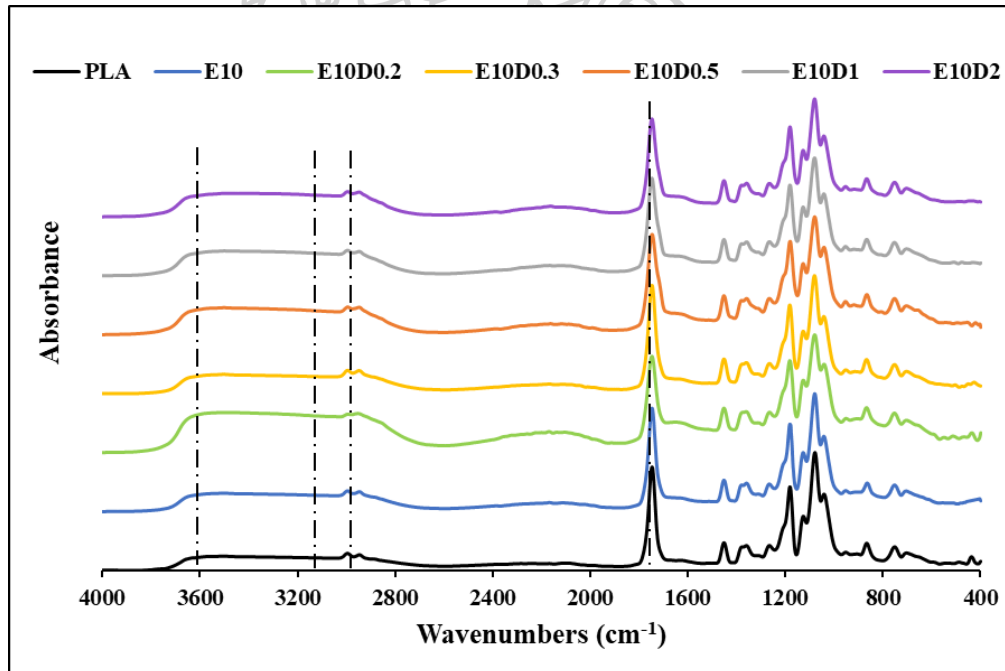


Figure 41 FTIR spectra of PLA/PBS/ENR (80/10/10) blends with various DCP contents.

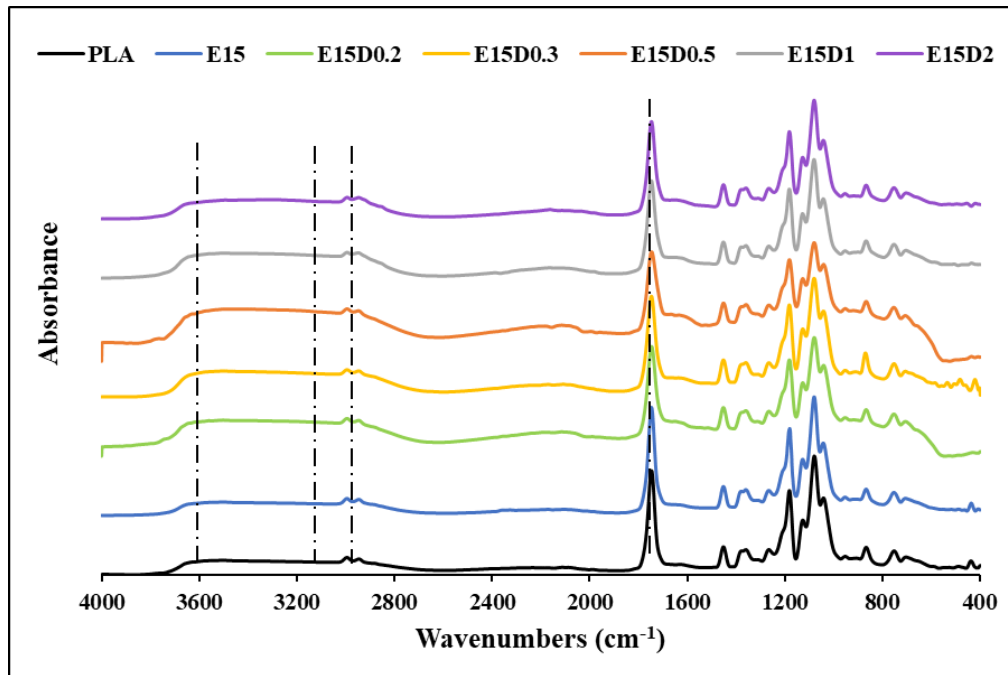


Figure 42 FTIR spectra of PLA/PBS/ENR (80/5/15) blends with various DCP contents.

5.2.3 Mechanical properties

(1) Young's modulus

The Young's modulus of PLA and PLA/PBS/ENR blends with various DCP is shown in Figure 43 and Table 8. The results showed that Young's modulus of PLA/PBS/ENR blends without DCP decreased when compared to PLA. All polymers are formed together as the amount of DCP is introduced in these systems, indicating that its fracture tried to change from brittle to ductile. For the PLA/PBS/ENR (80/15/5) blends, DCP was incorporated at 0.2-1 phr and it was higher Young's modulus than other blends, especially 0.3 and 0.5 phr of DCP. This indicated that the higher %wt of PBS increased, indicating both PLA and PBS had rigid strength, corresponding to Young's modulus increase. On the other hand, Young's modulus of PLA/PBS/ENR (80/10/10) and PLA/PBS/ENR (80/5/15) blends after DCP was added above 0.3 phr, still decreased due to the increasing ENR that could be observed from the empty spherical grooves in SEM micrograph.

(2) Tensile strength

The tensile strength of PLA and PLA/PBS/ENR blends with various DCP contents is shown in Figure 44 and Table 8. The results showed that the tensile strength of PLA/PBS/ENR blends with DCP decreased when compared to PLA. These results were similar to Young's modulus. All polymers are formed together as the amount of DCP is used to improve the properties in these blends. The PLA/PBS/ENR (80/15/5) blends, that DCP was incorporated at 0.2-2 phr, were higher the tensile strength than other ratios. On the other hand, the PLA/PBS/ENR (80/10/10) and (80/5/15) with DCP loading also had higher tensile strength than PLA/PBS/ENR blends without DCP. However, it indicated that DCP was incorporated and important in the blends which could help to improve the tensile strength and had better value than other blends without DCP loading.

(3) Stress at break

The stress at break of PLA and PLA/PBS/ENR blends with various DCP is shown in Figure 45 and Table 9, showed that the stress at break of PLA/PBS/ENR blends with various DCP slightly decreased. These results were similar to the previous properties. All PLA/PBS/ENR (80/15/5), (80/10/10), and (80/5/15) blends with various DCP loading, were also higher the stress at break than other blends, especially each PLA/PBS/ENR blends without DCP. As PLA/PBS/ENR (80/15/5) and (80/10/10) blends with DCP, which was incorporated above 0.3 phr, indicated that these blends needed lots of force to break because of their rigid and strength. However, the stress at break of PLA/PBS/ENR (80/15/5) and (80/10/10) blends with various DCP was still higher than PLA/PBS/ENR (80/5/15) blend with DCP, corresponding with the SEM micrograph is shown in Figures 38-40.

(4) Strain at break

The strain at break of PLA and PLA/PBS/ENR blends with various DCP is shown in Figure 46 and Table 9. The results showed that the strain at break of PLA/PBS/ENR (80/15/5) and (80/10/10) blends with various DCP, from 0.2-2 phr, slightly increased when compared to PLA while PLA/PBS/ENR (80/5/15) with DCP also decreased. It was the highest the percent strain at break of PLA/PBS/ENR (80/10/10) with 0.3 phr of DCP and other PLA/PBS/ENR blends with 0.3 phr DCP were higher than other blends. The results indicated that the incorporation

between PBS and ENR and the amount of DCP added could improve the percent strain at break and the flexibility of PLA. However, PLA/PBS/ENR (80/10/10) and (80/5/15) blends with above 0.3 of DCP still increased when compared with PLA/PBS/ENR blends [6, 7, 15, 50].

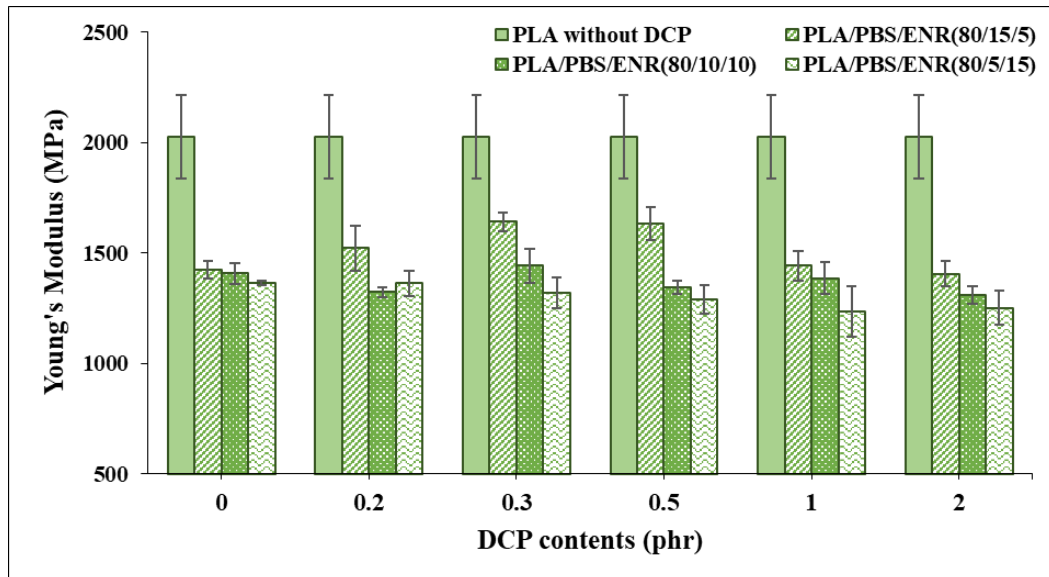


Figure 43 Young's modulus of PLA/PBS/ENR blends with various DCP contents.

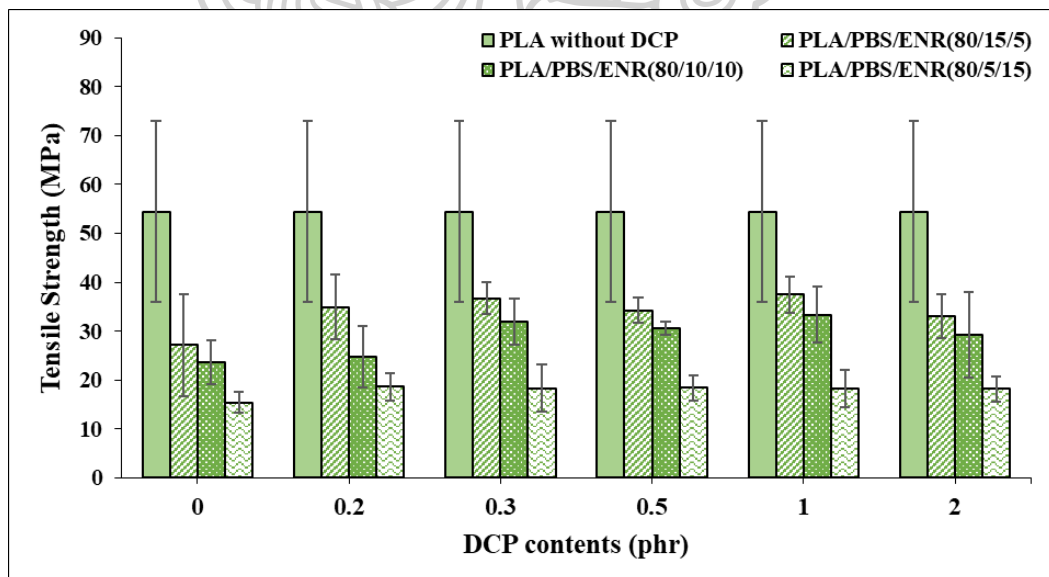


Figure 44 Tensile strength of PLA/PBS/ENR blends with various DCP contents.

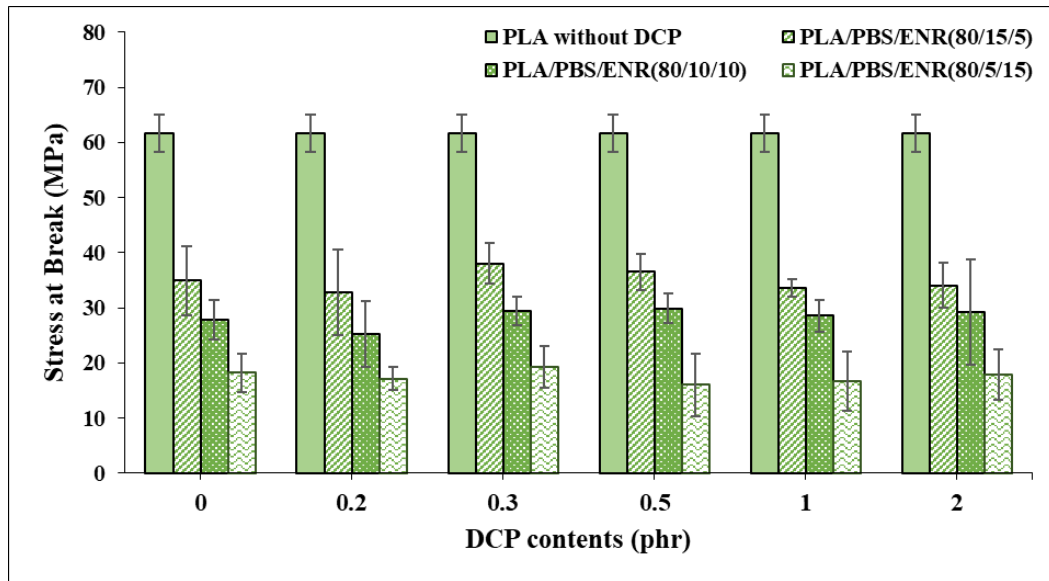


Figure 45 Stress at break of PLA/PBS/ENR blends with various DCP contents.

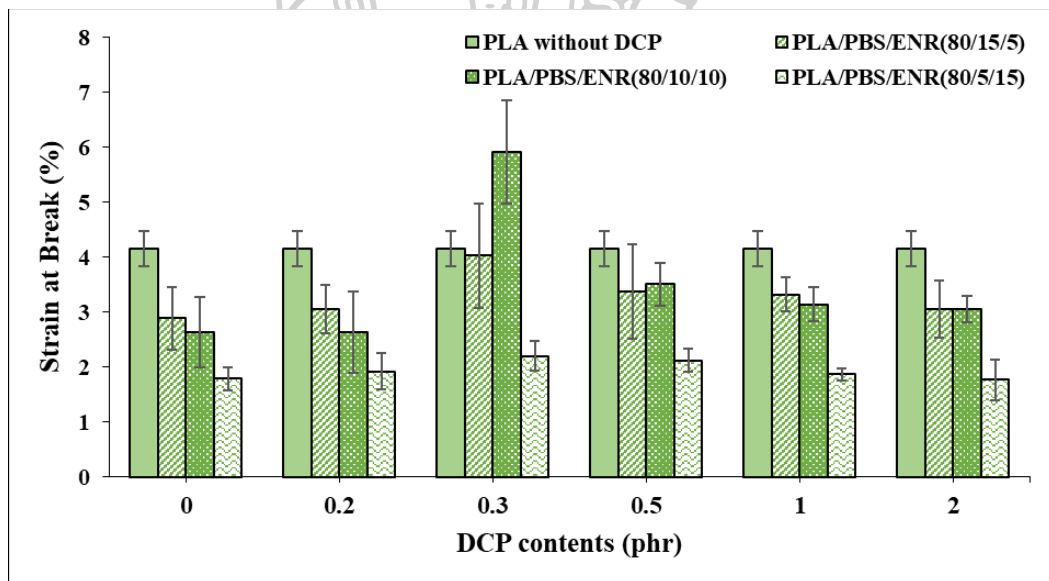


Figure 46 Strain at break of PLA/PBS/ENR blends with various DCP contents.

Table 8 Young's modulus and tensile strength of PLA/PBS/ENR blends with various DCP.

Samples	Codes	Young's Modulus (MPa)	Tensile Strength (MPa)
PLA	PLA	2024.37±189.92	54.41±18.50
PLA/PBS/ENR 80/15/5	E5	1425.01±40.97	27.15±10.43
PLA/PBS/ENR 80/10/10	E10	1407.85±46.64	23.71±4.45
PLA/PBS/ENR 80/5/15	E15	1364.63±11.78	15.45±2.07
PLA/PBS/ENR 80/15/5-0.2DCP	E5D0.2	1521.30±101.21	34.91±6.59
PLA/PBS/ENR 80/10/10-0.2DCP	E10D0.2	1322.97±21.14	24.76±6.22
PLA/PBS/ENR 80/5/15-0.2DCP	E15D0.2	1362.57±56.91	18.65±2.83
PLA/PBS/ENR 80/15/5-0.3DCP	E5D0.3	1641.17±43.82	36.70±3.29
PLA/PBS/ENR 80/10/10-0.3DCP	E10D0.3	1441.70±78.91	31.99±4.77
PLA/PBS/ENR 80/5/15-0.3DCP	E15D0.3	1318.25±70.95	18.36±4.88
PLA/PBS/ENR 80/15/5-0.5DCP	E5D0.5	1630.90±74.59	34.27±2.61
PLA/PBS/ENR 80/10/10-0.5DCP	E10D0.5	1343.65±30.97	30.60±1.37
PLA/PBS/ENR 80/5/15-0.5DCP	E15D0.5	1288.93±63.98	18.41±2.57
PLA/PBS/ENR 80/15/5-1DCP	E5D1	1442.78±66.70	37.49±3.69
PLA/PBS/ENR 80/10/10-1DCP	E10D1	1385.87±73.57	33.35±5.77
PLA/PBS/ENR 80/5/15-1DCP	E15D1	1234.91±113.52	18.29±3.83
PLA/PBS/ENR 80/15/5-2DCP	E5D2	1404.68±57.27	33.05±4.46
PLA/PBS/ENR 80/10/10-2DCP	E10D2	1308.86±40.98	29.27±8.84
PLA/PBS/ENR 80/5/15-2DCP	E15D2	1251.94±77.81	18.20±2.62



Table 9 Stress at break and strain at break of PLA/PBS/ENR blends with various DCP contents.

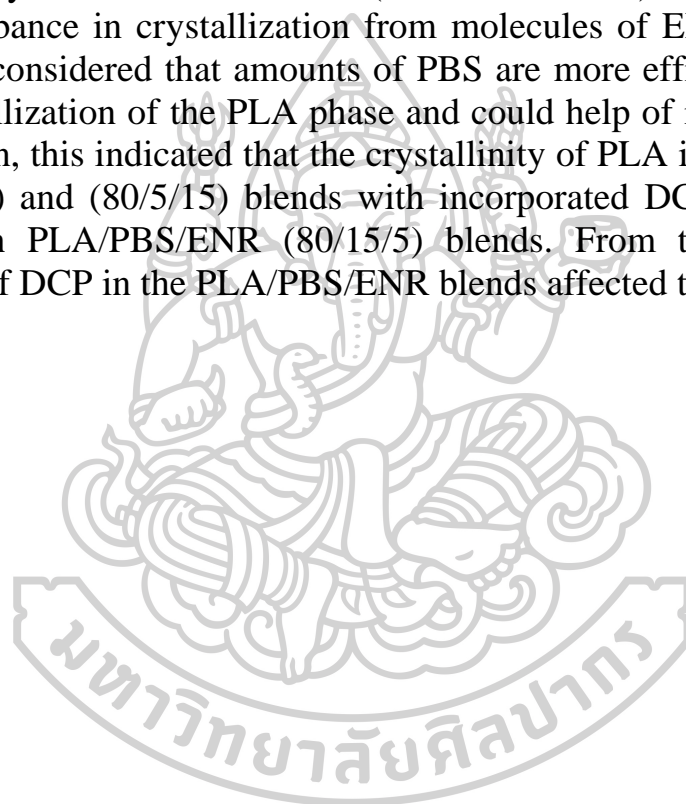
Samples	Codes	Stress at Break (MPa)	Strain at Break (%)
PLA	PLA	61.62±3.36	4.16±0.32
PLA/PBS/ENR 80/15/5	E5	35.00±6.27	2.89±0.64
PLA/PBS/ENR 80/10/10	E10	27.91±3.60	2.63±0.57
PLA/PBS/ENR 80/5/15	E15	18.25±3.49	1.79±0.21
PLA/PBS/ENR 80/15/5-0.2DCP	E5D0.2	32.87±7.78	3.05±0.73
PLA/PBS/ENR 80/10/10-0.2DCP	E10D0.2	25.19±5.94	2.63±0.45
PLA/PBS/ENR 80/5/15-0.2DCP	E15D0.2	17.16±2.13	1.92±0.33
PLA/PBS/ENR 80/15/5-0.3DCP	E5D0.3	38.08±3.68	4.03±0.94
PLA/PBS/ENR 80/10/10-0.3DCP	E10D0.3	29.46±2.62	5.92±0.95
PLA/PBS/ENR 80/5/15-0.3DCP	E15D0.3	19.26±3.84	2.2±0.27
PLA/PBS/ENR 80/15/5-0.5DCP	E5D0.5	36.55±3.29	3.38±0.39
PLA/PBS/ENR 80/10/10-0.5DCP	E10D0.5	29.86±2.67	3.51±0.86
PLA/PBS/ENR 80/5/15-0.5DCP	E15D0.5	16.02±5.72	2.12±0.21
PLA/PBS/ENR 80/15/5-1DCP	E5D1	33.68±1.57	3.32±0.31
PLA/PBS/ENR 80/10/10-1DCP	E10D1	28.58±2.90	3.14±0.31
PLA/PBS/ENR 80/5/15-1DCP	E15D1	16.67±5.36	1.87±0.11
PLA/PBS/ENR 80/15/5-2DCP	E5D2	34.11±4.14	3.05±0.25
PLA/PBS/ENR 80/10/10-2DCP	E10D2	29.26±9.56	3.05±0.52
PLA/PBS/ENR 80/5/15-2DCP	E15D2	17.91±4.59	1.77±0.37

5.2.4 Thermal properties

5.2.4.1 DSC analysis

The melting point temperature (T_m) of the PLA/PBS/ENR (80/15/5), (80/10/10), and (80/5/15) blends with various DCP contents are shown in Table 10 and Figures 47-49, respectively. From the study, the incorporation of DCP importantly changed the thermal behavior of the PLA/PBS/ENR blends. The results showed that the melting point temperature of all PLA/PBS/ENR blends was about 150°C. Although, each PLA/PBS/ENR blends with various DCP contents is shifted to a lower little temperature as shown in Table 10, indicating that it did not change in each PLA/PBS/ENR blends when compared with PLA. This indicated that DCP accelerated the melting point temperature of PLA/PBS/ENR blends. From the observation, the cold crystallization peak of PLA was around 120°C. The cold crystallization peak of PLA/PBS/ENR blends gradually weakened when DCP was incorporated which it could observe in Figures 47, 48, and 49, respectively. This indicated that the crystallinity of PLA in each blend was harder to form.

Table 11 shows the crystallinity (X_c) of the PLA/PBS/ENR blends with various DCP contents that were calculated from the melting enthalpy. While the melting enthalpy value for 100% crystalline (93.6 J/g for PLA) [60]. All of the PLA/PBS/ENR (80/15/5), (80/10/10), and (80/5/15) blends without DCP had low crystallinity when compared with PLA. After adding DCP, the crystallinity of PLA/PBS/ENR blends decreases. From the PLA/PBS/ENR (80/15/5) blends with DCP, the crystallinity decreased due to PBS and ENR including the amount of DCP. Although, the amount of DCP and PBS could increase the crystallinity as shown in section 1 (PLA/PBS blends) but decrease due to the disturbance in crystallization from molecules of ENR. Moreover, it could be considered that amounts of PBS are more efficient in assisting the crystallization of the PLA phase and could help of increasing X_c [8]. In addition, this indicated that the crystallinity of PLA in PLA/PBS/ENR (80/10/10) and (80/5/15) blends with incorporated DCP were easier to form than PLA/PBS/ENR (80/15/5) blends. From these results, the addition of DCP in the PLA/PBS/ENR blends affected the crystallinity.



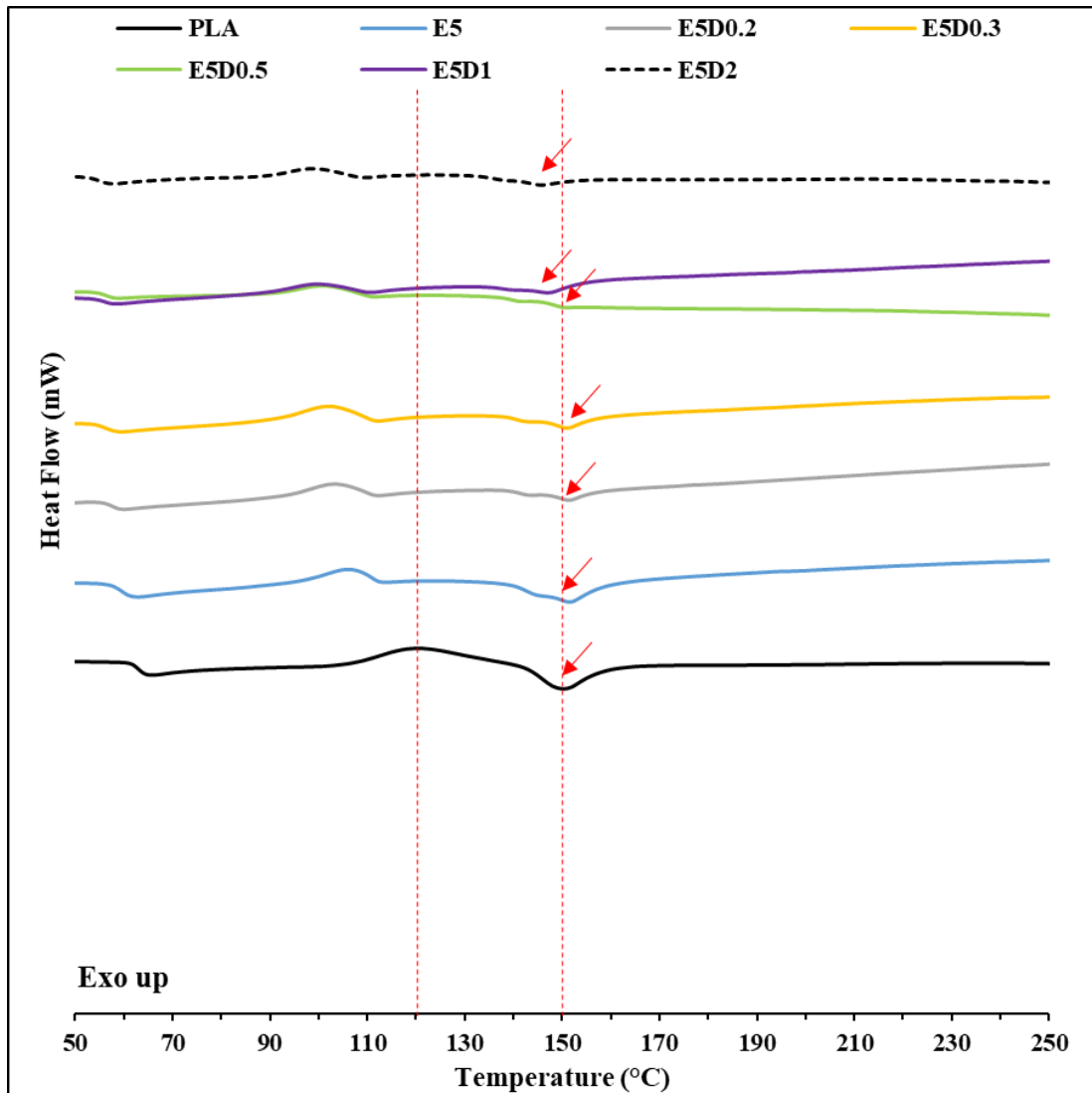


Figure 47 DSC of PLA/PBS/ENR (80/15/5) blends with various DCP contents.

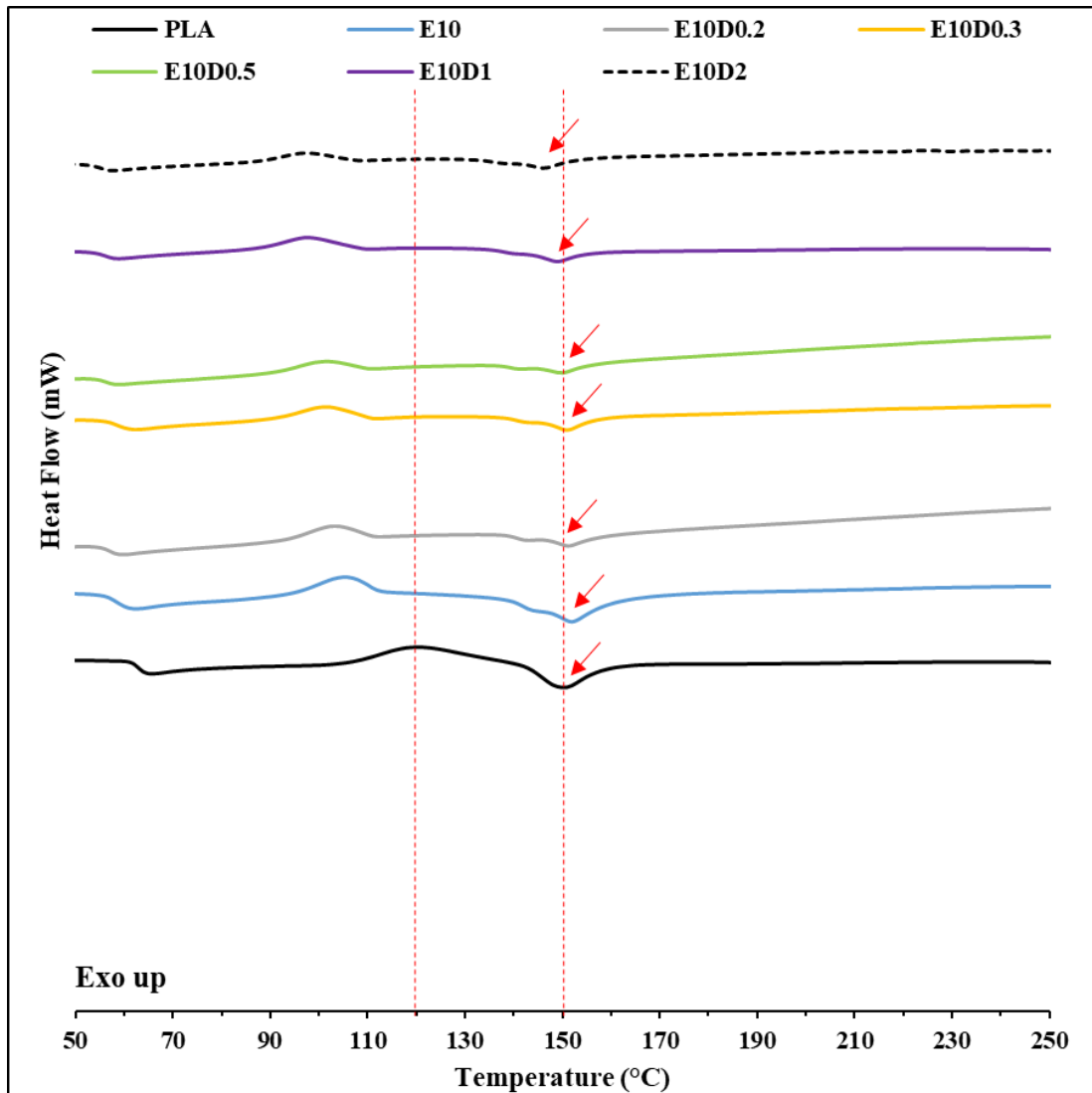


Figure 48 DSC of PLA/PBS/ENR (80/10/10) blends with various DCP contents.

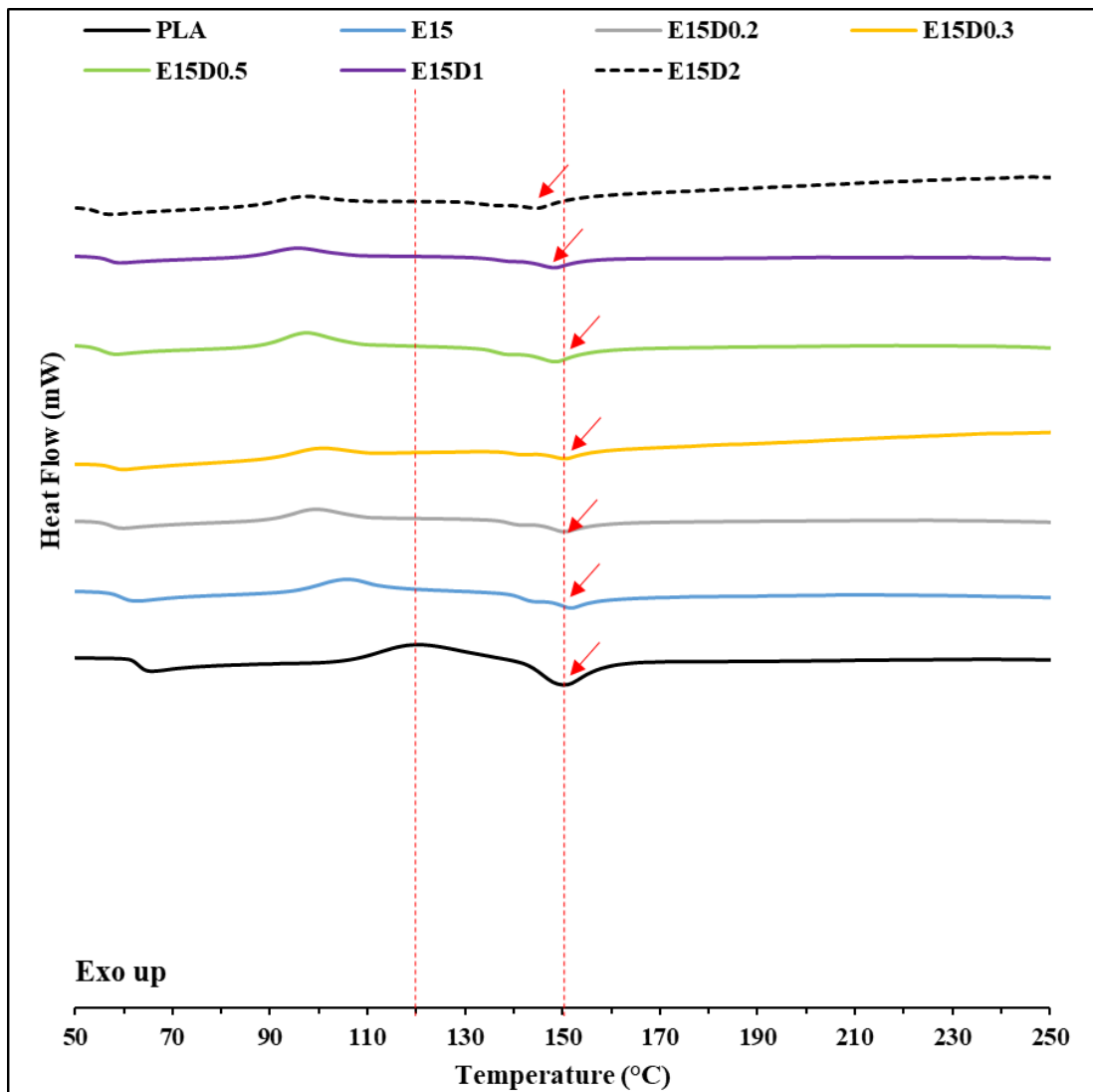


Figure 49 DSC of PLA/PBS/ENR (80/5/15) blends with various DCP contents.

Table 10 Melting point temperature of PLA/PBS/ENR blends with various DCP contents.

Samples	Codes	Melting point temperature (°C)
PLA	PLA	149
PLA/PBS/ENR 80/15/5	E5	152
PLA/PBS/ENR 80/15/5-0.2DCP	E5D0.2	152
PLA/PBS/ENR 80/15/5-0.3DCP	E5D0.3	151
PLA/PBS/ENR 80/15/5-0.5DCP	E5D0.5	151
PLA/PBS/ENR 80/15/5-1DCP	E5D1	148
PLA/PBS/ENR 80/15/5-2DCP	E5D2	145
PLA/PBS/ENR 80/10/10	E10	152
PLA/PBS/ENR 80/10/10-0.2DCP	E10D0.2	151
PLA/PBS/ENR 80/10/10-0.3DCP	E10D0.3	151
PLA/PBS/ENR 80/10/10-0.5DCP	E10D0.5	150
PLA/PBS/ENR 80/10/10-1DCP	E10D1	149
PLA/PBS/ENR 80/10/10-2DCP	E10D2	146
PLA/PBS/ENR 80/5/15	E15	152
PLA/PBS/ENR 80/5/15-0.2DCP	E15D0.2	150
PLA/PBS/ENR 80/5/15-0.3DCP	E15D0.3	151
PLA/PBS/ENR 80/5/15-0.5DCP	E15D0.5	148
PLA/PBS/ENR 80/5/15-1DCP	E15D1	148
PLA/PBS/ENR 80/5/15-2DCP	E15D2	145

Table 11 Crystallinity of PLA/PBS/ENR blends with various DCP contents.

Samples	Codes	Crystallinity (%)
PLA	PLA	41.5
PLA/PBS/ENR 80/15/5	E5	29.3
PLA/PBS/ENR 80/15/5-0.2DCP	E5D0.2	35.3
PLA/PBS/ENR 80/15/5-0.3DCP	E5D0.3	23.8
PLA/PBS/ENR 80/15/5-0.5DCP	E5D0.5	9.9
PLA/PBS/ENR 80/15/5-1DCP	E5D1	19.2
PLA/PBS/ENR 80/15/5-2DCP	E5D2	12.1
PLA/PBS/ENR 80/10/10	E10	35.6
PLA/PBS/ENR 80/10/10-0.2DCP	E10D0.2	34.4
PLA/PBS/ENR 80/10/10-0.3DCP	E10D0.3	10.0
PLA/PBS/ENR 80/10/10-0.5DCP	E10D0.5	24.8
PLA/PBS/ENR 80/10/10-1DCP	E10D1	24.3
PLA/PBS/ENR 80/10/10-2DCP	E10D2	21.3
PLA/PBS/ENR 80/5/15	E15	28.6
PLA/PBS/ENR 80/5/15-0.2DCP	E15D0.2	26.0
PLA/PBS/ENR 80/5/15-0.3DCP	E15D0.3	23.9
PLA/PBS/ENR 80/5/15-0.5DCP	E15D0.5	29.7
PLA/PBS/ENR 80/5/15-1DCP	E15D1	20.5
PLA/PBS/ENR 80/5/15-2DCP	E15D2	27.0

5.2.4.2 TGA analysis

Figures 50-52 show the thermal degradation of PLA/PBS/ENR blends with various DCP contents. The decomposition temperature of 5, 10, and 50% weight loss (T_{d5} , T_{d10} , and T_{d50}) of each blend is shown in Table 12. These results showed that the decomposition temperature decreased. Especially, the decomposition temperature at 10% weight loss was 330°C the all PLA/PBS/ENR blends (80/15/5, 80/10/10, and 80/5/15) with various DCP were shifted lower the decomposition temperatures than that of PLA. Then, the decomposition temperature at 50% weight loss, it could notice the decreasing the decomposition temperature of all PLA/PBS/ENR blends with DCP loading. The higher amount of ENR added in these blends, it had lower thermal stability when compared with PLA. In the comparison of the thermal stability, the PLA/PBS/ENR

blends (80/15/5) had higher than other blends, indicating that the higher amount of ENR affected thermal stability decreased [18, 50].

Furthermore, the degradation of PLA was proceeded by one step, as well as the degradation of PLA/PBS/ENR blends was two steps. From the results, the first step started between 270-380°C, presumably due to the main thermal degradation of PLA. In the second step, the degradation of PBS and ENR appeared at around a temperature of 340-450°C which is shown in Figures 50-52 [8, 65].

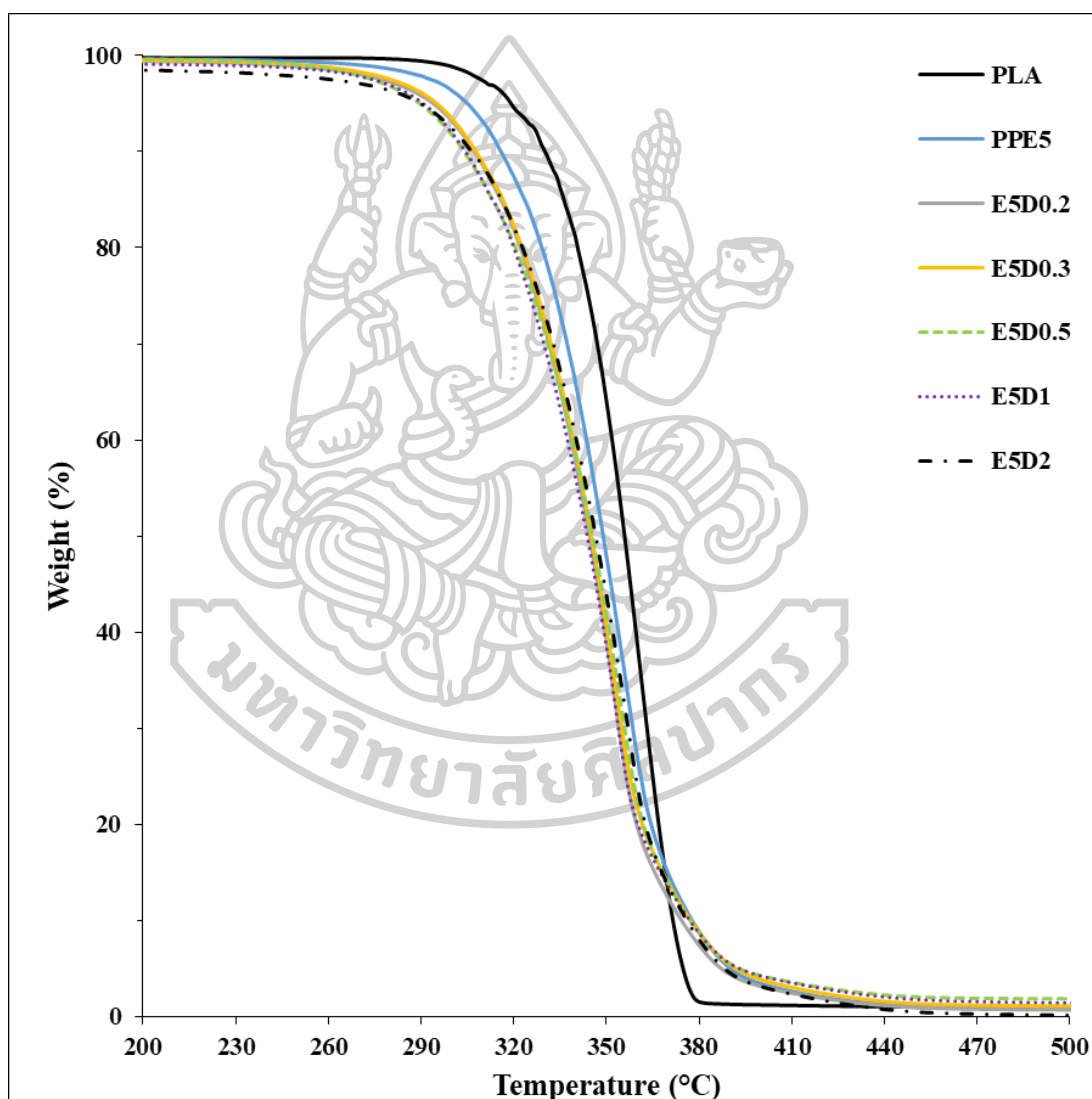


Figure 50 TGA of PLA/PBS/ENR (80/15/5) blends with various DCP contents.

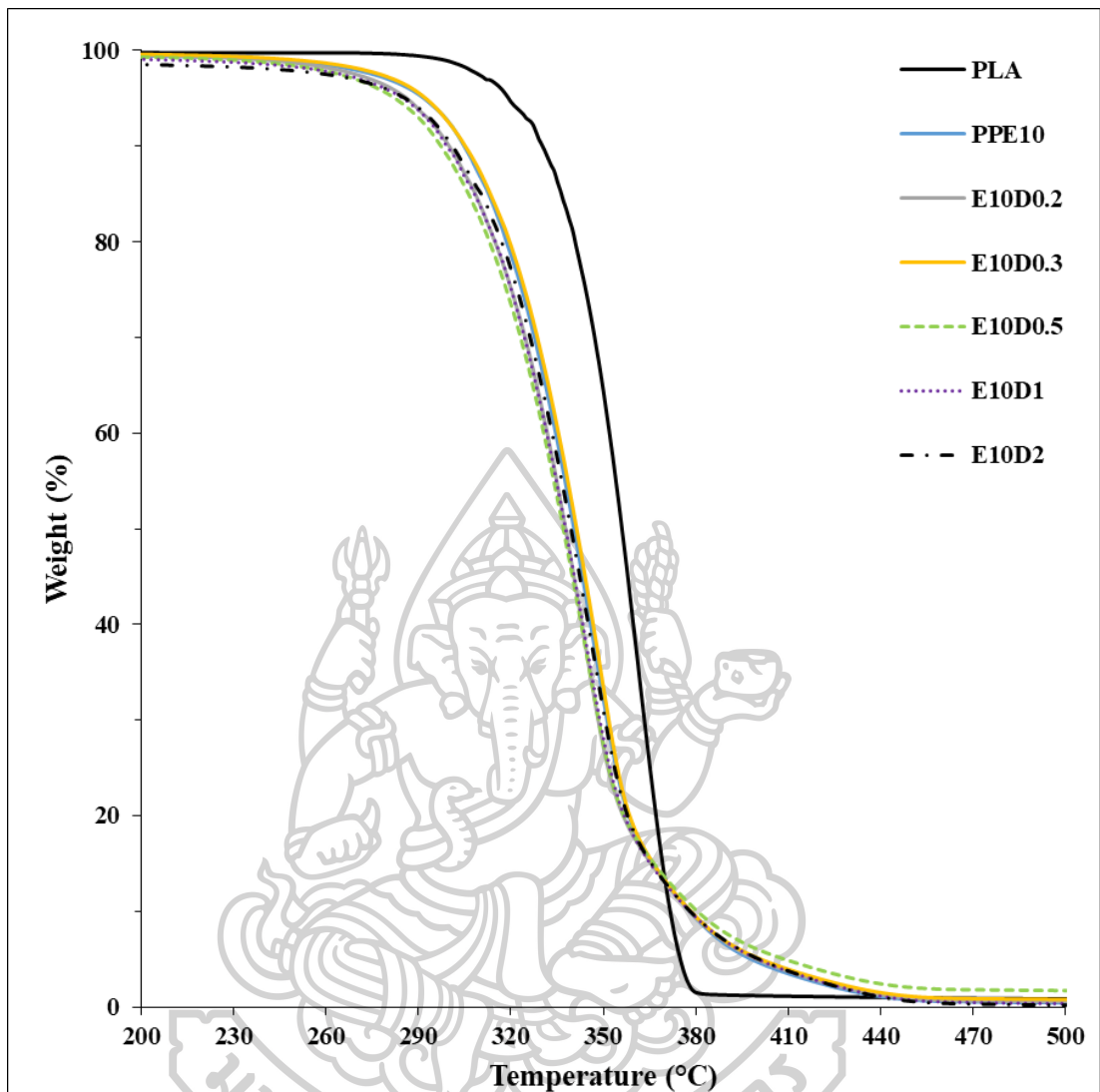


Figure 51 TGA of PLA/PBS/ENR (80/10/10) blends with various DCP contents.

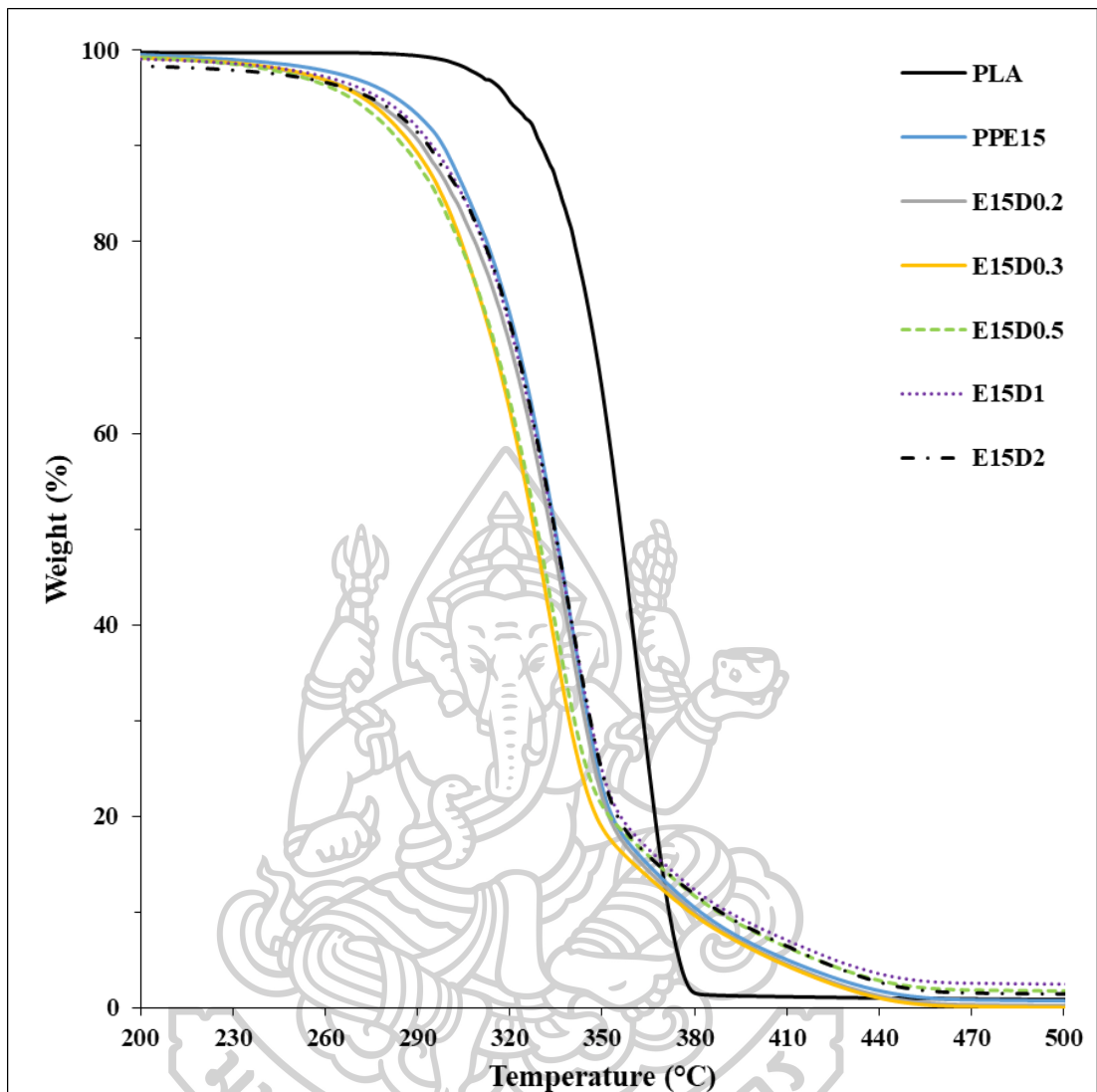


Figure 52 TGA of PLA/PBS/ENR (80/5/15) blends with various DCP contents.

Table 12 Decomposition temperature of PLA/PBS/ENR blends with various DCP contents.

Samples	Codes	Td5	Td10	Td50
PLA	PLA	319	330	356
PLA/PBS/ENR 80/15/5	E5	305	316	349
PLA/PBS/ENR 80/15/5-0.2DCP	E5D0.2	294	307	345
PLA/PBS/ENR 80/15/5-0.3DCP	E5D0.3	295	308	345
PLA/PBS/ENR 80/15/5-0.5DCP	E5D0.5	290	304	345
PLA/PBS/ENR 80/15/5-1DCP	E5D1	291	304	344
PLA/PBS/ENR 80/15/5-2DCP	E5D2	290	307	347
PLA/PBS/ENR 80/10/10	E10	291	305	340
PLA/PBS/ENR 80/10/10-0.2DCP	E10D0.2	286	300	338
PLA/PBS/ENR 80/10/10-0.3DCP	E10D0.3	292	305	341
PLA/PBS/ENR 80/10/10-0.5DCP	E10D0.5	282	297	337
PLA/PBS/ENR 80/10/10-1DCP	E10D1	285	299	338
PLA/PBS/ENR 80/10/10-2DCP	E10D2	286	301	339
PLA/PBS/ENR 80/5/15	E15	283	298	335
PLA/PBS/ENR 80/5/15-0.2DCP	E15D0.2	274	292	333
PLA/PBS/ENR 80/5/15-0.3DCP	E15D0.3	272	288	328
PLA/PBS/ENR 80/5/15-0.5DCP	E15D0.5	268	285	329
PLA/PBS/ENR 80/5/15-1DCP	E15D1	278	295	334
PLA/PBS/ENR 80/5/15-2DCP	E15D2	275	294	334

5.2.5 XRD analysis

The XRD patterns of PLA/PBS/ENR blends with various DCP were investigated to obtain further insight into the material's crystallinity, as shown in Figures 53-55. From XRD, a wide diffraction peak at $2\theta = 16^\circ$ was observed for PLA, indicating that the processing condition was amorphous. As XRD patterns of the PLA/PBS/ENR (80/15/5) and (80/10/10) blends are shown in Figures 53 and 54, which also have a high amount of PBS, showed the spectra peaks of PBS at $2\theta = 19.5^\circ$ and 22.5° due to its crystalline of PBS. For XRD patterns of the PLA/PBS/ENR (80/5/15) blends, which is a higher amount of ENR than the previous blends. The XRD patterns did not show the peaks of crystalline PBS.

Additionally, XRD could be determined the degree of crystallinity of the blends which can be calculated according to the same equation in section 1. The normalized area of peaks is shown in Table 13. The results showed that DCP acted as a crosslinker for the PLA/PBS/ENR blends. The crystallinity slightly increased the crystallites of PBS. This indicated

that the amount of DCP could affect the crystallinity of blends. This agreed with the DSC results, which showed the melting temperature of PLA blends slightly decreased. The high amount of DCP was incorporated, and the sharp and narrow peaks increased too as shown in Figure 32 (PLA/PBS blends).

Interestingly, these results contradict the degree of crystallinity calculated from DSC data, which revealed that PLA and the blends are amorphous crystallines rather than crystallines as observed by XRD. These are the results of different conditions and the distribution of amorphous and crystalline regions in the blends, which affect the crystallinity data obtained, as shown in Table 13 [58, 62, 63, 66, 67].

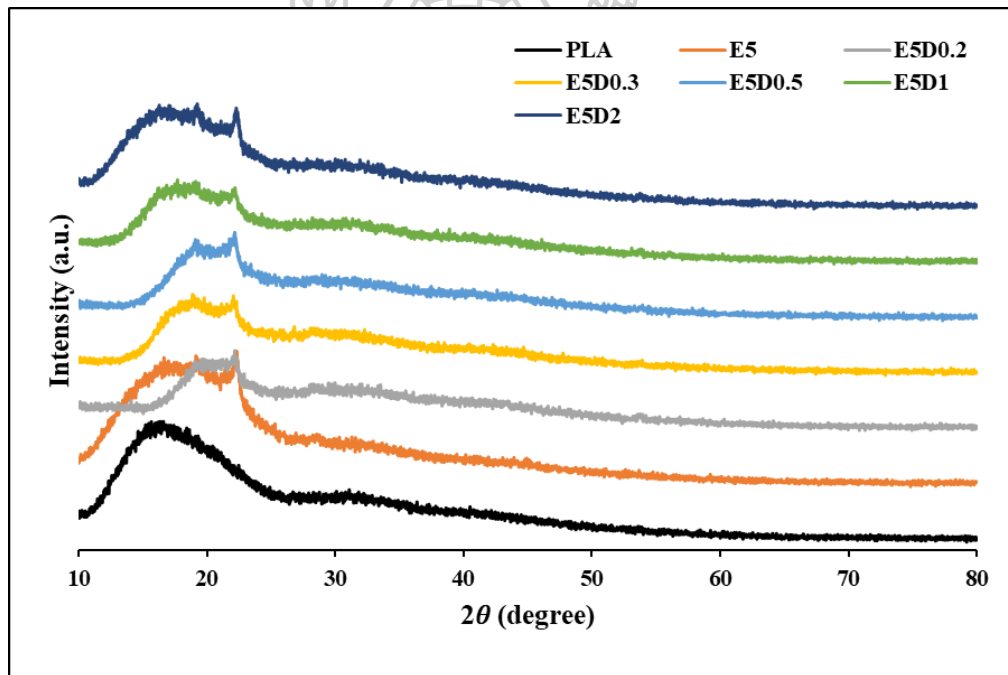


Figure 53 XRD of PLA/PBS/ENR (80/15/5) blends with various DCP contents.

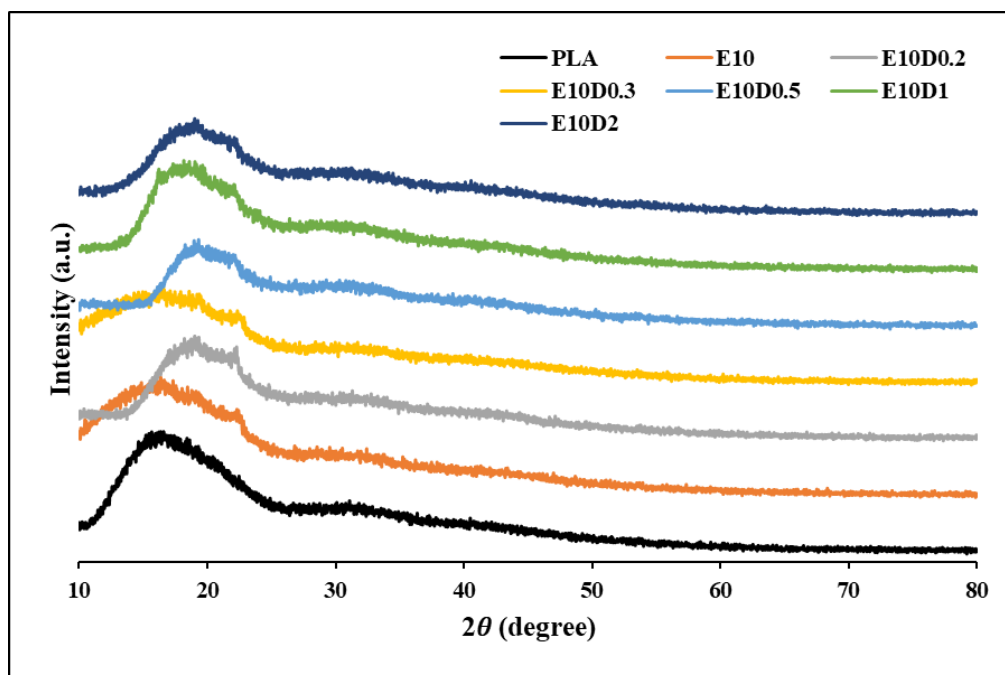


Figure 54 XRD of PLA/PBS/ENR (80/10/10) blends with various DCP contents.

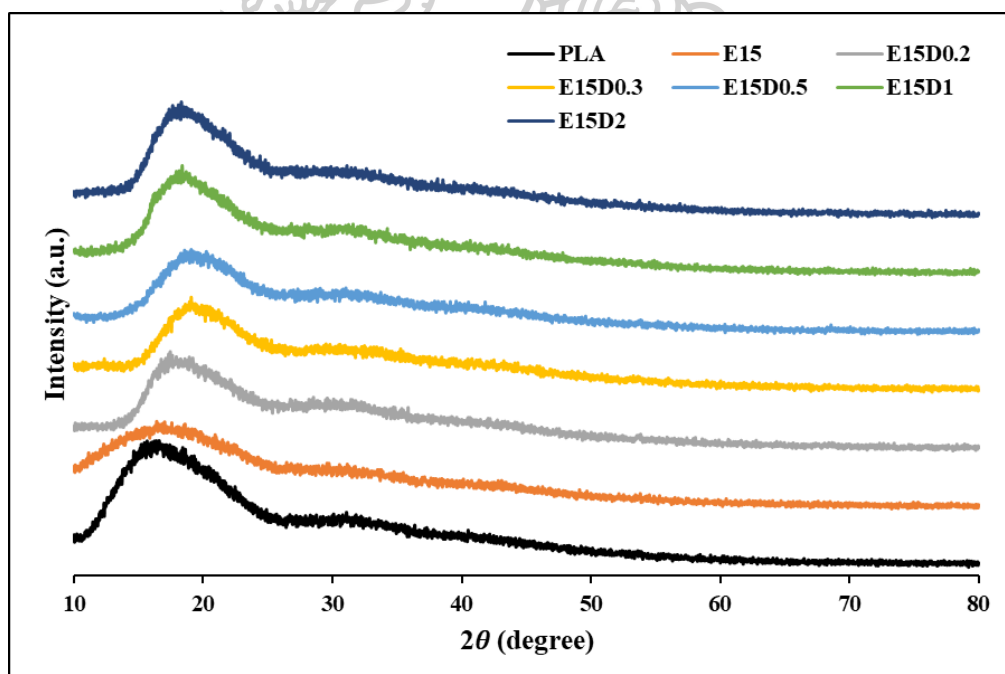


Figure 55 XRD of PLA/PBS/ENR (80/5/15) blends with various DCP contents.

Table 13 Normalized crystallinity of PLA/PBS/ENR blends with various DCP contents.

Samples	Codes	Area		Xc (%)
		Crystalline	Amorphous	
PLA	PLA	-	12696.21	-
PLA/PBS/ENR 80/15/5	E5	1093.05	13210.78	7.64
PLA/PBS/ENR 80/15/5-0.2DCP	E5D0.2	542.99	7596.35	6.67
PLA/PBS/ENR 80/15/5-0.3DCP	E5D0.3	473.21	9712.60	4.65
PLA/PBS/ENR 80/15/5-0.5DCP	E5D0.5	549.79	9476.65	5.48
PLA/PBS/ENR 80/15/5-1DCP	E5D1	678.49	8846.75	7.12
PLA/PBS/ENR 80/15/5-2DCP	E5D2	834.20	11180.61	6.94
PLA/PBS/ENR 80/10/10	E10	268.90	8082.27	3.22
PLA/PBS/ENR 80/10/10-0.2DCP	E10D0.2	399.08	10391.16	3.70
PLA/PBS/ENR 80/10/10-0.3DCP	E10D0.3	307.72	11413.58	2.63
PLA/PBS/ENR 80/10/10-0.5DCP	E10D0.5	290.86	10318.37	2.74
PLA/PBS/ENR 80/10/10-1DCP	E10D1	279.41	6978.11	3.85
PLA/PBS/ENR 80/10/10-2DCP	E10D2	298.67	9161.90	3.16
PLA/PBS/ENR 80/5/15	E15	-	7165.59	-
PLA/PBS/ENR 80/5/15-0.2DCP	E15D0.2	-	10267.36	-
PLA/PBS/ENR 80/5/15-0.3DCP	E15D0.3	-	9527.87	-
PLA/PBS/ENR 80/5/15-0.5DCP	E15D0.5	-	9937.74	-
PLA/PBS/ENR 80/5/15-1DCP	E15D1	-	10623.05	-
PLA/PBS/ENR 80/5/15-2DCP	E15D2	-	11127.67	-

5.2.6 UV-vis analysis

The UV absorption of PLA/PBS/ENR blends with various DCP was evaluated by using a UV-vis spectrophotometer in the wavelength range of 200-800 nm which is shown in Figures 56-58. The UV absorption is divided into two ranges which are the UV region and the visible region. A high absorption band of wavelength below 225 nm belonging to PLA absorption was observed, and its intensity of blends increased when PBS and ENR were added. It was seen that the beige color of ENR loading in blends increased. The absorption spectra showed a strong absorption band in the visible region at 400-800 nm due to discoloration of the blends as a result of ENR loading. When lots of ENR content were added, affecting to high intensity of blends in the visible region. The higher DCP content was incorporated in the blends, the more the absorption increased due to DCP loading. Heating decomposed DCP into free radicals during the blending process. It could help with the

extraction of hydrogens from PLA, PBS, or ENR chains as a result of the radical reaction propagating to form a branched structure between PLA, PBS, and ENR. PLA produces free radicals on tertiary C atoms, which are easily stabilized during reactive mixing. It is well known that PBS contains many secondary hydrogen (H) atoms and allows DCP to easily abstract Hydrogen [7, 8, 56].

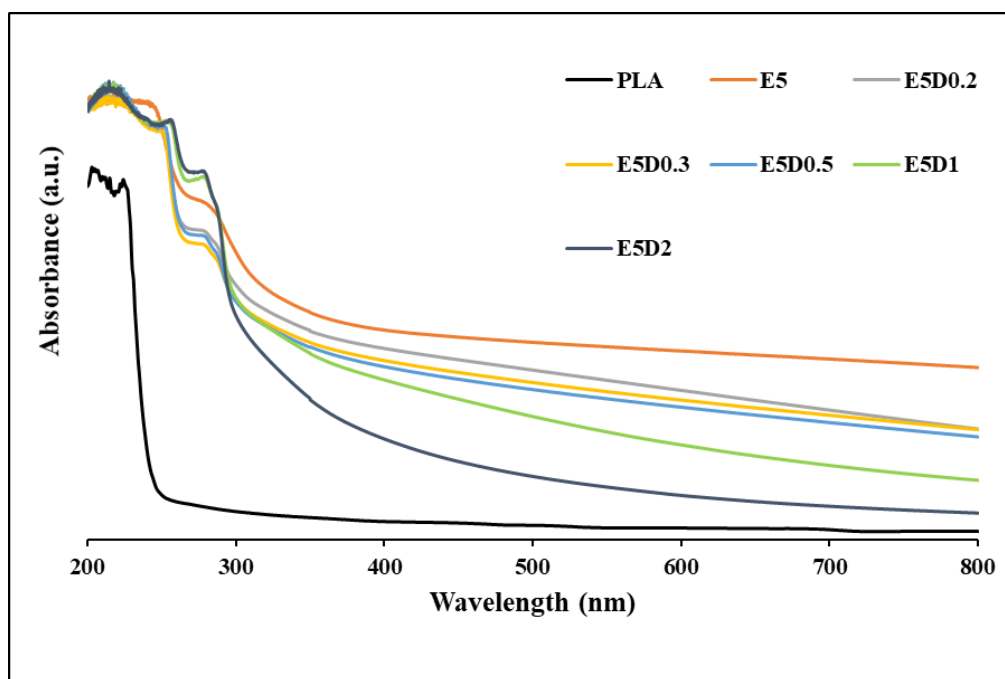


Figure 56 UV-vis of PLA/PBS/ENR (80/15/5) blends with various DCP contents.

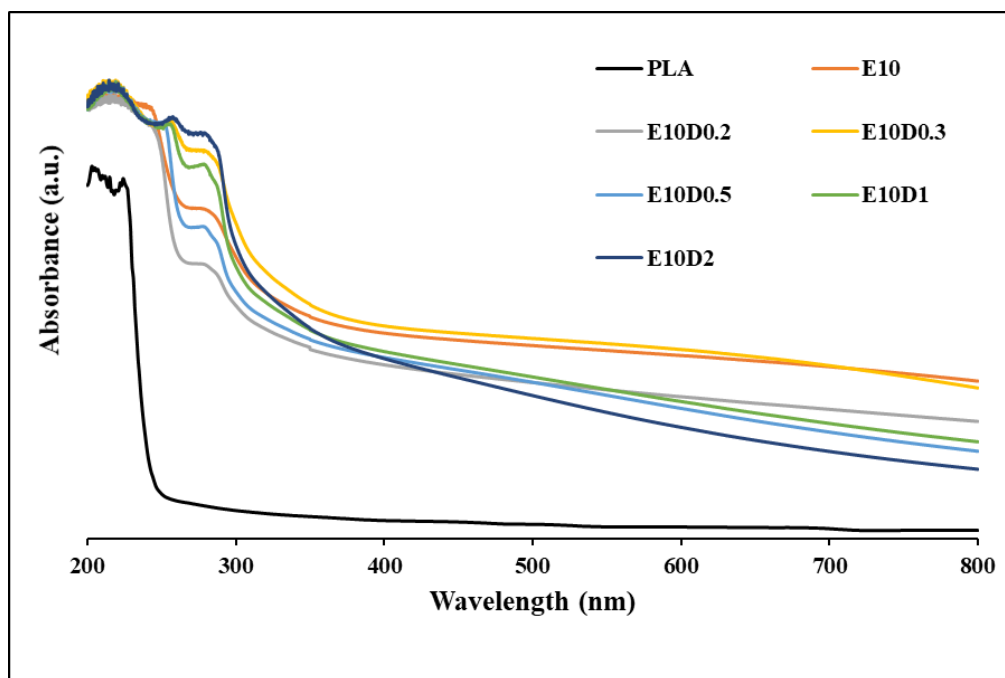


Figure 57 UV-vis of PLA/PBS/ENR (80/10/10) blends with various DCP contents.

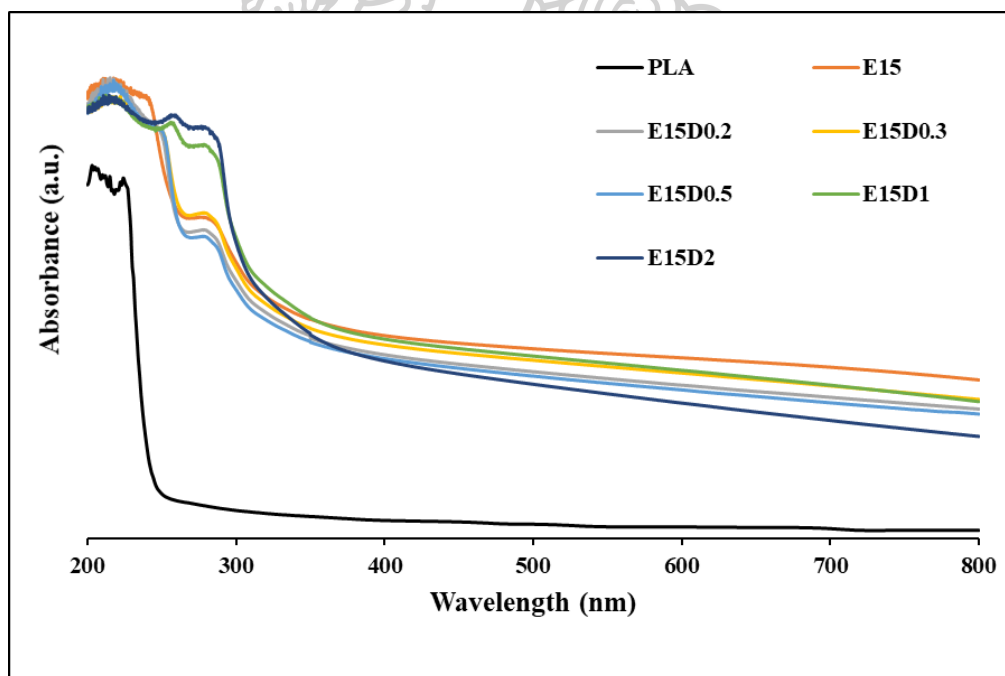


Figure 58 UV-vis of PLA/PBS/ENR (80/5/15) blends with various DCP contents.

5.3 The Samples of Polymer Blends from Thermoforming

The samples were prepared by thermoforming equipment in Polymer Innovation Laboratory as shown in Figure 59. The sample size was about 20×20 cm at a temperature of 250°C. The thickness of samples for thermoforming was about 0.3 mm. Figures 60-64 are only some samples that show the several forms of the packaging for both the PLA/PBS and PLA/PBS/ENR blends with DCP.



Figure 59 Thermoforming equipment in Polymer Innovation Laboratory.



Figure 60 Sample 1 of PLA/PBS (80/20) blends with DCP 0.3 phr.



Figure 61 Sample 2 of PLA/PBS (80/20) blends with DCP 0.3 phr.

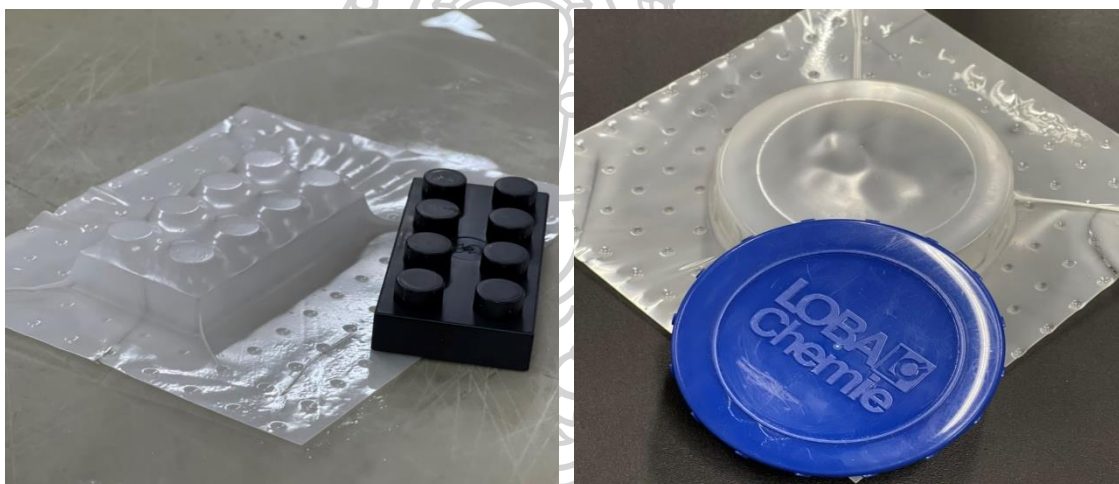


Figure 62 Samples 3 and 4 of PLA/PBS/ENR (80/10/10) blends with DCP 0.3 phr.



Figure 63 Samples 5 and 6 of PLA/PBS/ENR (80/10/10) blends with DCP 0.3 phr.



Figure 64 The sample 7 of PLA/PBS/ENR (80/15/5) blends with DCP 0.3 phr.

CHAPTER 6

CONCLUSION

The PLA/PBS, PLA/ENR, and PLA/PBS/ENR blends with DCP have been developed. From these results, the contents of over 0.3 phr of DCP could higher improve the percent strain at break more than PLA in PLA/PBS blends. For ternary blends, especially at PLA/PBS/ENR (80/10/10) blends had the highest percent strain at break when added 0.3 phr of DCP that it was better than the binary blends. After that, it could not affect the improvement of mechanical properties. The morphology analysis and SEM micrograph showed the effective miscibility changed to the mechanical properties with the addition of DCP and good dispersion state of all materials results in interfacial compatibility and enhanced the percent strain at break, compared with PLA. For FTIR showed the same peaks of polymer blends compared to PLA after adding all components. In addition, to thermal properties, the melting temperature of all of the PLA blends was approximately 150°C. Both the binary and ternary blends with various DCP contents had lower crystallinity than PLA. For thermal stability, the ternary blends are better than binary blends. In comparison, it can conclude that the ternary blends had better properties than the binary blends. For the ternary blends, at 80/10/10 with DCP 0.3 phr is a suitable ratio that can mold for some applications such as container packaging.

For further experiment, it is recommended to optimize conditions for either the binary or ternary blends. An alternative peroxide is also selected to improve the properties.

REFERENCES

1. Garlotta, D., *A literature review of poly (lactic acid)*. Journal of Polymers and the Environment, 2001. **9**(2): p. 63-84.
2. Qi, X., Y. Ren, and X. Wang, *New advances in the biodegradation of Poly (lactic) acid*. International Biodeterioration & Biodegradation, 2017. **117**: p. 215-223.
3. Nofar, M., et al., *Poly (lactic acid) blends: Processing, properties and applications*. International journal of biological macromolecules, 2019. **125**: p. 307-360.
4. Deng, Y. and N.L. Thomas, *Blending poly (butylene succinate) with poly (lactic acid): Ductility and phase inversion effects*. European Polymer Journal, 2015. **71**: p. 534-546.
5. Lim, L.-T., R. Auras, and M. Rubino, *Processing technologies for poly (lactic acid)*. Progress in polymer science, 2008. **33**(8): p. 820-852.
6. Xue, B., et al., *Fabrication of super-tough ternary blends by melt compounding of poly (lactic acid) with poly (butylene succinate) and ethylene-methyl acrylate-glycidyl methacrylate*. Composites Part B: Engineering, 2019. **172**: p. 743-749.
7. Ji, D., et al., *Morphology, rheology, crystallization behavior, and mechanical properties of poly (lactic acid)/poly (butylene succinate)/dicumyl peroxide reactive blends*. Journal of Applied Polymer Science, 2014. **131**(3).
8. Monika, et al., *Effect of dicumyl peroxide on a poly (lactic acid)(PLA)/Poly (butylene succinate)(PBS)/Functionalized chitosan-based nanobiocomposite for packaging: a reactive extrusion study*. ACS omega, 2018. **3**(10): p. 13298-13312.
9. Jompang, L., et al., *Poly (lactic acid) and poly (butylene succinate) blend fibers prepared by melt spinning technique*. Energy Procedia, 2013. **34**: p. 493-499.
10. Qiu, T., M. Song, and L. Zhao, *Testing, characterization and modelling of mechanical behaviour of poly (lactic-acid) and poly (butylene succinate) blends*. Mechanics of Advanced Materials and Modern Processes, 2016. **2**(1): p. 1-11.
11. Bhatia, A., et al., *Compatibility of biodegradable poly (lactic acid)(PLA) and poly (butylene succinate)(PBS) blends for packaging application*. Korea-Australia rheology journal, 2007. **19**(3): p. 125-131.
12. Cai, Z., et al., *The modification of properties of thermoplastic starch materials: Combining potato starch with natural rubber and epoxidized natural rubber*. Materials Today Communications, 2021. **26**: p. 101912.
13. Faibunchan, P., et al., *Novel biodegradable thermoplastic elastomer based on poly (butylene succinate) and epoxidized natural rubber simple blends*. Journal of Polymers and the Environment, 2018. **26**(7): p. 2867-2880.
14. Zhang, C., et al., *Thermal, mechanical and rheological properties of polylactide toughened by epoxidized natural rubber*. Materials & Design, 2013. **45**: p. 198-205.
15. Wang, R., et al., *Toughening modification of PLLA/PBS blends via in situ compatibilization*. Polymer Engineering & Science, 2009. **49**(1): p. 26-33.
16. Srimalanon, P., et al., *Effects of DCP as a free radical producer and HPQM as a biocide on the mechanical properties and antibacterial performance of in situ compatibilized PBS/PLA blends*. Polymer Testing, 2018. **67**: p. 331-341.

17. Wang, Y., et al., *Supertoughened biobased poly (lactic acid)–epoxidized natural rubber thermoplastic vulcanizates: fabrication, co-continuous phase structure, interfacial in situ compatibilization, and toughening mechanism*. *The Journal of Physical Chemistry B*, 2015. **119**(36): p. 12138-12146.
18. Zheng, M., et al., *Structure evolution of bio-based PLA/ENR thermoplastic vulcanizates during dynamic vulcanization processing*. *Polymer Testing*, 2020. **82**: p. 106324.
19. Yuan, D., et al., *Bio-based polylactide/epoxidized natural rubber thermoplastic vulcanizates with a co-continuous phase structure*. *Polymer Testing*, 2017. **64**: p. 200-206.
20. Ayu, R.S. and A. Khalina, *Effect of different polybutylene succinate (PBS)/starch formulation on food tray by thermoforming process*, in *Biopolymers and Biocomposites from Agro-Waste for Packaging Applications*. 2021, Elsevier. p. 85-100.
21. Jacquelin, N., et al., *Synthesis and properties of poly (butylene succinate): Efficiency of different transesterification catalysts*. *Journal of Polymer Science Part A: Polymer Chemistry*, 2011. **49**(24): p. 5301-5312.
22. Xu, J. and B.H. Guo, *Poly (butylene succinate) and its copolymers: research, development and industrialization*. *Biotechnology journal*, 2010. **5**(11): p. 1149-1163.
23. Phinyocheep, P., *Chemical modification of natural rubber (NR) for improved performance*, in *Chemistry, manufacture and applications of natural rubber*. 2014, Elsevier. p. 68-118.
24. Alias, N.F. and K.K. Marsilla, *Processes and characterization for biobased polymers from polybutylene succinate*, in *Processing and Development of Polysaccharide-Based Biopolymers for Packaging Applications*. 2020, Elsevier. p. 151-170.
25. Harada, M., et al., *Increased impact strength of biodegradable poly (lactic acid)/poly (butylene succinate) blend composites by using isocyanate as a reactive processing agent*. *Journal of Applied Polymer Science*, 2007. **106**(3): p. 1813-1820.
26. Thitithammawong, A., et al., *Thermoplastic vulcanizates based on epoxidized natural rubber/polypropylene blends: Selection of optimal peroxide type and concentration in relation to mixing conditions*. *European polymer journal*, 2007. **43**(9): p. 4008-4018.
27. Visakh, P., G. Markovic, and D. Pasquini, *Recent Developments in Polymer Macro, Micro and Nano Blends: Preparation and Characterisation*. 2016: Woodhead Publishing.
28. Sarath, C.C., R.A. Shanks, and S. Thomas, *Polymer blends*, in *Nanostructured polymer blends*. 2014, Elsevier. p. 1-14.
29. Wildi, R.H. and C. Maier, *Understanding compounding*. 1998: Hanser Publishers Munich, Germany.
30. Grove, D.A. and C. Harper, *Composite Processes*. *Handbook of Plastic Processes*, 2006: p. 475-527.
31. Selke, S.E., et al., *Plastics packaging: properties, processing, applications, and regulations*. 2021: Carl Hanser Verlag GmbH Co KG.
32. Davis, J.R., *Tensile testing*. 2004: ASM international.

33. Driver, W.E., *Plastics Chemistry and Technology*. 1979: Van Nostrand Reinhold Company.
34. Lampman, S., *Characterization and failure analysis of plastics*. 2003: Asm International.
35. Evaluation, I.S.U.C.f.N. and (CNDE). Available from: https://www.nde-ed.org/About/hs_intro002.xhtml.
36. Höhne, G. and W. Hemminger, H.-J. *Flammersheim Differential Scanning Calorimetry*. 2003, Springer-Verlag.
37. Gill, P., T.T. Moghadam, and B. Ranjbar, *Differential scanning calorimetry techniques: applications in biology and nanoscience*. Journal of biomolecular techniques: JBT, 2010. **21**(4): p. 167.
38. Cheremisinoff, N.P., *Polymer characterization: laboratory techniques and analysis*. 1996: William Andrew.
39. Gabbott, P., *Principles and applications of thermal analysis*. 2008: John Wiley & Sons.
40. Utracki, L.A. and C.A. Wilkie, *Polymer blends handbook*. Vol. 1. 2002: Kluwer academic publishers Dordrecht.
41. De Assumpção Pereira-da-Silva, M. and F. Ferri, *1—Scanning Electron Microscopy*. Nanocharacterization Techniques; Da Róz, AL, Ferreira, M., de Lima Leite, F., Oliveira, ON, Eds, 2017: p. 1-35.
42. Osahor, A., et al., *Rapid preparation of adherent mammalian cells for basic scanning electron microscopy (SEM) analysis*. Analytical biochemistry, 2017. **534**: p. 46-48.
43. Smith, B.C., *Fundamentals of Fourier transform infrared spectroscopy*. 2011: CRC press.
44. Gowariker, V.R., N. Viswanathan, and J. Sreedhar, *Polymer science*. 1986: New Age International.
45. Kothari, V. and V. Gupta, *Manufactured Fiber Technology*. 1997, Published by Chapman & Hall. p.
46. Choudhary, A., *The principle of Ultra Violet (UV) Spectrophotometer*. Medium.com, 2017.
47. Auras, R., B. Harte, and S. Selke, *An overview of polylactides as packaging materials*. Macromolecular bioscience, 2004. **4**(9): p. 835-864.
48. Hamad, K., et al., *Polylactic acid blends: The future of green, light and tough*. Progress in Polymer Science, 2018. **85**: p. 83-127.
49. Hassan, E., et al., *Dynamic mechanical properties and thermal stability of poly (lactic acid) and poly (butylene succinate) blends composites*. Journal of fiber Bioengineering and Informatics, 2013. **6**(1): p. 85-94.
50. Pongtanayut, K., C. Thongpin, and O. Santawitee, *The effect of rubber on morphology, thermal properties and mechanical properties of PLA/NR and PLA/ENR blends*. Energy Procedia, 2013. **34**: p. 888-897.
51. Tessanan, W., et al., *Improvement of mechanical and impact performance of poly (lactic acid) by renewable modified natural rubber*. Journal of Cleaner Production, 2020. **276**: p. 123800.
52. Chen, Y., D. Yuan, and C. Xu, *Dynamically vulcanized biobased polylactide/natural rubber blend material with continuous cross-linked rubber phase*. ACS applied materials & interfaces, 2014. **6**(6): p. 3811-3816.

53. Ma, P., et al., *In-situ compatibilization of poly (lactic acid) and poly (butylene adipate-co-terephthalate) blends by using dicumyl peroxide as a free-radical initiator*. Polymer degradation and stability, 2014. **102**: p. 145-151.
54. Mishra, J.K., Y.-W. Chang, and W. Kim, *The effect of peroxide crosslinking on thermal, mechanical, and rheological properties of polycaprolactone/epoxidized natural rubber blends*. Polymer bulletin, 2011. **66**(5): p. 673-681.
55. Cinelli, P., et al., *Cosmetic packaging to save the environment: Future perspectives*. Cosmetics, 2019. **6**(2): p. 26.
56. Huang, Y., et al., *Study on the effect of dicumyl peroxide on structure and properties of poly (lactic acid)/natural rubber blend*. Journal of Polymers and the Environment, 2013. **21**(2): p. 375-387.
57. Bureepukdee, C., S. Suttireungwong, and M. Seadan. *A study on reactive blending of (poly lactic acid) and poly (butylene succinate co adipate)*. in *IOP Conference Series: Materials Science and Engineering*. 2015. IOP Publishing.
58. Tiptipakorn, S., K. Hemvichain, and A. Pirombua. *Study of the effect of electron beam on thermal and mechanical properties of poly (lactic acid)/poly (butylene succinate) blends*. in *IOP Conference Series: Materials Science and Engineering*. 2019. IOP Publishing.
59. Cosme, J.G., et al., *Development of biobased poly (lactic acid)/epoxidized natural rubber blends processed by electrospinning: Morphological, structural and thermal properties*. Materials Sciences and Applications, 2016. **7**(4): p. 210-219.
60. da Silva, T.F., et al., *Effect of lignin as accelerator of the biodegradation process of poly (lactic acid)/lignin composites*. Materials Science and Engineering: B, 2019. **251**: p. 114441.
61. Zhou, J., et al., *Measurement and correlation of solubility and thermodynamic properties of dicumyl peroxide (DCP) in pure and binary solvents*. Journal of Molecular Liquids, 2020. **314**: p. 113268.
62. Silverajah, V., et al., *A comparative study on the mechanical, thermal and morphological characterization of poly (lactic acid)/epoxidized palm oil blend*. International journal of molecular sciences, 2012. **13**(5): p. 5878-5898.
63. Johns, J. and V. Rao, *Thermal stability, morphology, and X-ray diffraction studies of dynamically vulcanized natural rubber/chitosan blends*. Journal of materials science, 2009. **44**(15): p. 4087-4094.
64. Bijarimi, M., S. Ahmad, and R. Rasid, *Mechanical, thermal and morphological properties of poly (lactic acid)/epoxidized natural rubber blends*. Journal of Elastomers & Plastics, 2014. **46**(4): p. 338-354.
65. Wang, X., et al., *Influence of the lignin content on the properties of poly (lactic acid)/lignin-containing cellulose nanofibrils composite films*. Polymers, 2018. **10**(9): p. 1013.
66. Hu, X., et al., *Difference in solid-state properties and enzymatic degradation of three kinds of poly (butylene succinate)/cellulose blends*. RSC advances, 2017. **7**(56): p. 35496-35503.
67. Arruda, L.C., et al., *Influence of chain extender on mechanical, thermal and morphological properties of blown films of PLA/PBAT blends*. Polymer Testing, 2015. **43**: p. 27-37.





VITA

NAME Mr. Jesadakorn Sakdee

DATE OF BIRTH 17 October 1996

PLACE OF BIRTH Phichit

INSTITUTIONS ATTENDED 2015-2018: Bachelor's degree in Engineering at Department of Chemical Engineering, Silpakorn university

HOME ADDRESS 82/1, Thungnoi, Photale, Phichit, Thailand 66130

